A Sheffield Hallam University thesis

PREFACE

This dissertation is submitted for the degree of Master of Philosophy of the Council for National Academic Awards. During the period of his research the author has attended the following courses:

   (i)   Electron microscopy

  (ii)   Quantitative x-ray diffraction

 (iii)   Numerical analysis

  (iv)   High strength steels

The author has also attended the following conferences:

   (i)   Influence of second phase particles on the properties of steels. Scarborough (BISRA/ISI 24-24 March, 1971).

  (ii)   Modern metallography in Metallurgy, Liverpool (Inst. Met. 28th to 30th September, 1971.)

 (iii)   Grain boundary conference, London (Inst.Met.ISI 25th November,1971.)

The results obtained and the theories developed are to the best of my knowledge original except where reference is made to the work of others.

No part of this dissertation has been submitted for a degree at any University or College.

The effect of predrawing structure and carbon content upon the mechanical properties and structure of plain carbon steel wires has been investigated. Quenched and tempered, fully annealed, and isothermally transformed hypoeutectoid steels, and annealed pure iron have been used to provide a range of predrawing structures.

X-ray diffraction, optical and electron metallographic techniques have been used, quantitatively where possible, to follow the deformation process in its effects on structural parameters.

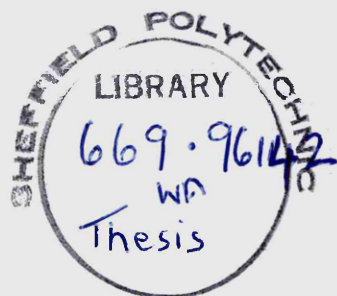The results obtained have been tabulated to permit the study of the variation in structural parameters relative to the deformation level and mechanical properties of the wire.

THE INFLUENCE OF PREVIOUS THERMAL HISTORY UPON THE PROPERTIES AND DEFORMATION CHARACTERISTICS OF COLD DRAWN PLAIN CARBON STEEL WIRES.

G.K.Wallis,
Department of Metallurgy
Sheffield Polytechnic.

November 1975

CONTENTS

The deformation of iron may be conveniently considered in two sections, single crystals, and polycrystals.

I.I. SINGLE CRYSTALS

I.I.I. CRYSTALLOGRAPHIC EFFECTS

In body centred cubic metals, unlike close packed structures, no single, well defined close packed plane exists, several planes having similar atomic packing densities. However, a single close packed direction exists, the $\langle 111 \rangle$, and slip is usually confined to this.

The $\langle 111 \rangle$ zone contains three planes of almost identical packing density, (110); (112); (123), and slip may occur on any of these. The deformation temperature appears to govern the active slip plane for most b.c.c. metals [1] :-

If T_m = melting temperature $^\circ K$ and T = deformation temperature $^\circ K$

$T < T_m/4$	active slip plane	$\{112\}$
$T = T_m/4 - T_m/2$	active slip plane	$\{110\}$
$T > T_m/2$	active slip plane	$\{123\}$

For iron it appears that slip may occur on any of the slip planes, and possibly simultaneously on more than one plane (pencil glide, wavy slip), but at low temperatures and high strain rates slip does tend to be confined to the $(110) \langle 111 \rangle$ system.

During deformation rotation of the lattice occurs, causing secondary slip systems to operate[2] Fig. I. illustrates this, with the simplifying assumption that slip is confined to the (IIO) plane. The initial stress axis is at point P on the stereographic projection, slip occurring on the (OII) [I$\bar{\text{I}}$I] primary system.

During deformation the position of the tensile axis moves along the hatched line, towards the [I$\bar{\text{I}}$I] point. On reaching the [OOI] - [IOI] boundary conjugate slip on the secondary system, (O$\bar{\text{I}}$I) [III] , occurs, the axis travelling along the [OOI] - [IOI] boundary towards [IOI] . Eventually the stress axis reaches the [IOI] direction, and the crystal is completely oriented.

Thus the critical resolved shear stress in the ($\bar{\text{I}}$OI) and (IOI) planes must be zero, and slip on these planes impossible since:-

$$\Upsilon = \sigma_t \cos \phi \cos \lambda \qquad \text{Equation I.I.}$$

Where Υ = resolved shear stress in the slip plane, along the slip
$$\text{direction.}$$

σ_t = applied stress

ϕ = angle between the stress axis and the normal to the
$$\text{slip plane.}$$

λ = angle between the stress axis and the slip direction.

Applying Equation I.I. to the other slip planes in the [III] and [II$\bar{\text{I}}$] zones the resolved shear stress in the (I2I) and ($\bar{\text{I}}$2I) planes is zero, since both are perpendicular to the stress axis. In the (23I) and (23I) planes, however

$$\Upsilon = 0.802 \ \sigma_t$$

whereas, in the (OII) $[\bar{1}11]$ and (O$\bar{1}$I) $[1\bar{1}1]$ systems

$$\gamma = 0.707\,\sigma_t$$

i.e. slip should occur preferentially in the (2$\bar{3}$I) $[\bar{1}11]$
and (231) $[1\bar{1}1]$ systems since the resolved shear stress is greater
in these system.

I.1.2. THE FLOW CURVE FOR SINGLE CRYSTALS

The effect of the crystal orientation is marked during testing of
single crystals. Keh [3], and Jaoul and Gonzalez [4] have shown that,
for certain orientations in which slip is limited to a single
system, a three-stage curve, similar to that obtained with face
centred cubic crystals can be obtained. Where the crystal is
oriented for multiple slip, however, a parabolic curve of the form

$$\sigma = \sigma_0 + \alpha\varepsilon^{\frac{1}{2}} \qquad\qquad \text{Equation : I.2}$$

where σ_0 and α are constants is obtained. [5]

I.1.3. THE EFFECT OF TEMPERATURE AND STRAIN RATE

The flow stress may be defined as the stress required to initiate
plastic deformation. In body centred cubic metals flow stress is
strongly temperature and strain rate dependent [6], particularly at
low temperatures. Two causes of the temperature dependence are
cited:

(i) A temperature dependent Peierls-Nabarro force.

(ii) The presence of interstitial impurities.

It seems probable that both these mechanisms are active, since experiments with ultra high purity materials reveal considerable temperature dependence of the flow stress. Conrad[6] concluded that the temperature dependence resulted from the Peierls-Nabarro force.

Zener and Holloman[7] suggested that plastic flow was a thermally activated process, i.e.

$$S = S(P.\varepsilon)$$

where P has the form $P = \dot{\varepsilon} e^{Q/RT}$

$\dot{\varepsilon}$ is strain rate

The hypothesis of thermally activated flow is now generally accepted, Zener and Holloman showing that the stress S was a function of log P. These theories imply an equivalence between temperature and strain rate.

I.2 POLYCRYSTALLINE IRON

I.2.I. CRYSTALLOGRAPHIC EFFECTS

While the available slip systems remain the same, it is obvious that the introduction of grain boundaries results in a restriction on crystal rotation. Since crystallographic orientation varies from grain to grain it must be assumed that the active slip system (s) in each grain are not identical. It has been shown that five independently operating slip systems are necessary for grain boundary coherence.[8,9]

Ultimately a preferred orientation must arise in the structure,

despite restraints introduced by the grain boundaries. However, high deformation levels are required, Dieter[10] quoting 80% as the necessary deformation level.

I.2.2. GRAIN BOUNDARIES AS BARRIERS TO DISLOCATION MOVEMENT

The plastic deformation of a metal involves the movement of large numbers of dislocations. It is well known that grain boundaries act as barriers to dislocation movement, " and that an increase in the area of grain boundary i.e. a decrease in grain size, results in increasing flow stress. Grain boundaries have been shown to consist of a region of atomic misfit 2-3 atomic distances wide."

Eshelby, Frank, and Nabarro[12] showed that the number of dislocations which could be compressed into the distance between a dislocation source, and a barrier is given by:

$$n = \frac{k \pi \gamma L}{Gb}$$

where   G is the modulus of elasticity in shear

b is the Burgers vector of the dislocation

n is the number of dislocations

k is a constant

γ is the shear stress acting on the dislocation source

L is the distance between the source and barrier

If we consider a source at the centre of a grain, diameter d, then the distance between source and barrier is d/2, and

$$n = \frac{k \pi \gamma d}{2Gb}$$

hence

$$= \frac{2 n G b}{k \pi d}$$

Equation I.3

Since n is the number of dislocations which can be compressed into the distance d/2, τ is the back stress exerted on the source by the pile up of dislocations. It is also the stress exerted on the barrier, i.e. the grain boundary.

I.2.3. GRAIN BOUNDARIES AS DISLOCATION SOURCES

Keh and Weissmann [13] observed that grain boundaries which were clearly defined in the undeformed condition, showed reduced sharpness after I-2% plastic strain. This was shown to be due to dislocation generation at the grain boundary. Similar effects have been observed by other workers [14,15], and there seems to be no reason why a barrier showing incoherency with the matrix should not act as a source of dislocations.

I.2.4. THE EFFECT OF GRAIN BOUNDARIES ON THE FLOW CURVE

The work of Hall [16], and of Petch and co-workers [17,18], relating the grain size of iron to the upper and lower yield points was an early step towards relating the structure of steel to its mechanical properties.

These workers derived the empirical relationship:-

$$\sigma_{L.Y.P.} = \sigma_i + k_{L.Y.P.} \, d^{-\frac{1}{2}}$$

Equation I.4

where σ_i was taken to be the stress required to overcome lattice friction, and $k_{L.Y.P.}$ is a constant.

Subsequently Petch et.al.[18] extended the theory to show a similar relationship for the flow stress and grain size.

$$\sigma_f = \sigma_i + k_f \, d^{-\frac{1}{2}} \qquad \text{Equation I.5}$$

In this equation σ_i and k_f have similar meaning to those of Equation I.4, but differ considerably in value. The authors interpreted the equation in the light of Taylor's work on the orientation factor relating the tensile yield stress to the critical resolved shear stress for yield τ_{max}.

$$\tau = \tau_o + k_s d^{-\frac{1}{2}}$$

$$\therefore \qquad \sigma_f = m\,\tau_o + m k_s \, d^{-\frac{1}{2}} \qquad \text{Equation I.6}$$

If the shear stress induced on a dislocation source distance r from the grain boundary by a slip line in the neighbouring grain intersecting the common grain boundary is τ_{max} then

$$k_s = \tfrac{1}{2} m \, \tau_{max} \, r^{\frac{1}{2}}$$

If τ_c is the shear stress required to operate the source, assuming τ_{max} is not generated in the slip plane.

$$\tau_{max} = \tfrac{1}{2} m \, \tau_c$$

$$k_s = m \, \tau_c \, r^{\frac{1}{2}}$$

$$k_f = m^2 \, \tau_c \, r^{\frac{1}{2}}$$

and

$$\sigma_f = m_o + (m^2 \, \tau_c \, r^{\frac{1}{2}}) d^{-\frac{1}{2}} \qquad \text{Equation I.7}$$

The original Hall Petch relationship has been modified on many occasions. Perhaps the most important contributions to the development of this approach have been those of Conrad [6,19], and McLean et.al. [20,21] Conrad suggested the following modifications:-

$$\sigma = \sigma^*(T, \dot{\varepsilon}) + \sigma_\mu(st.) + kd^{-\frac{1}{2}} \qquad \text{Equation I. 8}$$

where $(T\dot{\varepsilon})$ is the thermally activated stress component

σ_μ is the athermal stress component, proportional to the

shear modulus.

McLean considered the dislocation contribution to the flow stress, giving:-

$$\sigma = \sigma_0 + \alpha G b p^{\frac{1}{2}} \qquad \text{Equation I. 9}$$

where α is a constant

   G the shear modulus

   b the Burgess vector, and

   p the dislocation density

Dingley and McLean [21] suggested that the term $\alpha G b p^{\frac{1}{2}}$ should be unaffected by grain boundaries, any strengthening effect due to the latter being included in the σ_0 term. These authors concluded that:-

"After yield there is no significant grain boundary barrier hardening as there is at yield. The grain boundary hardening is mainly indirect, arising from different dislocation densities in different grain sizes. Dislocation strengthening is inversely proportional to dislocation spacing, with a proportionality constant that is nearly independent of temperature and dislocation pattern, which points to an intersection and (local) stress field dislocation hardening model."

Experimental evidence that finer grain size resulted in an increased dislocation density for a given strain was reported. A

similar analysis by Foltzmann and Man [22] produced the form:-

$$\sigma_f = \sigma_i + \sigma_u + k_f d^{-\frac{1}{2}}$$

where $\quad \sigma_u = \alpha \varepsilon_p^n \qquad$ where $\quad n \approx 0.43$

i.e. $\quad \sigma_f = \sigma_i + \alpha \varepsilon_p^n + k_f d^{-\frac{1}{2}} \qquad\qquad$ Equation I. 10

where ε_p is the plastic strain.

Evans and Rawlings [23] concluded that the flow curve of mild steel could be divided into two sections.

$< 10\%$ strain $\qquad \sigma_f = \sigma_0 + \alpha \varepsilon_p^n \qquad\qquad n \approx 0.45$

$> 10\%$ strain $\qquad \sigma_f = A + B \ln \varepsilon_p$

In the second equation, for strains in excess of 10%, decreasing grain size results in increasing A i.e. the term A contains the grain size effect. The equation for strains less than 10% was expanded to:-

$$\sigma_f = \sigma_0 + \alpha_0 \varepsilon_p^{0.5} + K d^{-\frac{1}{2}} \varepsilon_p^{0.5} \qquad\qquad \text{Equation I. 11}$$

where K is a constant depending on the purity of the metal, and α_0 the coefficient of work hardening for a metal of infinitely large grain size.

The observations of Jaoul [24] on the effect of grain size on the flow curve of mild steel indicated that their effect on the slope of the curve is very slight decreasing grain size increasing the initial flow stress, i.e. the yield point. Hull et.al. [15] state that:-
"Whilst grain boundaries may be sources of dislocations, they do not control the rate of multiplication."

while Keh and Weissmann [13] noted that grain boundaries acted as dislocation sources and Dingley and McLean [21] stated that the dislocation density in any two specimens strained to the same level was greater in the sample having the finest grain size. It seems probable, therefore, that grain boundaries exert an effect on the initial work hardening rate, possibly due to their action as dislocation sources, but that this effect disappears at higher strains.

The term σ_x introduced in Equation I.2.6, and retained in the final form of Equation I.2.10 refers, principally to the effect of precipitates on the flow stress of polycrystalline iron. σ_x will have a small, but significant effect when the proportion of precipitate is small. Increasing the proportion of precipitate would be expected to alter the flow stress of iron to a considerable extent.

2.1 THEORIES OF PRECIPITATE HARDENING

Theories of precipitation hardening may, for convenience, be divided into two groups:

(a) Hardening by coherent and semicoherent precipitates(precipitation hardening).

(b) Hardening by incoherent precipitates (dispersion hardening).

In the case of plain carbon steels i.e. ferrite plus a carbide precipitate, only the second form of hardening is of interest,and discussion of hardening by coherent or semi coherent precipitates has been omitted.

The theories of Orowan[24] are probably the most significant of those dealing with dispersion hardening, and most subsequent theories appear to be based on variations of this approach. Considering the dislocation line as flexible, passing through a matrix containing hard, approximately spherical particles.

The shear stress for yielding is given by:

$$\tau_y = \tau_s + \frac{Gb}{\pi(d-2r)}\,\phi\,\ln\left(\frac{d-2r}{2b}\right) \qquad \text{Equation 2.I}$$

$$\phi = \frac{1}{2}\left(1 + \frac{1}{1-\mu}\right) \qquad \text{where} \quad \mu = \text{Poisson's Ratio}$$

where

τ_y = shear stress for yielding

τ_s = yield stress of the matrix

G = shear modulus of the matrix

d = particle spacing (centre to centre)

r = particle radius

b = Burgers vector

It is obvious that Equation 2.I attributes the strengthening effect of the second particles to the particle spacing $(d-2r)^{-I}$, that as a dislocation line moves past the particles offering the resistance a dislocation ring is left behind, surrounding each particle. Zackay and Parker[25] summarised this effect:

"Alloys containing strong particles strain harden very rapidly because slip dislocations leave dislocation rings around particles they pass, and the effective interparticle spacing decreases rapidly as the number of rings increases."

Fisher, Hart, and Pry[26] derived an equation showing the effect of second phase particles, and the number of dislocation rings surrounding them:

$$\tau_h = 3\left(\frac{N}{r}\right) x^{3/2} \qquad \text{Equation 2.2}$$

is the increase in stress due to the second phase, N the number of rings surrounding each particle, of diameter r, and f the volume fraction of second phase present. However

$$f = \left(r/R\right)^2 \qquad \text{where R is the particle spacing}$$

Substituting in Equation 2.2

$$\tau_\lambda = 3 \frac{N}{r} \frac{r^3}{R^3} = \frac{3Nr^2}{R^3} = \frac{3Nf}{R} \qquad \text{Equation 2.3}$$

This equation suggests that the increase in hardness due to a second phase is proportional to the volume fraction of the second phase, and inversely proportional to the particle spacing.

Ansell and Lenel[27] suggested that the theories of Fisher et.al. explained the behaviour of dispersion hardened metals up to a certain particle size. For particle sizes greater than this they proposed that the dispersion strengthened metal yielded when the stress on each particle was sufficient to cause yield or fracture of the particle.

$$\text{Yield Stress} = \left(\frac{\mu b \mu^*}{2 \lambda c} \right)^{\frac{1}{2}} \qquad \text{Equation 2.4}$$

μ = shear modulus of matrix

μ^* = shear modulus of particle

b = Burgers vector

λ = particle spacing

i.e. Yield Stress $\quad \sigma_y = K \lambda^{-\frac{1}{2}}$

This equation ignores any effect of volume fraction of precipitate, unlike the Fisher theory, and, as Dieter[10] states:

"The hardness and strength (of steel) increase with carbon content, or volume fraction of the carbide phase. Further, for a given carbon content, the strength will be higher for a finer carbide spacing, than with a coarse particle spacing. Particle shape has a less important effect although, for a given volume fraction of carbides, lamellar carbides will be stronger than spheroidised carbides."

The approach of Unckel [28] differs from the foregoing. His theory states that:

$$\sigma_f = A e^{-By} + C \qquad \text{Equation 2.5}$$

A, B and C are constants, and y the interparticle spacing. As pointed out by Hyam and Nutting [29],

"This formulation has the merit that, at zero spacing, σ_f is equal to the flow stress of the second phase i.e. A, and at infinite spacing is equal to that of the matrix, C. The constant B is dependent on the way in which the shear forces decrease with distance from a particle."

Comparison of this equation with that of Evans and Rawlings for strains in excess of 10% given in the preceding chapter reveals considerable similarities.

2.2. EXPERIMENTAL RELATIONSHIPS BETWEEN STRUCTURE AND MECHANICAL PROPERTIES OF TWO PHASE ALLOYS

The first attempt to relate structure to strength in steels were those of Gensamer et.al.[30]. These authors showed that strength was inversely proportional to the logarithm of the interparticle spacing. Holloman [31] confirmed this relationship, and showed that the strain hardening rate of quenched and tempered, or isothermally transformed steels increased slightly with increased strength, but was essentially very similar for the same steel.

Hyam and Nutting [29], working with quenched and tempered steels concluded that none of the accepted theories of dispersion hardening [24,26,27,29] fitted the results obtained, and related the hardness to the mean predicted grain diameter. Turkalo and Low [32], working on similar materials, rejected the conclusions of Hyam and Nutting, and obtained a linear relationship between strength, and the logarithm of interparticle spacing i.e. the Gensamer relationship.

Turkalo and Low included precipitate particles, and grain
boundaries as barriers to dislocation movement.

2.3. THE EFFECT OF DEFORMATION ON THE STRUCTURE OF TWO PHASE METALS

Pickering et.al.[33] showed that, after 2% deformation cementite
lamellae in pearlitic steels could no longer be imaged clearly in
the electron microscope. This was shown to be due to the generation
of dislocations at the ferrite/cementite interface, and a high dis-
location density was observed in the pearlitic ferrite. The short
free ferrite path length severely limited dislocation movement.
Thus, to accommodate the deformation, a substructure must form,
probably accompanied by yielding and fracture of the cementite
lamellae. Puttick[34], and Kaldor[35] have shown clearly that plastic
deformation and fracture of cementite lamellae in pearlite can
occur, and Keh[36] has demonstrated plastic deformation of massive
cementite in rolled steel. Puttick concluded that:

"Deformation (in pearlite) is accommodated by fine slip in ferrite
parallel to the lamellae where the resolved shear stress is
sufficiently high, or by slip transverse to the cementite in un-
favourably oriented colonies. In the latter case the slip is
accompanied by plastic deformation of cementite, and some ferrite/
cementitate interfacial slip. In such colonies the ferrite slip
may also follow a zig-zag, or "arrowhead" path in the early stages
in the lamellar pattern, and may be nucleated at the ends of
cementite plates."

Additional evidence for a high density of faults in certain areas
of deformed pearlite was provided by Woltzmann, Danko, and Stout[37].
These authors studied the spheroidisation of deformed pearlite.
In all cases spheroidisation occurred most rapidly in areas of
heavily distorted lamellae.

In the case of quenched and tempered steels little evidence has
been found for the deformation and fracture of the carbide

particles. It would appear that the classical approach to a dispersion hardened structure will apply, and that deformation will cause the build up of dislocation rings around the particles.

CHAPTER 3. THE EFFECT OF WIREDRAWING ON THE STRUCTURE AND PROPERTIES OF CARBON STEEL

3.I. PRESENTATION OF DATA

Conventionally, wiredrawing data has been presented as a function of percentage reduction of area, or diameter until very recently. Even now much of the available data is published in this form. Recently, however, Godfrey[38], and Mohrnheim [39,40], have suggested the use of a logarithmic base scale. Godfrey's suggestion is that the deformation in wiredrawing should be presented as a true strain, based on the formula:

$$\text{True Strain on wiredrawing} = \log_e \frac{A_o}{A} = \log_e \left(\frac{D_o}{D}\right)^2 \qquad \text{Equation 3.I}$$

Mohrnheim [39,40], on the other hand, simply suggests presenting the results on axes having a "preferred number" series. The suggestion of Godfrey [38] appears to have the greater fundamental application.

3.2. THE PROPERTIES OF DRAWN WIRE

Sisco [4I], reviewing data published before 1937 came to the following conclusions:-

i) The principal effect of cold drawing is to increase strength and hardness, while reducing ductility.

ii) Irrespective of the original value the percentage elongation always drops to a low value after approximately 10% reduction.

iii) For carbon contents between 0.1% and I.4% the increase in tensile strength and yield strength is proportional to the amount of cold working, and is practically independent of

carbon content.

iv) Patenting before drawing results in higher drawn tensile strength, while annealing has the opposit effect.

v) Oil quenched and tempered steel has low drawability and drawn ductility.

Most of these conclusions would appear to have been upheld by the results of modern researchers.[42-48]

Examination of published data revealed close similarities in the pattern of work hardening of carbon steels containing up to 1% Carbon, where the structural matrix was ferrite. The form of the carbide did not appear to affect the basic curve shape.[41-48]

Initial deformation, up to 20% results in a logarithmic increase in strength, as measured by tensile strength or flow stress. Between 20% and 80% deformation tensile strength increases slowly in an approximately linear basis, and, for deformations in excess of 80%, increases very rapidly to the drawability. The ductility, as measured by percentage constriction, varies only slightly up to 80% deformation, and then decreases rapidly for .

spheroidised structures, however, as shown _,
et.al[42] the ductility decreases at a constant rate with increasing deformation. Sisco's conclusions regarding the use of percentage elongation as a measure of ductility have been fully confirmed by these authors.

3.3. THE STRUCTURE OF DRAWN WIRE

The early stages of deformation, up to 50-60% appear to result in some preferential distortion of pearlite grains containing lamellae approximately parallel to the wire axis[49]. After 91% deformation all the lamellae are aligned in the direction of drawing[44]. Deformation of unfavourably aligned appears to result in

a kinking, possibly, but not necessarily involving fracture of the carbides.[49] A subgrain network of dislocations is formed at an early stage, 15% deformation, and its prominence increases with increasing deformation.

Lamella aligned approximately parallel to the wire axis do not necessarily fragment, a reduction in thickness and spacing being observed by several authors [44,45,49]. Some "necking" of such lamellae was observed by Embury and Fisher [43]. Some fragmentation of carbides has also been reported, [44,45] together with a dislocation structure in the carbide phase.

The initial size of the ferrite substructure appear to be controlled by the lamellae spacing, Kardonskii et.al.[45] quoting figures of 300A° in patented steel, and 500-700A° in annealed steel. After deformation these reduce to 100-150A° and 350-400A° respectively. Dewey and Briers [50] confirm these dimensions for eutectoid steel deformed 98%. According to Embury and Fisher [43] the reduction in cell dimension perpendicular to the wire axis is directly proportional to the reduction in area throughout the deformation process.

Theory [10] predicts that deformed b.c.c. metals should have a 110 orientation, and several authors have reported this. [51,52] Dewey and Briers [50], on the other hand were unable to detect any preferred orientation by electron diffraction.

Deformation of spheroidised structures, formed either by prolonged annealing, or by tempering of quenched structures,i.e. coarse and fine particles respectively does not appear to result in any fragmentation of particles. [42,44] The ferrite cell size appears to

be related to the interparticle distance.

Several authors conclude that the function of the carbide phase is to "pin" and reinforce the substructure of the ferrite.[43,44,45,49,50]

3.4. THE RELATION BETWEEN STRUCTURE AND PROPERTIES

Two change points on the curves relating the mechanical properties to the degree of deformation have been established:-

i) After 10-20% deformation a decrease in the rate of work hardening, and a concurrent loss in tensile elongation.

ii) After 75-90% deformation a rapid acceleration in the rate of work hardening and a rapid decrease in percentage constriction.

No evidence is available to explain i), but it does not appear improbable that it is associated with the establishment of a substructure in the ferrite. The slight increase in percentage constriction sometimes observed has been attributed to fracture of the carbide phase [42]. It has been suggested that the overall length of the ferrite/cementite interface governs the strength.[42]

Most of the attempts to relate structure to strength have adopted modifications of the Hall-Petch approach [43,44,50], and Maurer et.al.[49] state that the strength of deformed steel was largely attributable to the substructure of the ferrite. In the modifications of the Hall-Petch theory postulated, the dislocation barrier spacing was taken as the subcell size, and Embury and Fisher show a plot of their data based on this approach. Chandhok et.al.[44] concluded that:

" A deformation mechanism can be described in terms of interactions among the basic variables of carbon availability, carbon mobility, and dislocation mean free path. The model involves dissolution of

Carbon from initial carbide particles, migration of carbon, and its interaction with dislocations."

i.e. that a continuous process of age hardening is operative, resulting in the pinning of the dislocation network by diffusion of carbon atoms to form a Cottrell atmosphere. This model was confirmed to some extent by high and low temperature deformation trials.

4.I RAW MATERIAL

A range of steels, and irons, with varying Carbon content were chosen to produce as wide a range of structures and strengths as possible. The material, and conditions selected were as follows:-

I. Pure Iron, with a range of grain size controlling the initial mechanical properties.

2. 0.18% Carbon Steel, with controlled carbide morphology controlling the mechanical porperties.

3. 0.44% Carbon Steels, with mechanical properties controlled by carbide morphology.

The materials for (2) and (3) were commercial steels readily available, but the first material was specially obtained.

4.I.I. HEAT TREATMENT

The structures required were obtained by a range of heat treatment methods. The following terminology is defined for clarity:-

(a) Austenitisation

The process of heating a steel above the AC_3 line on the Iron/Iron Carbide Phase Diagram (Fig.2) i.e. into the austenite phase field.

(b) Sub critical Annealing

The process of heating a steel to a temperature less than the AC_3

point, to obtain the required structure without austenitisation.

(b) Isothermal Transformation

The process of quenching a steel from the austenitic condition to a temperature below the AC_3 point, and maintaining this temperature for a period sufficient to permit transformation to the ferrite plus iron carbide structure by nucleation and growth of the final phase. (Fig.3)

4.I.2. PREPARATION FOR WIREDRAWING

This operation was identical for all steels. Following heat treatment, or after hot rolling, wire rod is heavily contaminated with adhering iron oxide scale. This must be removed before wire-drawing as the scale is highly abrasive, and, if present, would cause rapid wear and deterioration of the wiredrawing dies. The scale was removed chemically by immersion of the rod in a 20% v/v solution of Hydrochloric Acid in water, containing a small pro-portion of commercial inhibitor (Inhibisol) at $25^{\circ}C$ for 25-30 minutes. The rod was then washed in water to remove excess acid.

The rods were then immersed into a solution of Phosphoric Acid and Phosphates at $70^{\circ}C$ for 7 minutes. Excess solution was rinsed off with water, and the rod dried in ovens at $200^{\circ}C$ for IO minutes. This treatment serves two purposes:-

I. During wiredrawing the rod is required to "pick up" lubricant, in the form of soap granules or powder, and carry this into the die. The wiredrawing coat facilitates this.

2. Chemically cleaned rods exposed to the atmosphere corrode rapidly. While this may be desirable to a limited extent, the wiredrawing coat prevents oxidation, other than that required by intent.

4.1.3. PREPARATION OF PURE IRON

This material was obtained in the form of rod, nominally 6.35 m/m diameter, but of irregular cross section. The starting size for all the experimental wiredrawing had been selected as 5.6 m/m diameter (5 gauge) with a circular cross section. The 6.35 m/m rods were prepared for wiredrawing as described in Section 4.1.2., and drawn to 5.6 m/m diameter producing an even, circular cross section. This process introduced some grain deformation, which was desirable as it was intended to produce a raw material of the same chemical composition, but differing grain size by re-crystallisation. The effect of time and temperature on the grain size was studied on samples of the 5.6 m/m diameter material and the results established that annealing at $800^\circ C$, $850^\circ C$, and $900^\circ C$ would give the required grain size variation. Cooling rate did not appear to have any effect. Therefore the 5.6 m/m diameter material was separated into three small coils, and one coil heated for 15 minutes at each of the selected temperatures in a neutral salt bath, and then quenched to room temperature in clean water.

Finally the heat treated rod was again prepared for wiredrawing as in Section 4.1.2.

4.1.4. PREPARATION OF 0.18% CARBON STEEL

It is normal commercial practice to draw this material in the as

rolled condition, without any further heat treatment. The wire produced may be galvanised, or plastic coated, and used for various industrial purposes e.g. baling wire, wire baskets etc.

The as rolled condition was therefore chosen as one of the experimental conditions.

Attempts have been made to produce high tensile steel wire from low carbon steel [53] by production of a fine carbide dispersion in the initial rod. The production of this structure in low carbon steels requires a rapid quench rate after austenitisation. Previous work has shown that a 5% Sodium Hydroxide solution is a suitable quenching medium. The quenched structure was found to be very hard and brittle, indicating that a tempering treatment was required. A programme of experimental heat treatment indicated that an optimum blend of mechanical properties could be obtained by rapid quenching from 950°C into agitated 5% Sodium Hydroxide solution at 0°C, and tempering for 10 minutes at 400°C. This condition was selected for wire drawing. The austenitisation treatment, and tempering were carried out in neutral salt baths to prevent deoxidation of the rod surface.

In an attempt to determine the effect of carbon in solution on the tensile strength of drawn ferrite plus carbide structures a third condition was selected. Obviously a coarse carbide particle form was required, and the rod was therefore sub critically annealed at 650°C for 8 hours in a reducing atmosphere, producing a spheroidised carbide form evenly dispersed in a uniform ferritic grain structure. The heat treated rods were prepared for wiredrawing as described in Section 4.1.2.

Normal commercial practice is to "patent" steel of this composition before wiredrawing. Patenting may take one of three forms, following austenitisation:-

(a) Continuous cooling transformation in air (Air Patenting)
(b) Isothermal transformation on molten lead (Lead Patenting)
(c) Isothermal transformation in molten salt (Salt Patenting)

Salt patenting is mainly used outside the United Kingdom, but has recently shown signs of increasing popularity. The main advantage lies in the absence of toxic fume, but the structures produced tend to be slightly more coarse than lead patenting. Lead patenting was developed in the United Kingdom and produces a fine, uniform structure, but suffers from the emission of toxic fume. The air patenting process is principally employed for intermediate wiredrawing, ("ripping"), where the starting size for final wiredrawing is less than those obtainable by hot rolling in the rod mill, or where high tensile strength and controlled structure is not required.

The lead patenting process was selected, since the structure produced is very uniform. The rod was heat treated in a commercial lead patenting furnace of the continuous type, operating on the following cycle:-

Austenitisation 2 minutes at 900-950°C
Transformation 0.4 minutes at 540°C

Reference to Fig. 3 shows that these conditions should produce a fine pearlitic structure in a 0.44% Carbon steel.

Finally the heat treated rod was prepared for wiredrawing as
outlined in Section 4.I.2.

4.2. WIREDRAWING

4.2.I. WIREDRAWING DIES

Modern wiredrawing practice has replaced the steel drawplate,
containing a descending size of die holes, with a tungsten
carbide die. These were developed initially in Germany. The
modern wiredrawing die consists of a Tungsten Carbide/Cobalt
insert, shaped to the correct profile, in a steel case.
The production of dies is a skilled occupation and modern wire-
drawing mills have a "die shop" producing dies to the correct
size and profile. Wiredrawing dies are normally manufactured
by specialist companies to a specification set by the wire mill.
The dies are finished by the die department of the mill before
use. The following points are of great importance, referring
to Fig.4 :-

(a)   The entry angle should be sufficiently open to permit and
      increase flow of lubricant.
(b)   The angle of the die at the point of contact on wire entry
      should be 7°.
(c)   The parallel portion of the die should not exceed one third
      of the diameter of the drawn wire.
(d)   The parallel portion may taper slightly towards the exit,
      but should not taper towards the entry.
(e)   The exit of the die should be smoothly radiussed away to
      the full exit angle, to prevent stripping of the drawing
      coat.

Tungsten carbide dies were used throughout these experiments.

4.2.2. WIREDRAWING MACHINES

A modern wiredrawing machine normally consists of four basic
elements:-

(a)   The frame

(b)   The die holder, often a steel case, with a screw plug.
      The plug is removed, the die inserted with a washer in
      front, a second washer placed behind the die, and the plug
      tightened up to produce a water tight seal on the washers.
      The case is normally provided with entry and exit tubes for
      water cooling. The die holder is carried in a rectangular
      box section which also carries the lubricant.

(c)   "Killing rolls" which consist of a set of rolls, axis
      vertical. The wire is led around the rolls to induce a
      permanent "set" to the wire, which therefore falls naturally
      to a coil of slightly greater diameter than:-

(d)   The Block, normally a steel cylinder, which provides the
      force required to pull the wire through the die. The block
      is normally water cooled.

Modern wiredrawing machines are often multi-block, wire from
each block being fed off to the next die continuously. These
blocks are normally of the "accumulator" type, and the speed of
each block is individually adjusted to build up a reserve of
wire, i.e. wire accumulates on the block.

Two different machines were used for the experimental work:-

(a)   a 28 inch diameter block single hole machine, in which both the die and the block were water cooled.   Fig. 5

(b)   The final block of an 18 inch diameter block, 3 block machine, with water cooling on the die only.   Fig. 6

4.2.3.   WIREDRAWING PROCEDURE

All the materials were drawn on an equal draft schedule i.e. the reduction in area at each die was equal, of 10-15% Reduction per draft.   The leading edge was reduced on a small Pilger mill until the diameter was smaller than the die, and then threaded through the die.   This point was gripped in the jaws of a "dog", which could be hooked on to the block, and the wire drawn through the die, at 100 ft/minutes.   A dry mixture of 80% Calcium Stearate/20% Sodium Stearate was used as lubricant.

All the samples were drawn until further reduction resulted in fracture of the wire in the die i.e. to the limit of drawability.

Samples of drawn wire for mechanical testing and examination were always taken from the trailing end to avoid any possibility of material deformed on the Pilger mill being tested.

4.3.   MECHANICAL TESTING

4.3.1.   TENSILE TESTING

Two tensile testing machines were used:-

(a) An Instron 15,000 lb capacity machine

(b) An Avery tensile testing machine

The Avery machine was only used where the samples were too short for the Instron. No machining of wire samples is necessary. The specimens were painted with red lacquer, and marked at one inch intervals for elongation measurements.

Instron tests were carried out at a strain rate of 0.2 inches/minute using a 10 inch gauge length electromechanical extensometer, load/extension curves being recorded autographically. Extension after fracture was recorded on several gauge lengths, and reduction of area at the fracture point. All tests were started at 12 inches jaw separation and, wherever possible, extension to fracture recorded from the final jaw separation. Actual breaking load was recorded for many specimens.

Samples were prepared for the Avery machine in exactly the same manner as for the Instron machine, but the extension under load was measured with a 2 inch gauge length dial extensometer. Load and extension values were noted at regular intervals and load/extension curves plotted by hand. The strain rate was very low to permit accurate matching of load/extension readings. It was not possible to determine extension to fracture and actual breaking load on this machine.

4.3.2. WIREDRAWING LOAD

The load required to draw a wire may be expected to be a function of strain rate, the deformation resistance of the

material, and the friction in the die. Wiredrawing load could not be determined directly on any of the wiredrawing machines available due to lack of instrumentation, therefore the Instron tensile testing machine was used in a modified form. Samples were prepared from the 0.44% Carbon steel, with the fine dispersed carbide structure by stopping the wiredrawing machine with approximately 30 inches of wire not drawn. The drawn wire was cut I2 inches after the die, and the die removed from the die holder with the wire in position.

The lower gripping jaw, in the moving cross head was removed, and the drawn wire from the die exit passed through the cross head and gripped in the upper, stationary jaw. The lower cross head was lowered until tension was established, and the load required to draw the die over the wire recorded autographically at cross head speeds up to 50.8 cm/minute.

4.3.3. TORSION TESTING

The torsion test is frequently specified for wire, where the torsional ductility has a bearing on future application e.g. rope spinning. The normal test specified is number of twists to fracture, normally on a gauge length of I00 times the wire diameter. This test was made on all samples.

Some authorities regard the Shear Stress/Shear Strain curve as significant in the assessment of plasticity [IO], and full torque/ twist curves were prepared for the 0.I8% Carbon steel with coarse and fine carbide dispersion. The torque/twist data was converted to shear stress/ shear strain using the Nadai [IO] analysis

for values of shear stress above the elastic limit to calculate
Maximum Shear Stress. (See Appendix I). The testing equipment
used for these tests was as follows:-

(a) An Amsler horizontal torsion testing machine.(Large
                                                diameter wires).
(b) An Amsler vertical torsion testing machine.(Small diameter
                                                wires).
(c) A simple twisting apparatus, with no load measuring
     facility, with a counter for number of twists to fracture.

The horizontal machine consisted of a fixed jaw, which clamped
one end of the test specimen, and a moving jaw which clamped the
other end. The distance between the jaws could be adjusted to
give any required gauge length, normally a multiple of wire
diameter. The moving jaw was connected by a series of gears to
a dial showing the angle, in degrees, through which the specimen
was twisted, and load was applied by a pendulum, attached to the
fixed jaw, increasing displacement of the pendulum from the
vertical increasing the load applied. The load applied was in-
dicated on a dial gauge. Readings of load and angle of twist
were taken at regular intervals.

The vertical machine consisted of a torsion bar clamped at one
end to prevent any movement. The other end was held in a chuck
mounted on the upper face of a horizontal disc. The specimen
was clamped between a chuck mounted on the lower face of the disc,
and a second chuck connected to the twisting mechanism. The disc
holding the upper end of the specimen, and lower end of the torsion
bar was graduated around the rim , and a ring surrounding the disc

was graduated on its inner diameter in radians. The whole system was allowed to "float" from the suspension point of the upper end of the torsion bar. A tensile load, which was a small fraction of the tensile yield stress, was applied to maintain the specimen taut.

As the specimen was twisted the angle through which the torsion bar twisted measured the load applied, and the angle through which the specimen was twisted was measured separately. Readings of load and angle of twist were recorded at regular intervals. The maximum torque, and number of twists to fracture was recorded.

4.4 METALLOGRAPHY

4.4.I. SPECIMEN PREPARATION

Samples of rod in the heat treated condition, and wire after each reduction were prepared for examination. Samples were cut parallel and perpendicular to the wire axis for all conditions. The specimens were mounted in thermosetting plastic, using a laboratory press, at temperatures not exceeding I50^{o}C. The heating period was kept to a minimum throughout.

Initial grinding of the specimens was carried out on a Knuth-Rotor machine and I80μm grit silicon carbide paper with continuous water flow to remove grinding debris. The specimens were then hand ground on 280μm, 400μm and 600μm grit silicon carbide paper with continuous water flow, rotating the specimen through 90° at each change of grit particle size. Polishing was carried out on diamond impregnated pads, with particle sizes

of 12μ, 6μ, 1μ, and 0.5μ, using paraffin to remove polishing

debris. A final polish was obtained with medium grade alumina
of 12μ, 6μ, 1μ, and 0.5μ, using paraffin to remove polishing
suspension in water and heavy cloth.

The microstructure was revealed by etching with 2% Nitric Acid

in Alcohol for pure iron samples, and 5% Picric Acid in Alcohol

for steel samples. Finally the specimens were rinsed in alcohol

and dried in warm air.

4.4.2. OPTICAL MICROSCOPY

The specimens were examined on a Reichert Zetopan bench micro-

scope, with a range of magnification from 56 to 1760 diameters.

Photography and quantitative measurements were carried out on a

Vickers Projection Microscope at magnifications ranging from

200 to 2000 diameters. A stage micrometer was used to set the

magnification used for quantitative measurements.

Grain size measurements were made on the pure iron samples and

the 0.18% Carbon Steel with coarse carbide. Due to the grain

distortion resulting from wiredrawing the measurements were

made on specimens cut perpendicular to the wire axis. The

specimens were examined at a magnification suited to the grain

size, and the number of intercepts made on two mutually per-

pendicular lines, each 10 cm long, counted. A minimum of five

separate areas, selected at random, were examined for each

specimen. The results were then converted to grain boundary

spacing, D, using the formula:-

$$D = \frac{1}{N_L} \qquad \text{Equation 4.1.}$$

where N_L = number of intercepts/unit line length

Specimens were examined for evidence of non uniform grain deformation on the specimen cut parallel to the wire axis. Individual grains were measured parallel and perpendicular to the wire axis at edge and centre of the specimen. The ratio of the length to the diameter of grains at the surface and centre of the specimen and the Geometric Mean of these results was calculated.

4.4.3. ELECTRON MICROSCOPY

An A.E.I. EM6G electron microscope was used, with replica techniques only. After final polishing the specimens were etched electrolytically in Chromic Acid solution, rinsed with water and alcohol, and dried in a stream of hot air. The etched specimen was placed under the bell of an "Edwards" vacuum coating unit, in such a position relative to the carbon electrodes that self shadowing of the replica would be minimised, and the unit evacuated to low pressure. A carbon film was deposited on the etched surface of the specimen by evaporation of carbon from two carbon rods in contact which were resistance heated. The period required for coating was 1-2 seconds. Air was then allowed into the bell jar and the specimen removed. A rectangular grid was inscribed on the specimen with a scalpel. The coated specimen was then placed in a solution of oxalic acid and a platform wire electrode immersed adjacent to the specimen. The anode wire was then touched on the specimen, when gas evolution lifted the replica from the surface. The fragments

of carbon film were transferred to a cleaning solution of 2% Nitric Acid in Alcohol for 20 minutes before catching on a copper grid, rinsed in water, and dried.

Photographs of the structure of heat treated, and drawn samples, were taken at 10,000 diameters magnification, and enlarged to 20,000 diameters magnification. The interparticle spacing of the fine carbide dispersion in 0.18% Carbon steel was determined by linear intercept. Lines 10cm long were drawn on these photographs, and the number of particles intersected by the line counted. Then according to Fullman [54]

$$P = \frac{1 - f}{N_L} \qquad \text{Equation 4.2.}$$

where

N_L = number of particles intercepted / unit line length

f = volume fraction of carbide

P = interparticle spacing

(See Appendix II for determination of f)

The pearlite structure of the Lead patented 0.44% Carbon steel was characterised by the interlamellar spacing of the pearlite. According to Payne and Smith [55], the mean lamellar spacing of pearlite in a steel is given by:-

$$S_O = 1.65\, S_{min} \qquad \text{Equation 4.3.}$$

where S_O = mean spacing

S_{min} = minimum observed spacing

The replicas were examined at a magnification of 20,000 diameters and the spacing of the finest observed areas measured.

4.5 ORIENTATION DETERMINATION

4.5.1. SPECIMEN PREPARATION

A number of specimens were cut, perpendicular to the wire axis, and mounted in cold setting resin, with minimum distance between specimens (Fig.7). The total area of specimen in each mount was approximately 5 cm². Wires greater than 1 mm diameter were sectioned individually. Smaller wires were tightly bound in bundles, approximately 6 cm long, using fine stainless steel wire binding. The bundles were cut between bindings, and mounted in cold setting resin.

The samples were ground on wet silicon carbide paper until the mount thickness did not exceed 6 mm, and then ground and polished as described for metallographic mounts in Section 4.4.1. Two methods of texture determination were employed:-

> (a)   Inverse Pole figures
>
> (b)   Full spiral pole figures

4.5.2. INVERSE POLE FIGURE METHOD

A Phillips Diffractometer (Fig.8) was used to determine the peak intensity of $\{110\}\{200\}$, $\{211\}$, $\{220\}$, $\{310\}$, $\{222\}$ and $\{321\}$ reflections. This data was then normalised as suggested by Mueller, Chernock and Beck[56] i.e.

$$ P_{hkl} = \frac{I_{hkl}/I_{ohkl}}{\sum\limits_{n} \frac{I_{hkl}}{I_{ohkl}}} \qquad \text{Equation 4.4.} $$

where I_{ohkl} is the integrated intensity of the hkl reflection

in a deformed specimen.

4.5.3. 110 POLE FIGURES

Since, as stated in Section 3.3. the wire was expected to show a
110 parallel to the wire axis, full spiral pole figures were
determined for the 110 planes, which would be expected to appear
at 0, 60° and 90° to the wire axis. [57]
The Schultz reflection method was employed to show the 110 intensities.
This method is only accurate for up to 70° from the wire axis, hence
reflections at 0° and 60° would be anticipated with a perfect wire
texture.

A Siemens Texture Diffractometer, Fig.9, was employed for this work.
In the Schultz method the specimen undergoes two step-wise rotations
simultaneously, one about the wire axis, and the other perpendicular
to the wire axis.   The intensity of the diffracted radiation was
monitored continuously with a proportional counter, and recorded on a
chart to show the variation in diffracted intensity with specimen
rotation Fig.10. Since the rotation of the specimen was calibrated with
chart speed the intensity contours from the texture diffractometer trace
were readily plotted on spiral pole figure charts.

5.1 THE MECHANICAL PROPERTIES OF DRAWN WIRES

5.1.1. THE STRENGTH OF DRAWN WIRES

The strength at maximum load in the tensile test is hown as a function of wiredrawing strain in Fig.II. The 0.2% Proof stress in tension is shown as a function of wiredrawing strain in Fig.I2. The strength of drawn wires produced from 0.1U% Carbon steel annealed at $650^{O}C$, and quenched and tempered was also determined in torsion i.e. the Maximum Shear Stress, as shown in Fig.13 as a function of wiredrawing strain.

The tensile strength and 0.2% Proof Stress, as functions of wire-drawing strain ($\log_e$ Ao/A = 2 $\log_e$ Do/D) had certain features in common:-

a) a rapid increase in strength, which appeared to follow a power law of descending order.

b) a secondary increase in strength, which appeared to follow a power law of ascending order.

The results for the quenched and tempered wires differed from all other structures in that only the secondary hardening stage was observed. The maximum shear stress results in Fig.13 do not show these effects as clearly as the tensile properties, although similarities can be seen.

5.1.2. THE DUCTILITY OF DRAWN WIRES

The fractional reduction of area at fracture in the tension test

was converted to a true strain at fracture from the formula

$$E_f = \ln \frac{D_o^2}{D_f^2} = \ln \left(\frac{1}{1-R} \right) \qquad \text{Equation 5.1}$$

where
D_o = Initial diameter of test piece

D_f = Final diameter of test piece at the fracture
point.

R = Fractional reduction of area.

The results obtained using this conversion are shown as a function of wiredrawing strain in Fig.14.

The number of twists to fracture in the torsion test is a standard measure of ductility frequently used for drawn steel wires. This value was converted to a shear strain from the formula:

$$= \frac{N \pi D}{L} \qquad \text{Equation 5.2}$$

where
N = Number of twists to fracture

D = Test piece diameter

L = Test piece gauge length

The shear strain at fracture is shown as a function of wire-drawing strain in Fig.15.

The tensile ductility of the as heat treated specimens decreased with increasing carbon content. The effect of wiredrawing on tensile ductility was variable during the early stages, generally indicating a slight decrease. Further deformation resulted in slight recovery of ductility, followed by a rapid decrease as the

limit of drawability is approached. These features are clearly
evident in Fig.14.

The shear strain at fracture increased with initial deformation
for pure iron, and 0.18% Carbon steels. The extent of this initial
increase in ductility decreased with decreasing grain size or
particle spacing. Increasing levels of wiredrawing reduction
resulted in a rapid decrease in shear strain at fracture. The
level of deformation required to initiate this rapid decrease
increased with increasing grain size or particle spacing. The
0.44% Carbon steel, lead patented, onoy exhibited this second
stage decrease in shear strain, but the rate of decrease was less
than the other materials. The shear strain for all materials finally
entered a "common band" which demonstrated a slight recovery, or
increase in shear strain. This complex behaviour is shown in
Fig.15.

5.2 THE METALLOGRAPHY OF DRAWN WIRES

5.2.1. PURE IRON

The structures produced by annealing pure iron at 800°C, 850°C,
and 900°C are shown in Figs.16-18. The grain diameter of the
equiaxed ferrite increased with increasing annealing temperature.

The effect of wiredrawing on the structure was immediately obvious
on specimens cut parallel to the wire axis, although less so on
the specimens cut parallel to the wire axis. Grain boundary
coarsening was visible after 0.17 strain. Figs.19-22 show the
effect of increasing deformation.

The determination of grain boundary intercept distance was made increasingly difficult by grain boundary coarsening. Specimens cut parallel to the wire axis were used to measure grain elongation. The ratio of mean intercept distance parallel and perpendicular to the wire axis was determined at the surface and centre of the wire. The results, presented as a function of wiredrawing strain are shown in Fig.23.

The mean grain boundary intercept distance was determined on specimens cut perpendicular to the wire axis, until grain boundary coarsening made further measurements impractical. The results obtained were plotted as function of wiredrawing strain in Fig.24.

5.2.2. 0.18% CARBON STEEL

The initial structure of the 0.18% Carbon Steel, annealed at 650°C is shown in Fig.25. The structure consisted of fine equiaxed ferrite grains, with spheroidal carbides, principally forming a grain boundary network. The effect of deformation on this structure was similar to that described in Section.5.2.I. for pure iron, with the exception of the initial finer grain size. The mean grain boundary intercept distance was determined on specimens cut perpendicular to the wire axis. The results are shown as a function of wiredrawing strain in Fig.24.

The hot rolled 0.18% Carbon Steel, with the initial structure shown in Fig.26 consisted of fine equiaxed

ferrite grains, plus some pearlite colonies at interactions in the ferrite grain boundaries. The effect of wiredrawing on this structure was to elongate the ferite grains, and the pearlite colonies, until the latter gradually broke up. Elongation of the pearlite colonies after 2.3 strain is shown in Fig.27. Break up of the pearlite lamellea is evidenced in Figs.28 and 29, after 3.2 and 3.9 strain respectively, by angular particles of carbide in a fibrous structure of ferrite.

The initial structure produced by quenching and tempering the 0.18% carbon steel is shown in Fig.30. The carbides appear to be in two forms, rod shaped particles along crystallite boundaries and spheroids. This suggests that carbides are basically rod shaped, the plane of sectioning causing the apparent variation from spheroids to rods. The effect of wiredrawing on this structure is not immediately obvious, but after 1.1 strain the break up of rods is apparent, as shown in Fig.31. The continued break up of rod shaped particles to form spheroids is shown in Fig. 32 to 34.

The mean free ferrite path length through the carbide particles was determined, and plotted as a function of wiredrawing strain as shown in Fig.35.

5.2.3. 0.44% CARBON STEEL

The lead patented structure is shown in Fig.26. The structure consists of a semi continuous ferrite network with colonies of

fine pearlite. Some Widmannstatten ferrite was observed.

The early stages of wiredrawing did not appear to affect the structure, but examination at 1800 x magnification revealed slip lines in the pearlite after 0.13 strain. This is clearly illustrated in Fig.37. This structure was examined in greater detail by electron microscope the form of the slip in pearlite being shown in Figs.38-41. Continuing deformation appears to result in rotation of lamellae to lie parallel with the wire axis, and break up of unfavourably oriented lamellae. The rotation of lamellae was substantially complete by 2.5 strain. Further deformation resulted in an increasingly fibrous structure. Favourably oriented lamellae still appeared to retain their form, but unfavourably oriented lamellae were destroyed.

The spacing of the pearlite lamellae was determined on the electron microscope, and is shown as a function of wiredrawing strain in Fig.42.

The initial structure obtained by quenching and tempering the 0.44% Carbon steel is shown in Fig.43. This structure, and the effect of wiredrawing upon it, is similar in all respects to that of the 0.18% Carbon steel after quenching and tempering, as described in Section 5.2.2.

5.3. THE ORIENTATION OF DRAWN WIRES

5.3.1. INVERSE POLE FIGURES

The texture coefficients of the (002); (112);(022);(013);

(222); and (123) reflections from steel wires with increasing wiredrawing strain are shown in Fig.44 as a function of wiredrawing strain. The (022) plane reflection shows increasing intensity, while all the other reflections tend to decrease.

5.3.2. SPIRAL POLE FIGURES

Figs.45-47 show spiral pole figures from 0°-70° for the $\{110\}$ planes of 0.18% Carbon steel quenched and tempered, and annealed at 650^oC, and pure iron annealed at 850^oC, at varying stages of reduction. These show increasing intensities of of the poles at 0°, and 60° to the wire axis. The ratio of the intensity of the pole at 0° to the intensity of the poles at 60°, i.e. $Io^o{}_{/}I_{60^o}$ was calculated, and is shown as a function of the $\{110\}$ pole $^{60^o}$ for the plane parallel to the wire axis.

5.4. WIREDRAWING LOAD

Load measurements, for differing drawing speeds on the Instron machine, were made for each die used in drawing the 0.44% Carbon Steel quenched and tempered before drawing. The actual load, as load per projected area of the reduction was plotted as a function of Mean Strain Rate//tanα, where α is the half angle of the wiredrawing die, as shown in Fig. 49. Referring to Fig. 49 curves 2-5 increase to a peak value, and then devrease slightly, while curve No. 2 increases to a peak and then decreases to a steady state. There is a suggestion that increased values of Mean Strain Rate/Tan may result in a decrease to steady state for curves 2-5.

CHAPTER 6. DISCUSSION OF RESULTS

6.1 SELECTION OF PARAMETERS

6.1.1. STRENGTH PARAMETERS

The strength of metals may be represented by any, or all, of several parameters. The following were determined for materials used in this work:-

(a) Limit of Proportionality (Elastic Limit) in tension and torsion.

(b) 0.01% Proof Stress in tension and torsion.

(c) 0.1% Proof Stress in tension and torsion.

(d) 0.2% Proof Stress in tension and torsion.

(e) The Ultimate Tensile strength.

(f) The Maximum Shear Strength.

The tensile test data was available for all materials used, while torsion test results were limited to 0.18% Carbon steels.

Much of the published data on the mechanical properties of drawn wires is confined to the Ultimate Tensile strength σ_u. Two groups of authors, Embury and Fisher[43], and Hirano et.al.[58] published data for the 0.2% Proof Stress in tension σ_f in addition to the Ultimate Tensile Strength. The choice of strength parameter was severely limited by this fact. Comparison of experimental with published data was impossible, unless the Ultimate Tensile Strength σ_u, or 0.2% Proof Stress in tension σ_f, was used. The data available for comparison was limited if the latter was chosen.

Duckfield[59] states that, for cold drawn carbon steel:-

$$\sigma_f = K \, \sigma_u \qquad \text{where } K \simeq 0.85$$

This implies that the variation in carbon content and strain has no effect on the relationship between 0.2% Proof Stress, and ultimate Tensile Strength i.e. does not affect the shape of the tensile test curve. Intuitively this does not appear to be correct. It may well be that, when the carbon content approaches the eutectoid value the ratio of 0.2% Proof Stress to Ultimate Tensile Strength approaches a

constant value, but it appears unlikely that this would be the
case over the full range of carbon steels, and structures employed
in wiredrawing.   Nevertheless this point was checked for the
materials used in this work, and for carbon steels up to 0.93%
carbon steel from various sources 43,58.   The actual values of
the ratio 0.2% Proof Stress:Ultimate Tensile Strength obtained
for iron and steel wires are tabulated below:-

Material	Heat Treatment	σ_f/σ_u as Heat Treated	σ_f/σ_u For cold drawn wires Mean Value	Range in Values
Pure Iron	Annealed	0.679	0.984	0.944-1
0.18%C Steel	Annealed	0.619	0.913	0.831-0.791
0.18%C Steel	As hot rolled	0.623	0.844	0.810-0.959
0.44%C Steel	As hot rolled[58]	0.611	0.871	0.784-0.944
0.44%C Steel	Air patented [58]	0.605	0.880	0.857-0.907
0.44%C Steel	Lead patented	0.605	0.787	0.747-0.829
0.69%C Steel	As hot rolled[58]	0.493	0.844	0.802-0.880
0.69%C Steel	Lead Patented[58]	0.563	0.850	0.758-0.878
0.8%C Steel	As hot rolled[58]	0.471	0.841	0.801-0.887
0.8%C Steel	Lead patented[58]	0.625	0.863	0.814-0.935
0.93%C Steel	Lead patented	0.782	0.952	0.907-0.983

The effect of cold drawing on   is obviously very marked. The as hea
treated values of   appear to depend on carbon content with the
difference in heat treatment having a marked effect at 0.69% and
0.8% carbon, probably due to the interlamellar spacing of the pearlite
It is noticeable that the mean value of σ_f/σ_u appears fairly constant
for the Hirano[58] results on cold drawn wires, independent of carbon
content and heat treatment, but that the range in σ_f/σ_u values varies
from 0.05 to 0.16.   The tabulated values for σ_f/σ_u suggest that the
ratio σ_f/σ_u decreases with increasing carbon content to a plateau
at 0.69%-0.8% carbon content, but then increases i.e. the mean value
of σ_f/σ_u for drawn steels as a function of carbon content will be an
inverted parabolic.   The range in values of σ_f/σ_u for drawn steels
suggest that the constant value for σ_f/σ_u suggested by Duckfield[59]
should be treated with caution.

The variation in the ratio σ_f/σ_u is probably due to the effect of

a second phase on the work hardening rate during the tensile test. Pure iron, or annealed low carbon steels have a structure consisting almost completely of equiaxed ferrite grains. This structure has a very low rate of work hardening, linked with very high ductility, hence σ_f/σ_u is high. The introduction of a second phase reduces ductility, and increases work hardening rate until a fairly constant value of σ_f/σ_u is reached, in the region of 0.8-0.9. Further increase in the Carbon content decreases ductility still further until the 0.2% Proof Stress begins to approach the Ultimate Tensile Strength. Finally the ductility falls to the point where the tensile test does not reach 0.2% strain.

The materials used in this work included a wide range of carbon contents, and, therefore, a wide range of ductility and work hardening rates in the tensile test. The values of Ultimate Tensile Strength obtained were subject to variation resulting from this e.g. the tensile strain to fracture of pure iron was far in excess of that for 0.44% Carbon steel. The Ultimate Tensile Strength was, therefore, rejected as unsuitable for use as a strength parameter. Proof Stress data has the advantage of being a value obtained at a constant level of test deformation, but is subject to inaccuracies in plotting the elastic portion of the test. These inaccuracies are greatest in the Limit of Proportionality, and least in the 0.2% Proof Stress, due to the gradient of the tensile test curve at the particular sections considered i.e. a high gradient at the limit of proportionality, and a low gradient at the 0.2% Proof Stress. Some published data was available for the 0.2% Proof Stress and this was therefore chosen as the strength parameter for all future discussion, unless otherwise specified.

6.1.2. DUCTILITY PARAMETERS

The ductility of a metal may be represented by any, or all of several parameters. Some conventional measures used for wire specimens may be listed as follows:-

1. % Reduction of Area at Fracture in the tensile test

2. % Elongation after fracture in the tensile test

3. Number of twists to fracture in torsion

4. Number of reverse bends to fracture

Each of these measures has certain disadvantages for experimental work in the conventional form. The % Reduction of Area to fracture is difficult to measure accurately when the form of fracture is less than the ideal cup and cone type. Basic work requires a true strain measure, however, and % Reduction of Area is readily converted from Equation 5:1.

The % Elongation in the tensile test is actually a combination of several factors. Since the ends of the specimen are gripped the plastic deformation theoretically commences at each grip, and increases until the fracture point, at the centre of the test length. Practically variations occur from this state, but the tensile elongation can be seen to be the sum of the elongations occuring over each section of length. Thus the test length will affect the elongation. The % Elongation may be simplified to consist of two elements, local and uniform elongation. These may be calculated but the results are subject to variation resulting from the specimen test length. This measure of ductility was therefore not included in the test results, since, while every effort to maintain constant specimen length was made, specimens of varying lengths had to be used in some cases.

The number of twists to fracture is possibly the most fundamental measure of ductility employed in wire testing. The test is normally made on a specimen with the gauge length set to a constant multiple of the wire diameter. This is readily converted to shear strain using Equation 5:2. The shear strain is a direct measure of the capacity of the material to undergo further cold work, since only the resolved shear stress actually deforms the metal either in work or test. Hence the shear strain is an extremely important parameter in studying the workability of metals.

The reverse bend test is an engineering test, and can give a good indication of formability. The stress system is complex however, and the results are not readily convertable to true strain values. This test has not been considered.

The discussion of ductility parameters given above indicates the reasons for the choice of parameters used to measure ductility. The basic requirements of the ductility parameter were:-

(a)   It should be readily converted to a true strain value

(b)   It should be a recognisable form of conventional test

(c)   It should be insensitive to test conditions, or

(d)   It should be possible to minimise the effect of test conditions.

(e)   Specimen end effects should be minimised, or absent.

The selected parameters, reduction of area in the tensile test converted to a true strain, and the maximum shear strain were selected, as best meeting the above requirements. The first, true strain at the fracture point in the tensile test, only considered plastic deformation, while shear strain included elastic and plastic deformation.

6.2 THE STRUCTURE OF DRAWN WIRES

The metallographic structure of drawn wires is a variable, dependent on the chemical composition and heat treatment of the original rod, and the deformation to which the wire has been subjected. The orientation of the structure is independent of these factors in so far as hypoeutectoid carbon steel wires as concerned. The effect of deformation on the metallography of wires is discussed in the following sections from the viewpoint of the ferrite matrix (pure iron) the introduction of a second phase, iron carbide or cementite, and the morphology of that phase. The orientation of the wires is restricted to the ferrite matrix.

6.2.1. THE ORIENTATION OF DRAWN WIRES

The wire texture [110] parallel to the wire axis in body centred cubic metals has been reported frequently [52,57] and the results obtained in this work, shown as a function of strain in Fig.44 confirmed the increasing (110) Plane intensity parallel to the wire axis. The angles between {110} planes in a cubic cell are 0, 60° and 90°, and since, by definition, the angle between a crystallographic plane and direction having the same indices is 90° the angle between {110} planes and ⟨110⟩ directions is 0, 60° and 90°. A (110) pole figure would, therefore, be expected to show poles at 0° and 60° to the wire axis. The (110) pole figures for pure iron, and 0.18% Carbon steels show this clearly in Figs.45-47.

At this stage the work has confirmed the results reported previously. A method of quantifying the degree of orientation present is now required. The texture coefficients from inverse pole figures,

normalised as suggested by Mueller et al [56] showed a power type of relationship with strain, i.e.

$$P_{hkl} = a\varepsilon^{\pm n}$$

where a and n are constants. The constant appeared to be positive for the (110) plane, and negative for (200); (211); (310); (222); (321) planes. Some variation was noted in the results. The techniques employed required a fairly constant area of wire in cross section in the mount. As the wire diameter decreased as increasing number of wires were in each mount, and the difficulties of ensuring true axis vertical wires increased. Therefore the scatter in data shown is considered to be due to the slight variation in the angle between the axis and reflecting face of the specimens.

The specimens employed in pole figures determination were of the same form, and therefore suffered from the same problems. The area of specimen was maintained constant from specimen to specimen to retain relativity of reflected intensity. The slight variation of axiality resulted in some lack of definition, particularly for the pole at 60° to the wire axis.

The ratio of intensity for the poles at 0 and 60° to the wire axis, plotted as a function of strain in Fig.48 showed marked similarity with the texture coefficient of the (110) plane in Fig.44, i.e.

$$I_0/I_{60} = a\varepsilon^{n}$$

Certain points (1.97 and 2.60 strain in pure iron, and 1.13 and 1.97 strain in annealed 0.18% Carbon steel) appeared to diverge from this pattern, but this was considered to be a result of errors in mounting

as explained above.

The texture coefficient and I_0/I_{60} ratios of the as heat treated materials were not coincident, and the data was therefore transformed to pass through the origin i.e.

$$P' = P^{\bullet}_{(hkl)} - P^{o}_{(hkl)}$$

and $$P' = \left(I_0/I_{60}\right)^{\bullet} - \left(I_0/I_{60}\right)^{o}$$

where P' is the transformed data,

$$P^{\bullet}, \left(I_0/I_{60}\right)' \quad \text{refers to deformed material}$$

$$P^{o}, \left(I_0/I_{60}\right)^{o} \quad \text{refers to as heat treated rod}$$

The graph of P' as a function of strain then passes through the origin. Examination of this data suggested that the relationship should be linear with $\mathcal{E}^{\frac{1}{2}}$, and this is shown in Fig.50. The relationship being clearly linear, a regression of P' an $\mathcal{E}^{\frac{1}{2}}$ was made, omitting the points referred to above, giving the line shown in Fig.50. The regression equation:-

$$P' = 1.123 \, \mathcal{E}^{\frac{1}{2}} - 0.19 \qquad \text{Equation 6:1}$$

explained 96.5% of the variation in P'. The constant (-0.19) gives an indication of the degree of experimental error. It should be realised that this equation is derived from two methods of quantitatively assessing the texture of drawn wires.

6.2.2. THE STRUCTURE OF DEFORMED FERRITE

Consider the structure of pure iron, in the annealed condition i.e. equi-axed ferrite. The let:-

l = the grain dimension parallel to the rod axis

d = the grain dimension perpendicular to the rod axis

By definition, in equi-axed ferrite the ratio l/d is unity. Extending the concept to drawn structures, indicated by a suffix after the letter, i.e. l_1 and d_1 respectively, from constancy of volume

$$l_1 \, d_1 = ld$$

for an ideal grain. The grain boundary should function as in in-scribed grid and, provided the initial grain dimension is known, a grid of known dimensions. Since grain size will not be constant, but a distribution about a mean value, affected by the plane of sectioning, the data may be best considered in the form of a ratio i.e. $\frac{l}{d}$. This ratio should be a function of strain, and independent of grain size.

For drawn wire if

l_1 = initial length of rod

l_2 = final length of wire

d_1 = initial rod diameter

d_2 = final rod diameter

True (natural) strain $= \log_e \dfrac{l_2}{l_1} = \log_e \dfrac{d_1^2}{d_2^2} = 2 \log_e \dfrac{d_1}{d_2}$

The same symbols l_1 ; l_2 ; d_1 ; d_2 may be taken as referring to an ideal grain, for which

$$\frac{l_1}{d_1} = 1 \qquad\qquad \frac{l_2}{d_2} = R$$

Then, from constancy of volume in the wire

$$l_1 \, d_1^2 = l_2 \, d_2^2$$

$$l_2 = \frac{l_1 \, d_1^2}{d_2^2}$$

$$d_2 = \left(\frac{d_1^2 \, l_1}{l_2}\right)^{\frac{1}{2}} = \frac{d_1 \, l_1^{\frac{1}{2}}}{l_2^{\frac{1}{2}}}$$

$$\frac{l_2}{d_2} = \frac{l_1 \, d_1^2}{d_2^2} \quad \frac{l_2^{\frac{1}{2}}}{d_1 \, l_1^{\frac{1}{2}}}$$

but

$$\frac{l_1}{d_1} = 1$$

Therefore

$$\frac{l_2}{d_2} = \frac{d_1^2 \, l_2^{\frac{1}{2}}}{d_2^2 \, l_1^{\frac{1}{2}}} = R$$

Since

$$\mathcal{E} = \log_e \frac{d_1^2}{d_2^2} = \log_e \frac{l_2}{l_1}$$

$$R = e^{\,3/2\,\mathcal{E}} \hspace{3cm} \text{Equation 6:2}$$

Equation 6:2 should predict the relationship between the ideal l/d ratio R, and strain. However Fig.23 shows that the ideal relationship does not hold after two deformations i.e.0.3 strain, and,moreover, that that rate of divergence from ideal is less for grains close to the surface than it is for grains at the centre of the wire. The divergence in all grains is negative,i.e. the measured value of R is less than that predicted. This divergence results from the fact that the wiredrawing deformation id at a maximum at the wire surface. These results indicate that measurement of R values can give a valuable indication of the deformation present in cold drawn material, but the estimated value will be low, affected by the position of the grain relative to the axis,and the error will increase with increasing deformation.

Measurement of the length, and perpendicular height of deformed ferrite

grains become increasingly difficult in specimens cut parallel to the wire axis, due to grain boundary coarsening and the difficulty of ensuring the plane of section. Specimens cut perpendicular to the wire axis should not suffer from the latter defect, but can only be used to determine the grain dimension perpendicular to the wire axis. Practically, due to the form of grain boundary deformation resulting from wiredrawing, grain boundary coarsening, and the presence of slip lines, measurement of grain boundary spacing rapidly became inaccurate at deformations in excess of 2.0 strain. An equation predicting the value of the grain boundary spacing may be derived from Equation 6:2 as follows:-

Let d_o , l_o be the grain dimensions perpendicular and parallel to the wire axis before deformation and d_x , l_x be the grain dimensions perpendicular and parallel to the wire axis after $_x$ strain.

$$\frac{1}{6} \; \pi \; l_o \, d_o^2 = \text{grain volume} = \frac{1}{6} \, d_o^3 \pi$$

$$\frac{l_x}{d_x} = 1^{1.5 \varepsilon x}$$

$$\therefore \quad d = e^{-1.5 \varepsilon x} l_x$$

$$\frac{1}{6} \, \pi \, l_x d_x^2 = \frac{1}{6} \, \pi \, d_o^3$$

$$\therefore \quad l_x = \frac{d_o^3}{d_x^2}$$

$$\text{i.e.} \quad d_x = \frac{d_o^3}{d_x^2} \, e^{-1.5 \varepsilon x}$$

$$\therefore \quad d_x = d_o e^{-0.5 \varepsilon x}$$

$$\text{i.e.} \quad d = d_o e^{-0.5 \varepsilon} \qquad \qquad \text{Equation 6:3}$$

Hence a graph of log d as a function of strain should be linear. This is shown in Fig.51 for pure irons, and 0.18% Carbon steel annealed at 650°C. A regression of log d on strain gave the

following equations:-

1. PURE IRON

Annealed at 900°C $\qquad$ $d = 55.76\,e^{-1.0166\varepsilon}$ $\quad$ ($d_0 = 82.90 \times 10^{-4}$ cm)

Annealed at 850°C $\qquad$ $d = 41.30\,e^{-1.0029\varepsilon}$ $\quad$ ($d_0 = 46.40 \times 10^{-4}$ cm)

Annealed at 800°C $\qquad$ $d = 19.97\,e^{-0.7288\varepsilon}$ $\quad$ ($d_0 = 24.40 \times 10^{-4}$ cm)

2. 0.18% CARBON STEEL

Annealed at 650°C $\qquad$ $d = 11.40\,e^{-0.9351\varepsilon}$ $\quad$ ($d_0 = 17.73 \times 10^{-4}$ cm)

These equations drawn in Fig.51 show clearly that equation 6:3 predicts the form of relationship between grain boundary spacing i.e. an exponential relationship, but the values of the constants do not match. The gradient of the equation is greater than predicted, as was suggested by the "kinking" of the grain boundaries, and the presence of slip lines which were difficult to distinguish from grain boundaries. Thus the regression equations show the actual rate of increase in barriers visible on the light microscope, while Equation 6:3 predicts the reduction on grain spacing due to strain, assuming that no new boundaries are created.

6.2.3. THE STRUCTURE OF DEFORMED FERRITE PLUS PARTICULATE CARBIDES

The 0.18% Carbon Steel annealed at 650°C, Quenched and Tempered before drawing, and the 0.44% Carbon steel quenched and tempered before drawing comprise this group of structures. Effectively, due to the low carbide content, and large(relatively) particle size the 0.18% Carbon steel annealed at 650°C has been discussed in the preceding section on drawn ferrites.

The structure of the quenched and tempered steels, before drawing,

consited of rod or plate type carbide particles at boundaries, and
spheroidal particles in a random pattern. Some indication of needle
shaped particles was observed in the 0.44% carbon steel. The particles
shaped changed considerably during deformation. Rod or plate carbides
were absent after 1.14 strain on the 0.18% carbon steel, being
replaced by spheroidal particles. Two possible mechanisms may be
considered, to explain the change in morphology. The fracture and
shear of lamellar carbides is established in the literature[34,43].
It seems possible that fracture of rod and plate carbides could
result from deformation. However, the particles observed did not
show any indication of angularity. The rate of decrease in mean free
ferrite path length, shown as a function of wiredrawing strain $\mathcal{E}_{wD} = \mathcal{E}log_{\epsilon}\frac{P_o}{P_{\epsilon}}$ in Fig.35 suggests that an equation similar to Equation 6.3 may
apply i.e.

$$P_{\epsilon} = P_o \, e^{-0.5\mathcal{E}} \qquad\qquad \text{Equation 6.4}$$

A regression of logarithm mean free ferrite path length on wire-
drawing strain for the data in Fig.35 indicated a linear relationship:

$$\bar{P_{\epsilon}} = 2483^{-0.37\mathcal{E}}$$

where $\bar{P_{\epsilon}}$ = Mean free ferrite path length, in Angstroms.

The experimental value of $\bar{P_o}$ was 3461Å, considerably greater than
the value of 2483Å in the above regression equation. The minimum v
value of P_o from any line was 2559Å. The experimental values of the
mean free ferrite path length in Angstroms as a function of wire-
drawing strain is plotted on logarithmic/linear areas in Fig.25,
with the regression line drawn in. The line of equation 6:4, based
on the measuree value of   is also shown. Statistically the data
give the best fit to the regression equation, but the fit with
equation 6:4 is sufficiently good to suggest that this equation
does predict the rate of decrease in mean free ferrite path length.

The fracture of lamellar carbides as a result of wiredrawing is fully reported[34,43] and examination of drawn structures of the 0.44% Carbon steel lead patented before drawing showed confirmatory evidence after 0.15 strain. The 0.18% Carbon steel as rolled clearly contains fragmented carbides in the later stages of deformation. Apparent rotation of carbide lamellae, with a favourable orientation, to lie parallel to the wire axis was observed, but fracture of such lamellae was observed.

The 0.18% Carbon steel as rolled was omitted from the quantitative metallography, since the structure varied from polygonal ferrite to pearlite colonies which, in terms of barrier spacing, were small, dense areas. However the 0.44% Carbon steel lead patented before drawing consisted principally of pearlite.

Payne and Smith[55] gave an equation for conversion of the minimum observed learlite spacing to the mean pearlite spacing:-

$$S_o = 1.65 \, S_{min} \qquad \text{Equation 4:3}$$

This expression is strictly valid only for a structure in which the carbide lamellae were in random orientation with respect to the plane of section, which would not necessarily be the ease for drawn wires. Therefore the minimum observed pearlite spacing was used inccalculations on drawn wires.

The minimum pearlite spacing of wires is shown as a function of pearlite spacing in Fig. 42. This suggests that an equation similar to Equation 6:3 and Equation 6:4 may apply i.e.

$$S_\epsilon = S_o e^{-05\epsilon} \qquad \text{Equation 6:5}$$

The data shown in Fig.42 are re-plotted in Fig.53 on

logarithmic/linar axes. A regression of log S_ε on
wiredrawing strain was calculated, giving the following
equation

$$S_\varepsilon = 1238\varepsilon^{-0.42\varepsilon}$$

where   = Minimum lamellar spacing in Angstroms.

This regression line, together with the line calculated from
Equation 6:5 is shown on Fig.53. The value of the regression
constant, 1238, was very close to the value of   determined
experimentally, i.e. 1250 Angstoms and deviation of experimen
tally determined values of   from Equation 6:5 is slight.

The reduction in pearlite spacing resulting from cold working
is well known, and has often been reported e.g. by Embury and
Fisher[43]. This implies that the ferrite may slip out from
between the carbide lamellae, implying that the latter are
rigid, and remain whole during the complete deformation
process. The fracture of carbide lamellae during deformation
was observed after 0.15 strain in this work, and other mechanisms
such as thinning and kinking of carbide lamellae have been
reported[45,60]. The microstructure of heavily deformed 0.18%
carbon steel (Fig.29) shows the complete breakdown of the
pearlitic structure. Flow of ferrite to fill voids resulting
from fracture of the carbide lamellae is considered far more
probable than flow of ferrite out from between lamellae. The
latter type of flow may occur but would probably be restricted
to areas at the end of lamellae.

6.3 THE STRENGTH OF DRAWN WIRES

6.3.1. THE STRENGTH BEFORE DEFORMATION

The as heat treated materials would be divided into two basic groups
typified by structure:-

(a) Ferritic structures (single phase)

(b) Ferrite plus carbide structures (two phase)

The materials in group (a) included the as hot rolled and annealed
0.18% Carbon steel, while group (b) consisted of quenched and tempered

0.18% Carbon and 0.44% Carbon steels plus 0.44% Carbon steel lead patented before drawing.

The pure iron samples, 0.18% Carbon steel annealed, and as rolled were all found to follow the Hall-Petch relationship as shown in Fig.54. A regression of flow stress (in Kgf/mm^2) on the reciprocal square root of grain size was linear, and explained 94% of the variation in flow stress:-

$$\sigma_f = 1.21 + 925.00 d^{-\frac{1}{2}}$$ Equation 6:b

where d = grain size in cm x 10^{-4}

The as heat treated conditions for the quenched and tempered 0.18% and 0.44% Carbon steels, and 0.44% Carbon steel lead patented did not provide sufficient data for a rigorous analysis, and all the relationships proposed in the literature gave similar amounts of scatter about a straight line.

Since the presence of a second phase often obscures the ferrite grain boundary, Equation 6:4 requires a modifying factor. This could be additive e.g. for dispersion hardened material the modifying factor may take the form $\alpha f P^{-1}$ or $\alpha f P^{-\frac{1}{2}}$, while the Gensamer[30] relationship would require a factor of log (particle spacing). As stated above the data available did not permit rigorous analysis, and a similar degree of scatter was observed for all the materials.

6.3.2. THE WORK HARDENING BEHAVIOUR OF SINGLE PHASE IRON

The pure iron samples, annealed at 800,850 and 900°C effectively consisted of a series of samples in which the grain size, and strain varied semi independently. Fig.12 shows that the samples had similar flow stress at the same strain values, although the larger grain size

resulted in a slightly lower tensile strength.

The shape of the initial work hardening curve suggests a logarithmic relationship between strength and strain. The flow stress, as a function of log. strain is shown in Fig.55. It is apparent that the relationship is linear for values of strain between 0.1 and 2. Similarly the flow stress of drawn iron was found to have a linear relationship with the reciprocal square root of the grain barrier spacing. Hence it was apparent that flow stress of pure iron was a function of log strain, and the reciprocal square root of the grain boundary spacing. The grain boundary spacing was shown to be a function of the intial spacing, and strain in Section 6.2. It is necessary, therefore, to derive a value for the coefficient of log strain, which is independent of the grain size. This was done by a multiple regression technique, which effectively calculates the partial regression coefficient for each variable while holding the second variable constant at its mean value. The results of this analysis for pure iron gave

$$\sigma_f = K + \alpha \log \varepsilon + \beta d^{-\frac{1}{2}} \qquad \text{Equation 6:5}$$

where $K = 38.69$ $\qquad$ σ_f = Flow stress in Kgf/mm^2

$\alpha = 14.89$ $\qquad$ ε = strain

$\beta = 26.03$ $\qquad$ d = grain size cm x 10^{-4}

The significance of the partial regression coefficients exceeded 0.1% i.e. a probability of a true relationship greater than 0.999. Since the grain size has been related to the initial grain size and strain Equation 6:5 may be modified to give:-

$$\sigma_f = K + \alpha \log \varepsilon + \beta (d_0 e^{-\phi \varepsilon})^{-\frac{1}{2}}$$

Hence $\sigma_f = K + \alpha \log \varepsilon + \beta d_0^{-\frac{1}{2}} e^{\phi \varepsilon/2}$ $\qquad$ Equation 6:6

where d_0 = a constant proportional to initial grain size

ϕ = constant determined in Section 6.2

The predicted values of the expression

$$\alpha \log \varepsilon + \beta \, d_o^{-\frac{1}{2}} e^{\phi \varepsilon / 2}$$

were calculated, for the wires produced from pure iron annealed at 900°C, and the results deducted from the experimental values of the flow stress.

$$K^1 = \sigma_f - \alpha \log \varepsilon - \beta d_o^{-\frac{1}{2}} e^{\phi \varepsilon / 2}$$

The values of K^1 obtained ranged from 27.88 to 42.45 (the value 27.88 was obtained at ε = 5.28, the next lowest value of K^1 was 35.63) with an average value of 38.39, compared with the value derived from the regression of 38.69. This confirmed the validity of Equation 6:6 over the full range of deformation for pure iron samples.

6.3.3. THE WORK HARDENING BEHAVIOUR OF TWO PHASE STRUCTURES

The quenched and tempered structures differed from the others materials in that a high degree of initial rapid hardening was not observed. The pearlitic steel, 0.44% Carbon, lead patented, did exhibit rapid initial hardening complete at 0.3 strain. This absence of initial rapid hardening in the quenched and tempered structures may have resulted from a high carbon in solution. These steels were highly sensitive to ageing at 200°C after drawing suggesting that the carbon in solution was high. The sensitivity to ageing of 0.18% Carbon steel after drawing is shown in Fig.56. The initial rapid hardening observed in the 0.44% Carbon steel, lead patented before drawing was essentially completed much more rapidly than for pure irons. Similarly the rapid initial hardening in the 0.18% Carbon steels was completed in the order:-

1. Quenched and tempered

2. As hot rolled

3. Annealed

i.e. in order of increasing barrier spacing. It appeared
that the particles of the second phase acted as far more
efficient barriers to dislocation movement, or as more
efficient dislocation sources.

The regression equations for mean ferrite path length, and
lamellar spacing derived in Section 6.2.3. and 6.2.4. may be
substituted into Equation 6:6. The results of this should
then give an equation for the prediction of flow stress based
on the strain. The derived equations were as follows:-
0.18% Carbon steel, quenched and tempered

$$\sigma_f = K + \alpha \log \varepsilon + \beta P_0^{-\frac{1}{2}} e^{0.37 \varepsilon / 2}$$

0.44% Carbon steel, lead patented

$$\sigma_f = K + \alpha \log + \beta S_0^{-\frac{1}{2}} e^{0.42 \varepsilon / 2}$$

A graph of σ_f as a function of $e^{\varepsilon / 2}$ for these materials should
indicate whether Equation 6:**8** is valid. This is shown in
Fig. 57. The flow stress shows a mainly linear relationship
with $e^{\varepsilon / 2}$ confirming the validity of Equation 6:**8** for two
phase structures. The variation from linearity in the early
stages of deformation are due to the effect of log . The
values of the constants α and β in the above equation are
unknown. The data available is such that values of the terms
$\log \varepsilon$ and $\left[S_0^{-\frac{1}{2}} e^{\alpha \varepsilon / 2} \right]$ can be calculated for each material.
A multiple regression analysis of the values of σ_f for these
would permit the calculation of α and β. This analysis
was carried out, with the following results:-
0.18% Carbon steel, quenched and tempered

$$\sigma_f = 100.7^{0.37 \varepsilon / 2} - 11.71 \log \varepsilon - 18.98$$

0.44% Carbon steel, lead patented

$$\sigma_f = 117.25^{0.42 \varepsilon / 2} - 24.56 \log \varepsilon - 59.95$$

Embury and Fisher[43] proposed a modification of the Hall-Petch equation
based on a proposed relationship between the barrier spacing of cold
drawn 0.93% Carbon steel, and swaged Ferrovac E, and the plastic
strain $\varepsilon_{W.D.}$. The following shows the derivation of the Embury and
Fisher relationship from the Hall-Petch equation.

The Hall-Petch equation states that:-

$$\sigma_f = \sigma_i + K_f d^{-\frac{1}{2}}$$

where
σ_f = Flow Stress

σ_i = constant

K_f = constant

d = grain size

$$d = d_0 \, e^{-0.5\varepsilon} \qquad \text{Equation 6:3}$$

where
d = grain size of drawn wire after ε plastic strain

d_0 = grain size of undeformed material

Substituting the term for d in the Hall-Petch equation gives

$$\sigma_f = \sigma_i + K_f \left[d_0 \, e^{-0.5\varepsilon} \right]^{-\frac{1}{2}}$$
$$\sigma_f = \sigma_i + K_f \, d_0^{-\frac{1}{2}} e^{\varepsilon/4}$$

The Embury and Fisher[43] equation was

$$\sigma_f = \sigma_i + \frac{K}{\sqrt{2}\sqrt{r}} e^{\varepsilon/4}$$

i.e.
$$\sigma_f = \sigma_i + \frac{K}{\sqrt{2}} \, r_0^{-\frac{1}{2}} e^{\varepsilon/4}$$

Embury and Fisher, working with thin film electron microscopy
techniques, measured barrier spacings based on the sub cells re-
sulting from cold work. The initial sub cell size was stated to be
a function of interlamellar spacing in pearlitic structures, and to
require 25% plastic strain for dislocation generation in swaged pure
iron (0.29 strain). No indication of the level of strain required to

produce the substructure was given.

The present work has concentrated on the effect of barriers to
dislocation movement visible by light microscopy or replica,
techniques. Theoretically, assuming no redundant work, or variation
in deformation across the section Equation 6:3 should predict the
deformation of barriers to dislocation movement, but will not pre-
dict the creation of new barriers as a result of that deformation.
The Embury and Fisher equation also lacks this factor.

Rapid initial hardening has been noted, and referred to elsewhere
in this text. This hardening is of a descending order, being
logarithmic in form. The level of strain at which the effect
approaches zero varies, apparently with increasing barrier spacing.
The rate of hardening appears less for pure iron than for steels,
but continues to affect flow stress to a greater degree of plastic
strain. This suggests that the initial hardening is related to the
formation of a substructure. The initial hardening, as discussed
earlier, was found to be logarithmic in form, and a logarithmic
term was introduced into the work hardening equation. There were
some indications that the value of the constant of the logarithm
of strain incfeased with increasing second phase, probably due to a
greater rate of dislocation generation in the structure.

The basic difference between the equations derived to explain work
hardening in this work, and those of Embury and Fisher[43] lie in the
fact that statistical methods of analysis have been used to calculate
equations of best fit for two variables. The Embury and Fisher
results imply that the flow stress of cold worked steels is dependent

on the barrier spacing, but the equation proposed assumes that the number of barriers is a constant, while the spacing of barriers decreases. Equation 6:5 implies that initially the rate of multiplication or generation of dislocations, logarithmic in form, is the main contributor to work hardening, but that barrier spacing effect then becomes significant. The logarithmic term representing dislocation generation or multiplication then changes sign, suggesting annihilation of sub cell boundaries, in the multiple regression technique, i.e.

$$\varepsilon < 1 \quad \log \varepsilon \text{ is negative} \qquad \varepsilon > 1 \log \varepsilon \text{ is positive}$$

6.4 THE DUCTILITY OF DRAWN WIRES

6.4.1. THE VARIATION IN TENSILE DUCTILITY

The tensile ductility as shown in Fig.14 was highly sensitive to the chemical composition; that of the pure iron samples both as heat treated and after drawing was 6-7 times greater than any of the steels. The effect of small quantities of a second phase, even in the spheroidised form, was very marked. The effect of increasing the second phase content was very slight when compared with the effect of its introduction.

Deformation of these structures had little effect on the tensile ductility, although, as may be expected the pure iron samples showed the greater effect. The effect of the wiredrawing was to reduce the value of tensile ductility slightly. The average value of tensile ductility for each raw material was calculated, giving the following results.

Material	Tensile Ductility		
	Mean	Maximum	Minimum
Pure Iron annealed at 900°C	6.663	7.49	5.63
Pure Iron annealed at 850 C	6.6.85	7.33	5.79
Pure Iron annealed at 800 C	6.585	7.39	5.00
0.18% C Steel annealed at 650 C	0.903	1.43	0.49
0.18% C steel as rolled	0.697	1.05	0.54
0.18% C steel quenched and tempered	0.901	1.31	0.24
0.44% C steel lead patented	0.669	0.80	0.51
0.44% C steel quenched and tempered	0.685	0.78	0.35

These results show clearly that the tensile ductility is more dependent on the second phase content than on the morphology, or spacing of the ohase, and the level of deformation. Generally the maximum value of the tensile ductility occurred in the as heat treated material, or early in the drawing process, and the minimum value occurred at the limit of drawability.

6.4.2. THE VARIATION IN TORSIONAL DUCTILITY

The torsional ductility was actually the shear strain to fracture in the torsion test. The results of this are shown in Fig.15. During the initial stages of wiredrawing the test results initially suggest a wide and inconsistent fluctuation in ductility, with no set pattern. Careful examination of the data, however, revealed certain facts:-

1. All the data tended to fit a common band, at around 1.0 shear strain, in the later stages of wiredrawing.

2. The initial value of ductility decreased with grain size in ferritic structures.

3. The initial value of ductility appeared to decrease with decreasing free ferrite path length in two phase structures.

4. A tendency to increase the value of ductility on the first reduction was most marked in the pure iron, less so in the 0.18% Carbon steel, and absent in the 0.44% Carbon steel.

5. The order in which the materials entered the common band of ductility was in order of increasing structural parameter i.e. the 0.44% Carbon steel was first, and pure iron annealed at 900°C last. The only exception to this was the pure iron annealed at 800°C, which preceded the 0.18% Carbon steel annealed at 650°C.

6. The common band appeared to have a logarithmic relationship with wiredrawing strain i.e. tended to increase slightly at a decreasing rate. The common band which all the materials entered is apparent at 1.5-2.0 wiredrawing strain.

The features described above suggested a "ranking" of the materials related to the pattern of changes in torsional ductility. This ranking gives the order:-

1. Pure iron annealed at 900°C

2. Pure iron annealed at 850°C

3. 0.18% Carbon steel annealed at 650°C

4. Pure iron annealed at 800°C

5. 0.18% Carbon steel as hot rolled

6. 0.18% Carbon steel quenched and tempered

7. 0.44% Carbon steel, lead patented

Generally this ranking indicates the order of decreasing initial torsional ductility, and the reverse order of entry to the common band. With only one exception this list is also ranked in order of

decreasing structural barrier distance within the material, and increasing second phase content. This suggests that the torsional ductility is structure sensitive, and that the controlling factor is barrier spacing. The apparent exception to this rule, pure iron annealed at $800^{\circ}C$ may be explained by variation in grain size. The pure iron samples did exhibit grain size variation, largely due to the fact that the deformation prior to annealing, 56%, was rather low, and the irregular cross section of the initial rod caused this figure to be variable. The reason for the initial increase in ductility of the ferrites is difficult to explain, since it was very rapid, and also very short lived. It does, however, appear to be linked with the grain size of the initial material. One feature of the initial stages of drawing will be an increase in dislocation density, and it is possible that the torsional ductility is related to dislocation density. The rapid decrease in ductility to the common band could then be attributed to the formation of a substructure.

The relationship between structure and strength has been discussed in Section 6.1 and a direct relationship proposed. Hence, if the torsional ductility is related to the structure, then a plot of ductility as a function of flow stress should be of interest. This is shown in Fig.58, from which it can be seen that a distinct relationship does exist, which appears to be dependent upon the flow stress.

7. CONCLUSIONS

1. The effect of wiredrawing on the barrier spacing of pure iron and hypoeutectoid steel wires is an exponential reduction in barrier spacing. Theoretically the barrier spacing should

follow the equation:-

$$d = d_0 \, e^{-0.5\varepsilon} \qquad\qquad \text{Equation 6:3}$$

Actual measurements of spacing confirm the basic equation form, but considerable variation from the predicted constants was detected.

2. Direct substitution of Equation 6:3 into the Hall-Petch equation

$$\sigma_f = \sigma_i + Kd^{-\frac{1}{2}}$$

resulted in the equation used by Embury and Fisher[43]

$$\sigma_f = \sigma_i + \frac{K}{\sqrt{2}\sqrt{r_0}} \, e^{\varepsilon/4}$$

This was again found to be in the correct form, but variance from the constants predicted was again observed.

The work hardening of hypoeutectoid steels was therefore shown to follow the equation

$$\sigma_f = \sigma_i + \phi \log \varepsilon + \beta \, d_0^{-\frac{1}{2}} \, e^{\varphi\varepsilon/2} \qquad\qquad \text{Equation 6:8}$$

The values of all the constants in the equation were shown to vary with the chemical composition of the wire.

3. The ductility of the drawn wire, as measured by the shear strain to fracture appeared to be related to the flow stress.

4. The ratio of tensile strength to flow stress was shown to be a variable, dependent largely on the chemical composition of the wire.

5. The drawn wires showed a $\langle 110 \rangle$ texture, the intensity of which was related to the strain by the equation

$$P = a\varepsilon^{\frac{1}{2}}$$

ACKNOWLEDGEMENTS

1. Smallman, R.E.   "Modern Physical Metallurgy"

2. Honeycombe, R.W.K. "Plastic Deformation of Metals

3. Keh, A.S.   Phil.Mag.12 , 9 (1965)

4. Jaoul, B and Gonzalez, D J.Mech.Phys.Solids, 9, 16

5. Mordike, and Haasen Phil.Mag.7 ,459, (1962)

6. Conrad, H.   NPL Symp."The relation between structure
           and mech.properties of solids" HMSO(1963)

7. Zener, C and Holloman, J.H. A.App.Phys.15, Jan (1944)

8. Von Mises, R.   Z.Angew.Math.Mech.8, 161 (1928)

9. Taylor, G.I.   J.I.M.81, 491 (1928)

10. Dieter, G.E.   "Mechanical Metallurgy"

11. Mc Lean, D.   "Grain Boundaries in Metals"

12. Eshelby,Frank and Nabarro Phil,Mag.42, 351 (1951)

13. Keh,A.S.and Weissmann, S. Proc.1st Inst.Conf."Electron Microscopy
           and Strength of Crystals"Berkely,Calif.1961

14. McLean, D.   "Mechanical Properties of Metals"

15. Hull,D,McIvor,I.D.& Owen,WS Proc.Symp."Relation between structure and
           properties of solids"NPL 1963 (HMSO)

16. Hall, E.O.   Proc.Phys.Soc.64B, 747 (1951)

17. Petch, N.J.   J.I.S.I. 173, 25 (1953)

18. Armstrong,R.Codd,I.Douthwaite, R.M. and Petch,N.J.
           Phil.Mag.7,45 (1962)

19. Conrad, H.   "Iron and its Dilute Solid Solutions"
           Interscience-Wiley

20. McLean, D.   Can.J.Physics,45,973 (1967)

21. Dingley,D.J. and McLean,D Acta Met.15,885,May 1967

22. Holtzmann,M and Man,J. J.I.S.I. 204, 230 (1966)

23. Evans,J.T. & Rawlings,R. Met.Sci.J.2,221 (1968)

24. Orowan,E.   Symp.on Internal Stresses in Metals
           (1948)Inst.of Metals,London.

25. Zackay,V.F.and Parker,E.R. Proc.2nd Berkely Inst.Conf."High
           Strength Materials"

26. Fisher,J.C.Hart,E.W.and Pry,R.H.   Acta Met.**1**,May 1953,336

27. Ansel,G.S. and Lenel,F.V.   Acta.Met.**8**,Sept.1960,612

28. Unckel,H.A.   Metallugia,March 1952 p115

29. Hyam,E.D.and Nütting, J.   JISI **184**,p.148 Oct.1956

30. Gensamer,M.Pearsall,E.B., Pellini, W.S. and Low, J.R.Jr.

    Trans.A.S.M.Dec.1942 p.983

31. Holloman, J.H.   Trans.A.S.M.**32**, p.123(1948)

32. Turkalo,A.M.and Low,J.R.Jr.   Trans.Met.Soc.AIME,**212**

    Ded.1958,p.750

33. Pickering,F.B.Burns,K.W. and Keown,S.R.

    Fifth Inst.Cong.for Electron Microscopy

34. Puttick, K.E.   J.I.S.I.Feb.1957, 161

35. Kaldor, M.   Acta.Met.**10**, 887,Sept.(1962)

36. Keh, A.S.   Ibid **11**, 2202, (1963)

37. Holtzmann, A.H., Danko, J.C. and Stout, R.D.

    Trans.Met.Soc.AIME Aug.1958 p.475

38. Godfrey, H.J.   Wire and Wire Prod.Jan.1963 p51

39. Mohrnheim, A.F.   Wire.Oct.1965 p.193

40. Mohrnheim, A.F.   Wire and Wire Prod.Feb.1966 p.243

41. Sisco, F.T.   "Alloys of Iron and Carbon"Vol.II

    Chap.5 McGraw Hill, 1937

42. Starodubov, K.F., Babich, V.K., and Gasik, L.I.

    Izvest.VUZ Chem.Met.Nov.1961

    155/158

43. Embury, J.D. and Fisher, R.M.   Acta.Met.**14**, Feb.1966,p.147

44. Chandhok,V.K.,Kasak, A, and Hirth, J.P.

    Trans.ASM **59**, p.285 (1966)

45. Kardonskii, V.M., Kurdjumov, G.V. and Perkas, M.D.

Met.I.Term.Obrab.Met.

1/2 1964 pp.62-68

46. Vitelli, V.J.   Wire and Wire Prod.Dec.1962 p.1763

47. Sazanova, A.A. and Shafranovskii, I.E.

Stal.Nov.1962 1051-1052

48. Tovpenetz, E.S.   Izvests.VUZ,Chem.Met.1966

6,151-155

49. Maurer,K.L. and Rosegger,R.   Berg.Hutt Monatsch 111.

(9)P.412 (1966)

50. Dewey,H.A.P.?and Briers,G.W.   J.I.S.I. Feb.1966, p.102

51. Hibbard, W.R.Jr.,Roswell, A.E. and Shuetz, A.E.

J. of Metals Sept.1951 p.808

52. Peck, J.F., and Thomas, D.A.   Trans.Met.Soc,AIME Dec 1961,

221, p.1240

53. Nishioka, T.   Tetsu to Hagane 44 1958, 2

pp 151-157

54. Fullman, L.R.   J. of Metals 1953 p.447

55. Payne, D.P. and Smith,B.F.   Symp."Continuous Heat Treatment

of Wire and Rod".

56. Mueller,M.H., Chernock, W.P. and Beck P.A.

Trans.Met.Soc.AIME Feb.1958 p.39

57. Barrett,C.S. and Massalski,T.B.   "Structure of Metals"3rd Ed.

McGraw Hill

58. Hirano, H. Takahashi, E, and Sano, S.

Wire October, 1965 p.1529

59. Duckfield, B.J.   "Wire Industry"Aug.1973 p.618

60. Pickering, F.B.   Iron and Steel April/March 1965
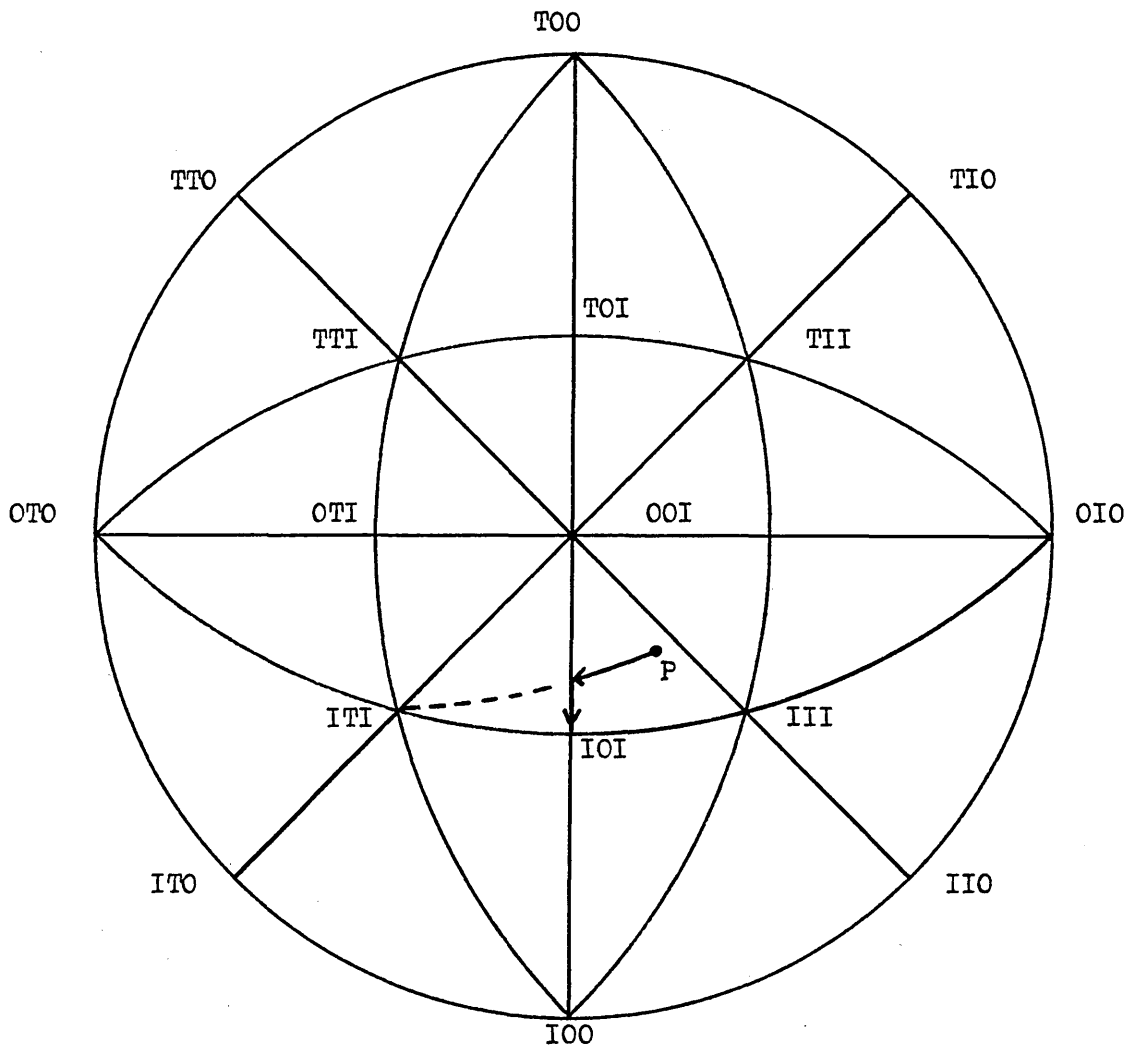
FIG.1. ROTATION OF SPECIMEN AXIS DURING DEFORMATION OF A BODY
CENTRED CUBIC METAL
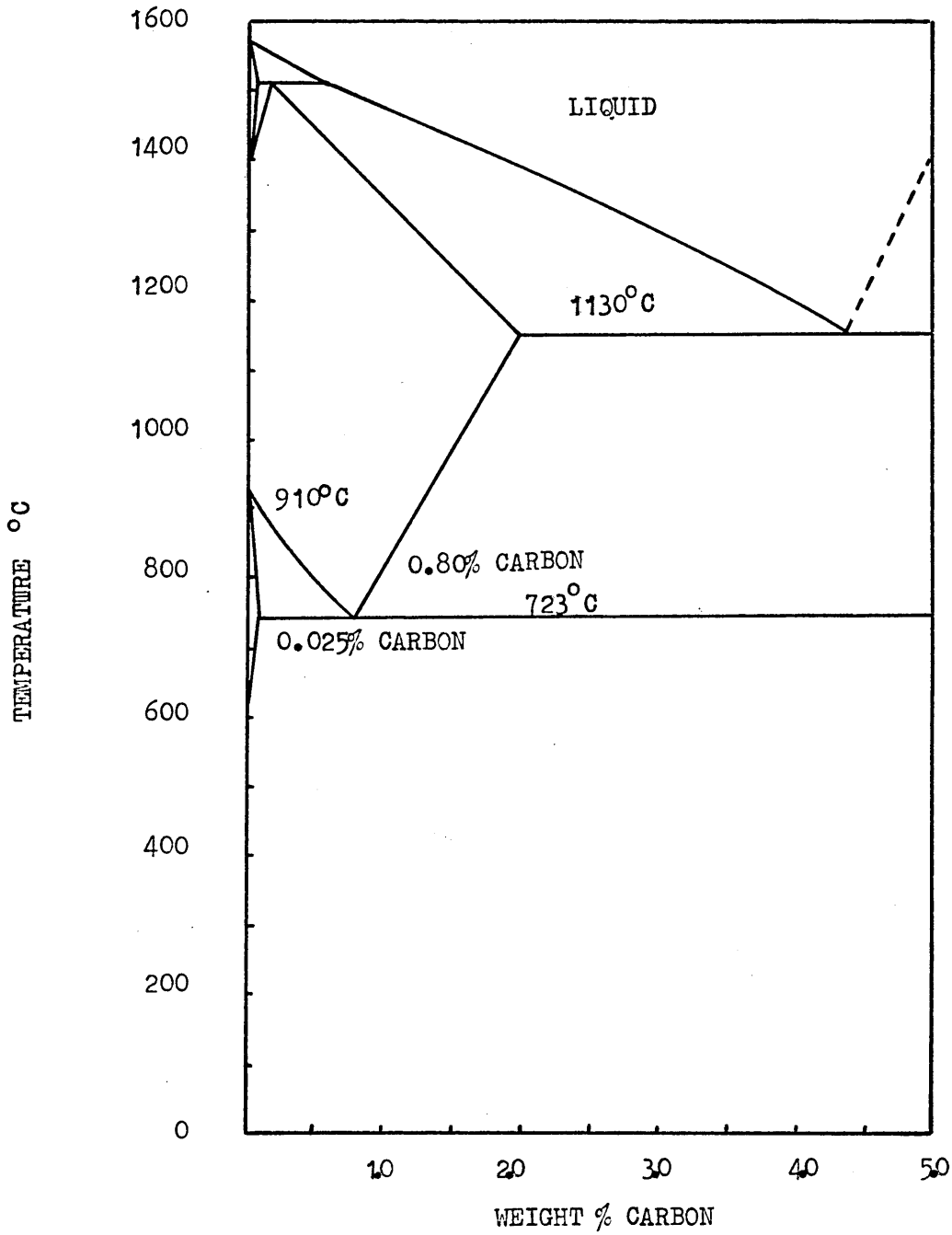
FIG. 2 IRON/CARBON PHASE DIAGRAM

FIG.3

ISOTHERMAL TRANSFOR...
DIAGRAM FOR 0.44% CA...
STEEL

CARBIDE INSERT

STEEL CASE

14°

30°

ENTRY ANGLE

EXIT ANGLE
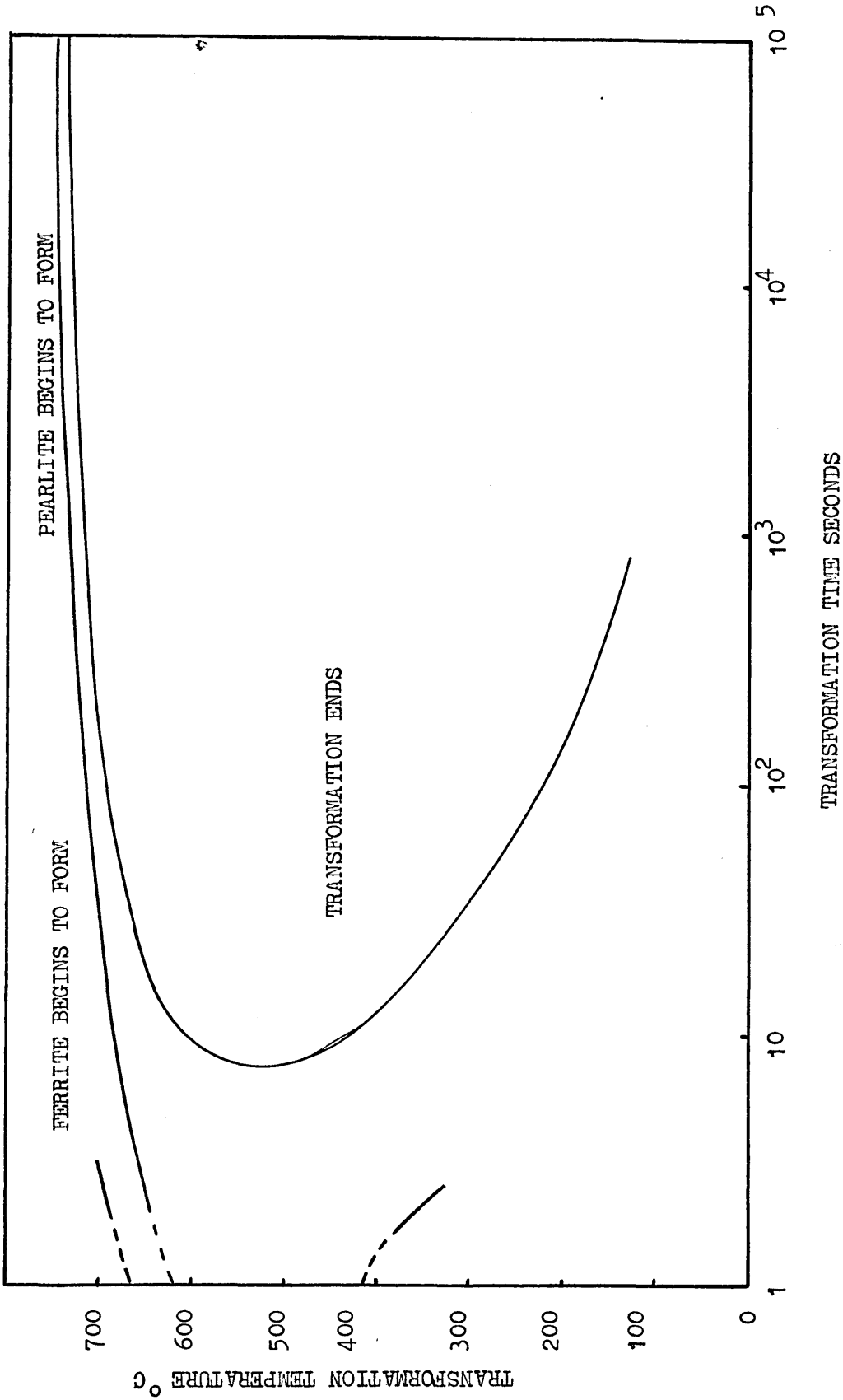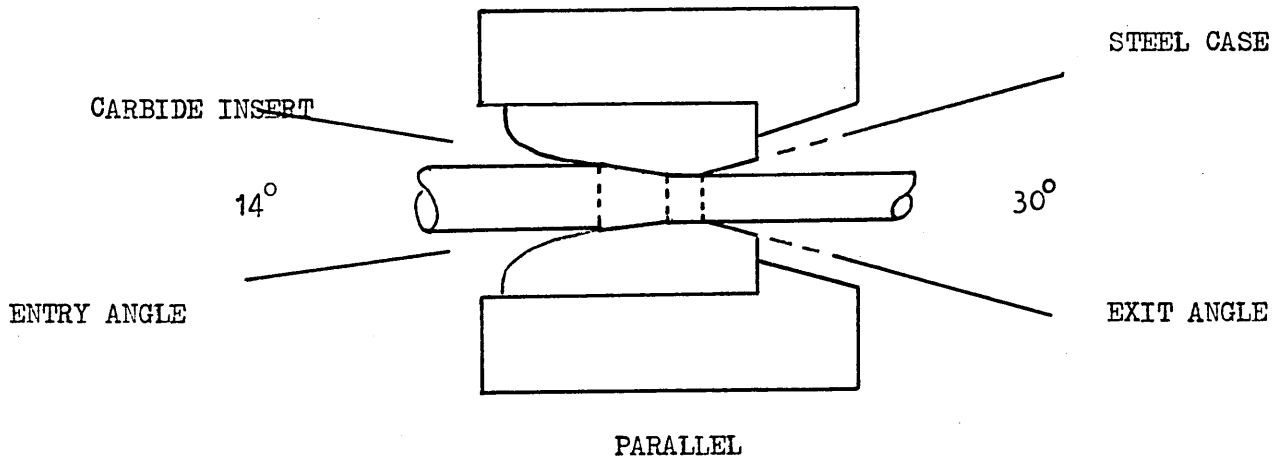
PARALLEL

NOTES

1. DRAWING ANGLE OF 14° TO BE SMOOTHLY BLENDED IN TO
   PARALLEL PORTION.

2. LEAD IN TO BE 30° AND BLENDED INTO DRAWING ANGLE.

3. WIRE TO IMPACT ON 14° ANGLE.

4. PARALLEL LENGTH NOT TO EXCEED $\frac{1}{3}$ DRAWN DIAMETER
   OR EXCESS HEAT GENERATION MAY RESULT.

FIG.4 FEATURES OF A GOOD WIREDRAWING DIE

FIG. 5.

28" DIAMETER SINGLE DIE "BULL BLOCK" USED TO DRAW WIRE.
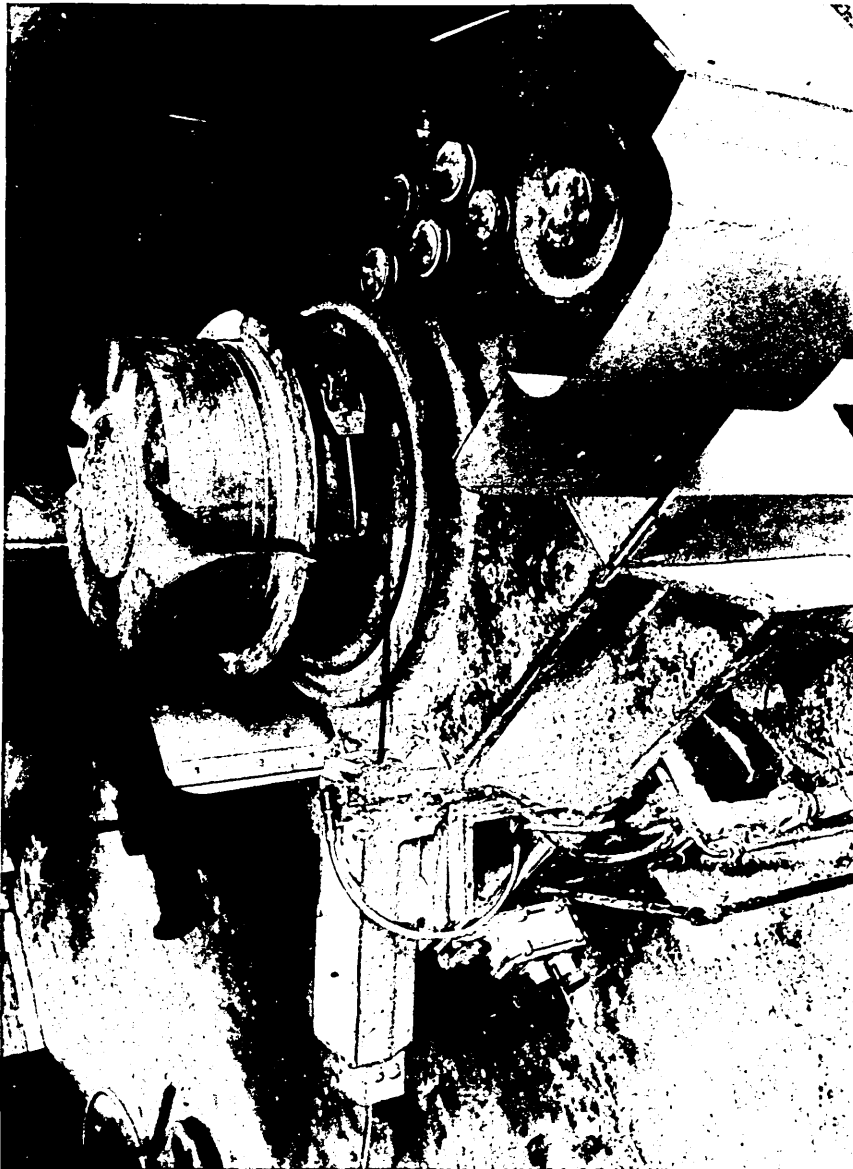
FIG. 6.

18" BLOCK DIAMETER 3 DI
WIREDRAWING MACHINE
USED TO DRAW FINE WIRE
SIZES.

6-9 M/M

COLD SETTING RESIN
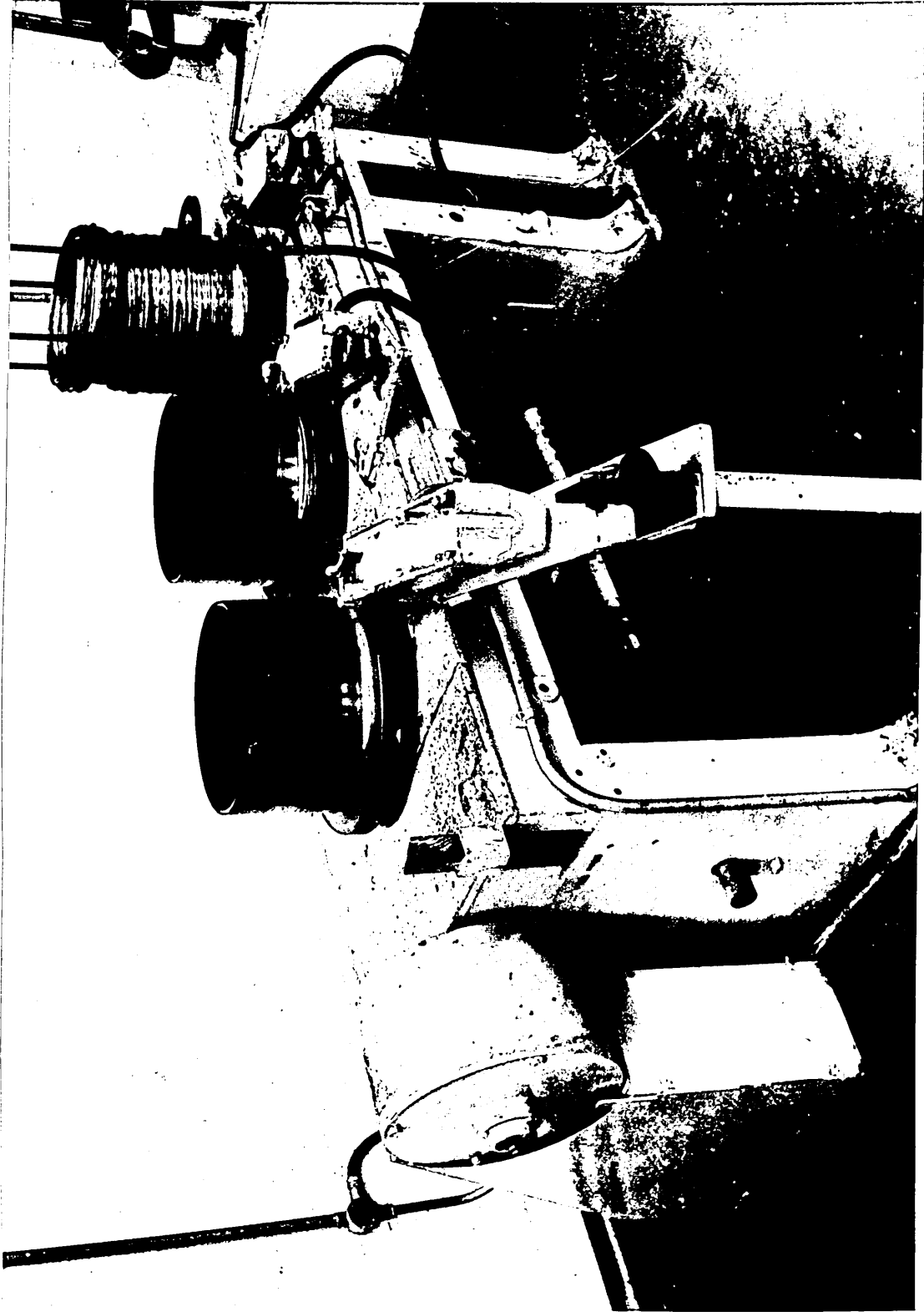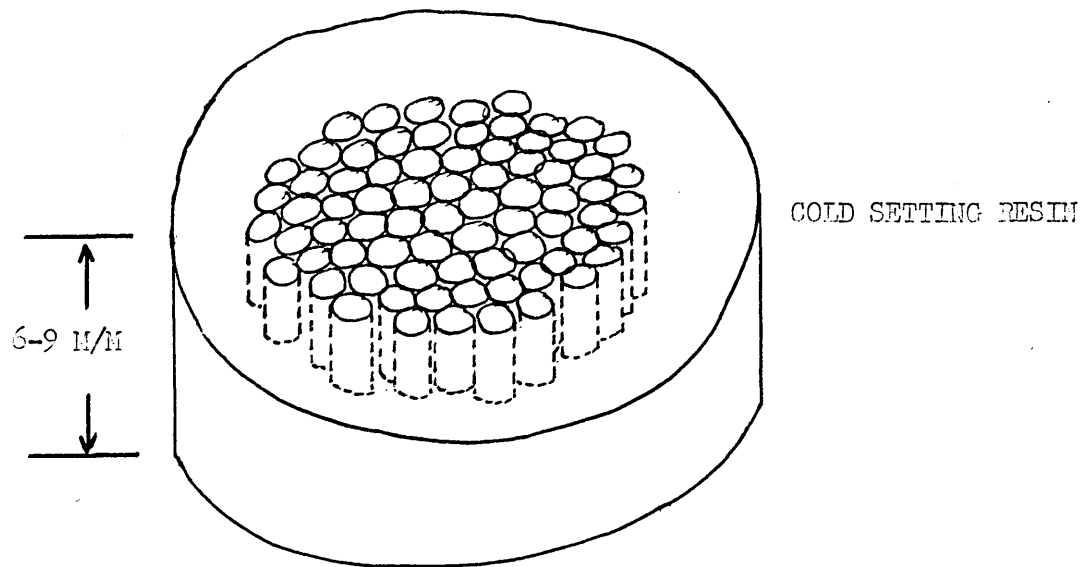
CLOSELY PACKED WIRE SPECIMENS CUT
PERPENDICULAR TO WIRE AXIS.

FIG.7. MOUNTING METHOD USED TO PREPARE WIRE SPECIMENS
FOR ORIENTATION DETERMINATION.
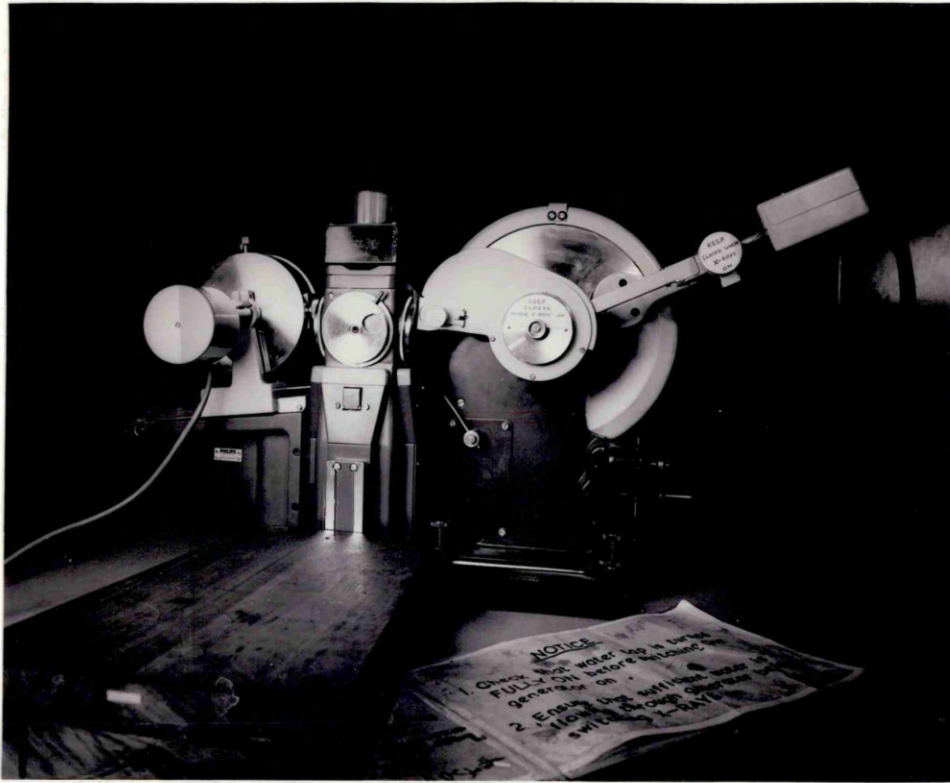
FIG.8

THE PHILIPS DIFFRACTOMETER USED TO DETERMINE INTENSITY OF
REFLECTIONS FOR TEXTURE COEFFICIENTS
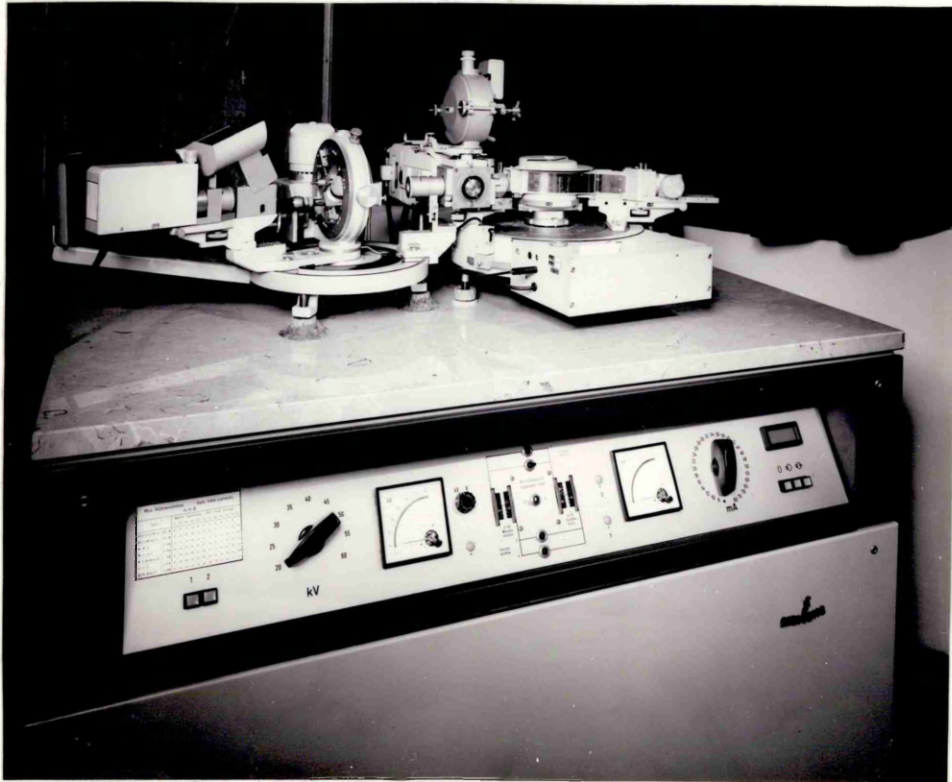
FIG.9

SIEMENS TEXTURE DIFFRACTOMETER USED TO DETERMINE FULL
SPIRAL POLE FIGURES
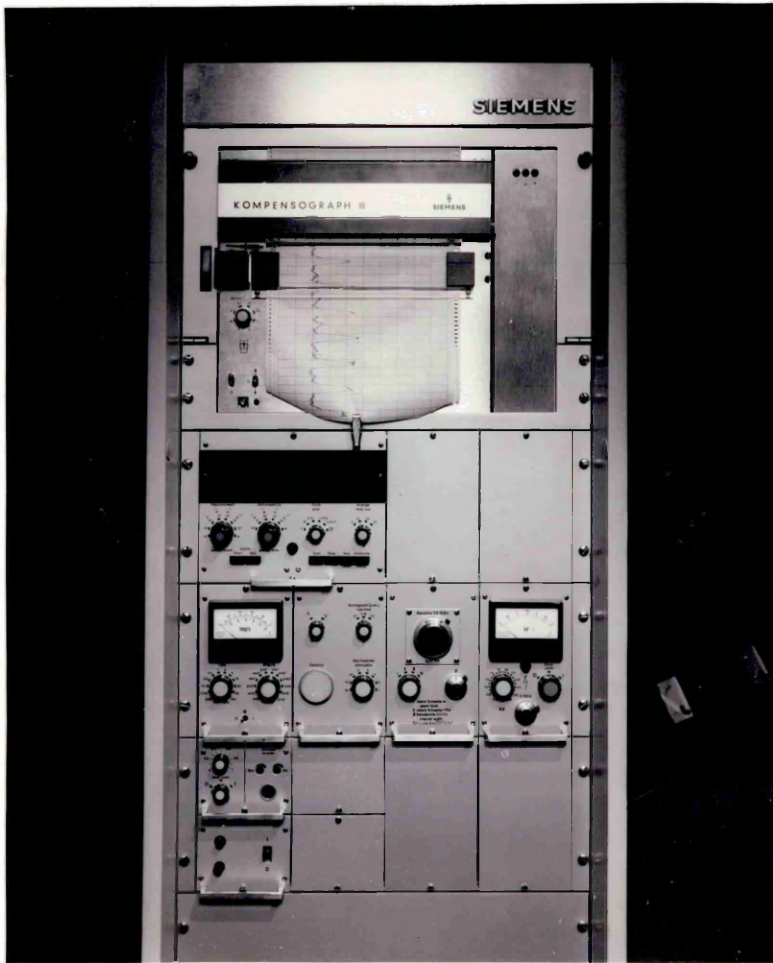
FIG.10

TYPICAL TRACE FROM SIEMENS TEXTURE DIFFRACTOMETER
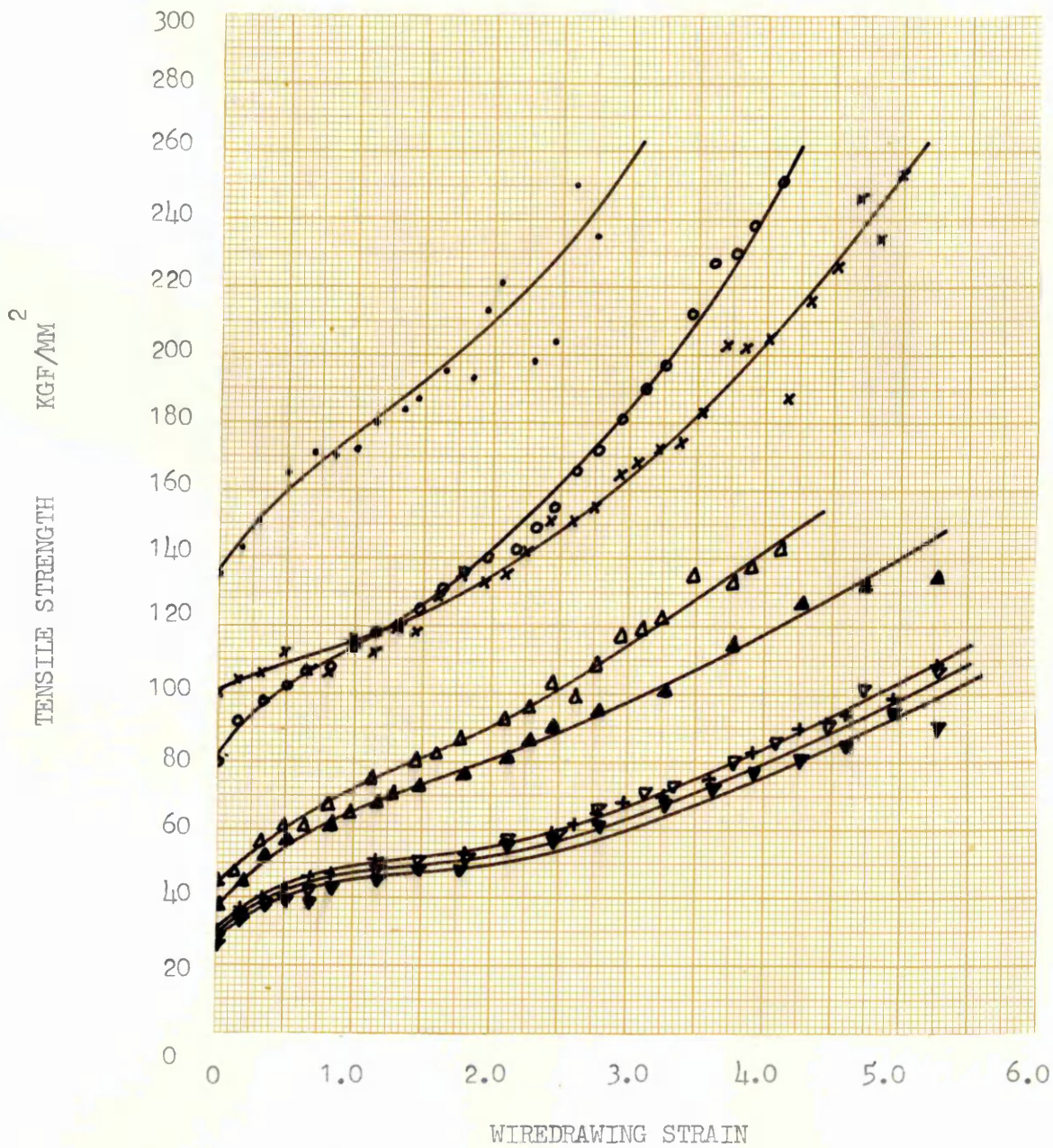
KEY TO SYMBOLS

  • 0.44 % CARBON STEEL QUENCHED AND TEMPERED
  o 0.44% CARBON STEEL LEAD PATENTED
  X 0.18% CARBON STEEL QUENCHED AND TEMPERED
  △ 0.18% CARBON STEEL ANNEALED
  + PURE IRON ANNEALED AT 800°C
  ▼ PURE IRON ANNEALED AT 850°C
  ▽ PURE IRON ANNEALED AT 900°C

FIG.11 .THE TENSILE STRENGTH OF DRAWN IRON AND STEEL AS A
       FUNCTION OF WIREDRAWING STRAIN
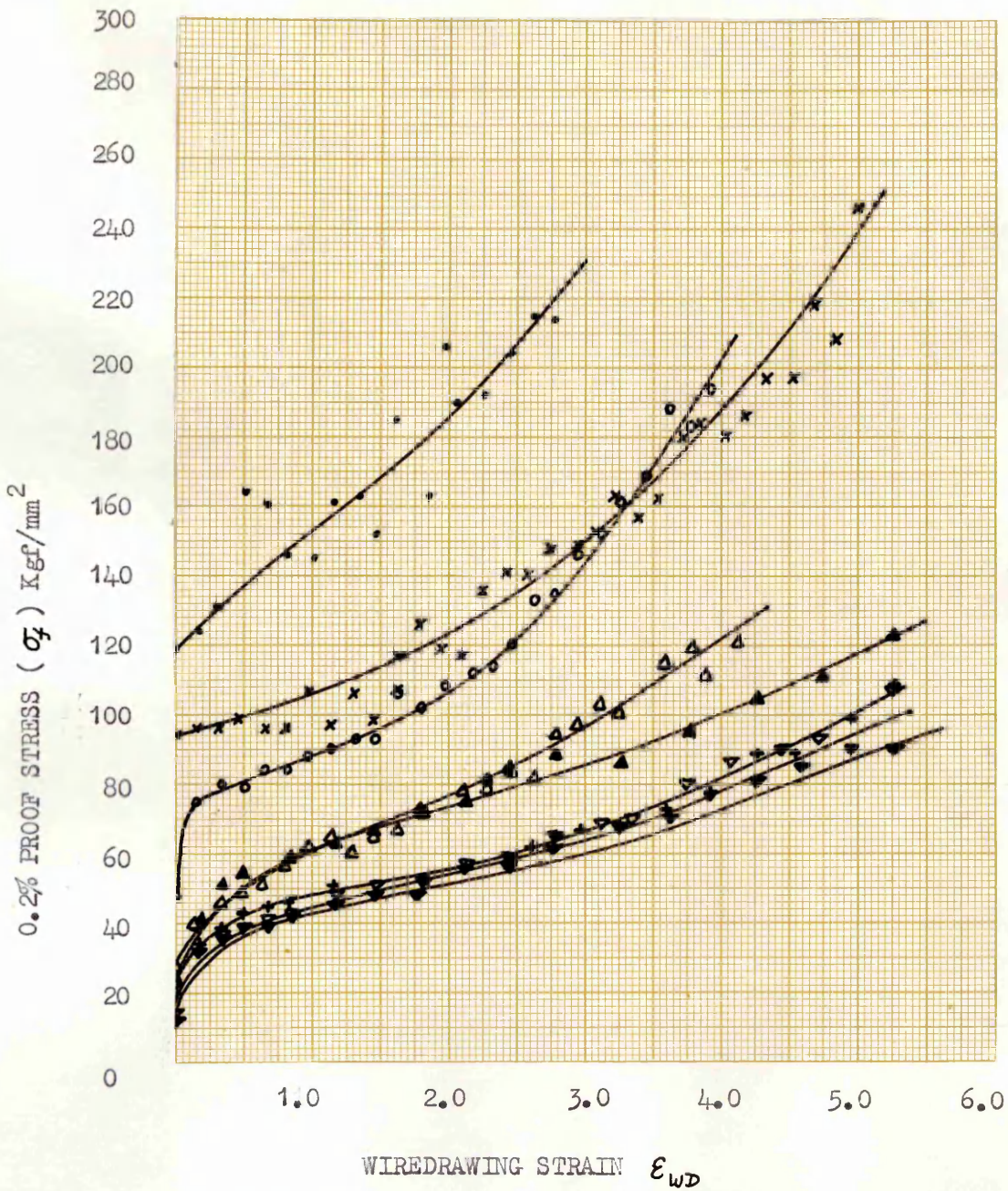
FIG. 12

THE 0.2% PROOF STRESS σ_f OF DRAWN IRON AND STEEL AS A FUNCTION OF WIREDRAWING STRAIN.
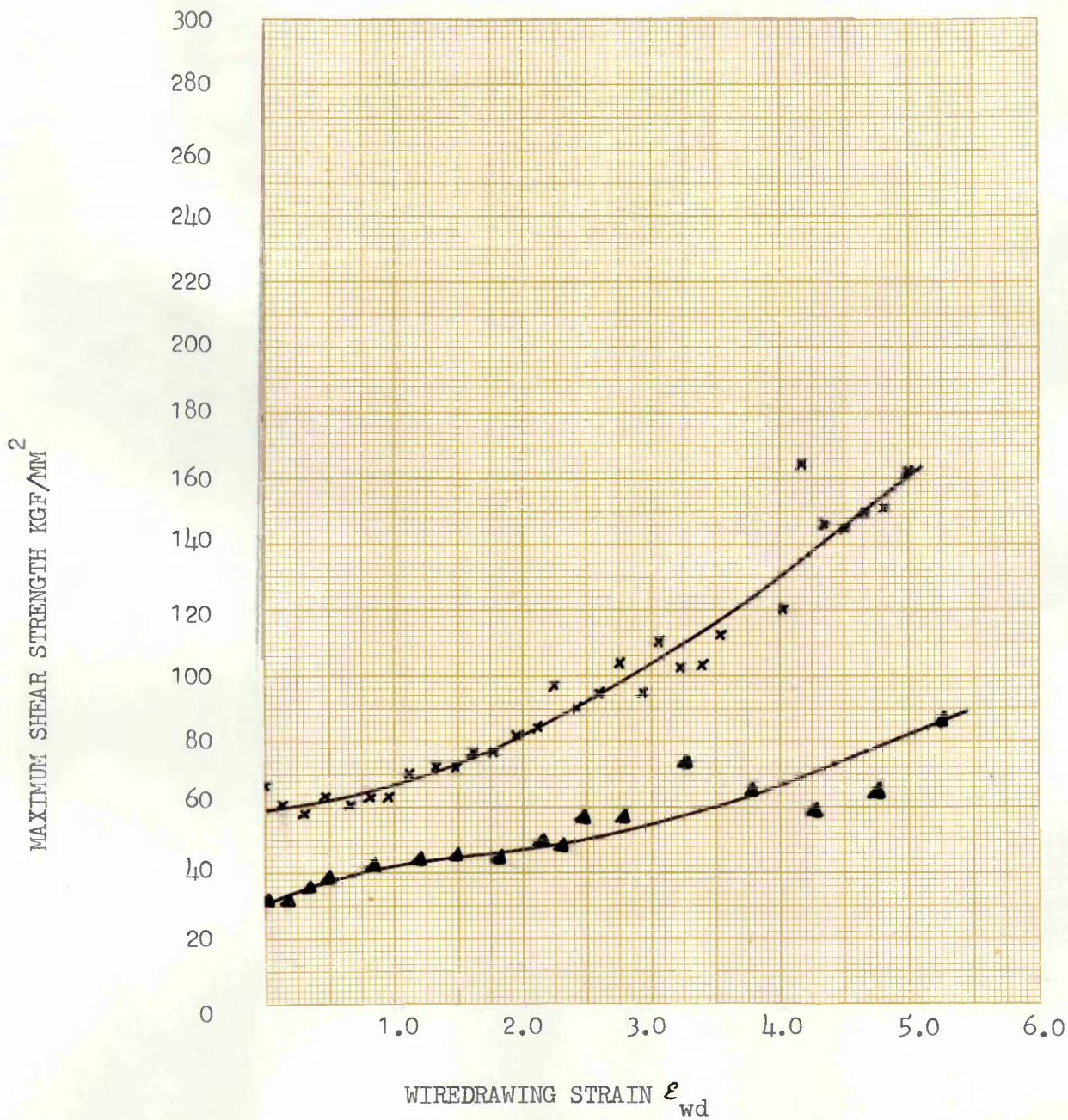
KEY TO SYMBOLS

x 0.18% CARBON STEEL QUENCHED AND TEMPERED

▲ 0.18% CARBON STEEL ANNEALED AT 650°C

FIG.13

MAXIMUM SHEAR STRENGTH OF DRAWN 0.18% CARBON STEEL WIRE

AS A FUNCTION OF WIREDRAWING STRAIN

KEY TO SYMBOLS

- •   0.44% CARBON STEEL QUENCHED AND TEMPERED
- o   0.44% CARBON STEEL LEAD PATENTED
- ✗   0.18% CARBON STEEL QUENCHED AND TEMPERED
- △   0.18% CARBON STEEL AS ROLLED
- ▲   0.18% CARBON STEEL ANNEALED AT 650°C
- +   PURE IRON ANNEALED AT 800°C
- ▼   PURE IRON ANNEALED AT 850°C
- ▽   PURE IRON ANNEALED AT 900°C

FIG.14

THE TENSILE DUCTILITY AT FRACTURE OF DRAWN IRON AND STEEL WIRES AS A
FUNCTION OF WIREDRAWING STRAIN
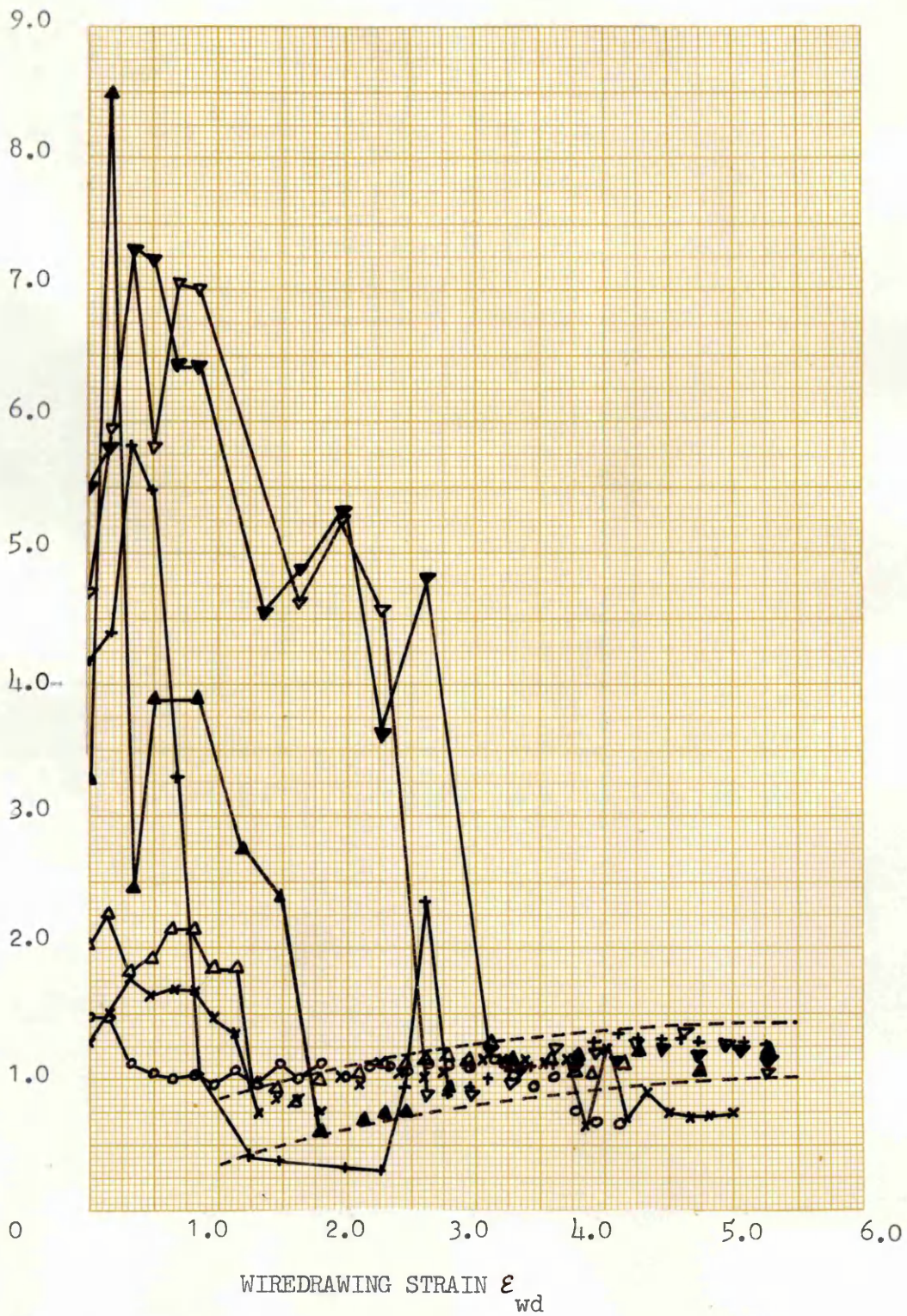
KEY TO SYMBOLS

- • 0.44% CARBON STEEL QUENCHED AND TEMPERED
- o 0.44% CARBON STEEL LEAD PATENTED
- × 0.18% CARBON STEEL QUENCHED AND TEMPERED
- △ 0.18% CARBON STEEL AS ROLLED
- ▲ 0.18% CARBON STEEL ANNEALED AT 650°C
- + PURE IRON ANNEALED AT 800°C
- ▽ PURE IRON ANNEALED AT 850°C
- ▼ PURE IRON ANNEALED AT 900°C

FIG.15

THE MAXIMUM SHEAR STRAIN AT FRACTURE OF DRAWN IRON AND STEEL WIRES AS
A FUNCTION OF WIREDRAWING STRAIN
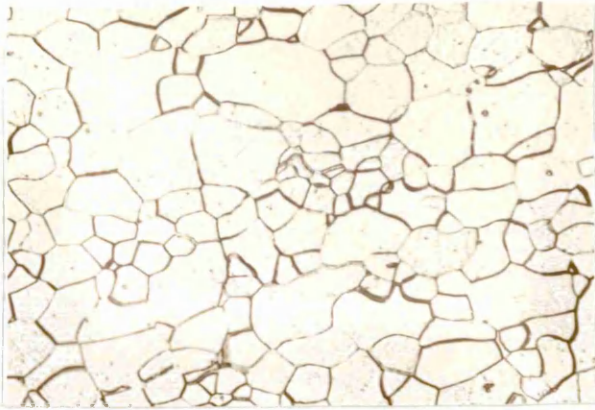
FIG.16

THE MICROSTRUCTURE OF PURE
IRON ANNEALED AT 800°C
LIGHT MICROSCOPE X500
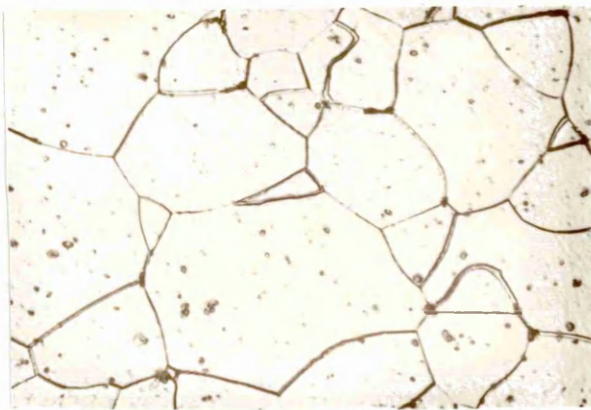
FIG.17

THE MICROSTRUCTURE OF PURE
IRON ANNEALED AT 850°C
LIGHT MICROSCOPE X500
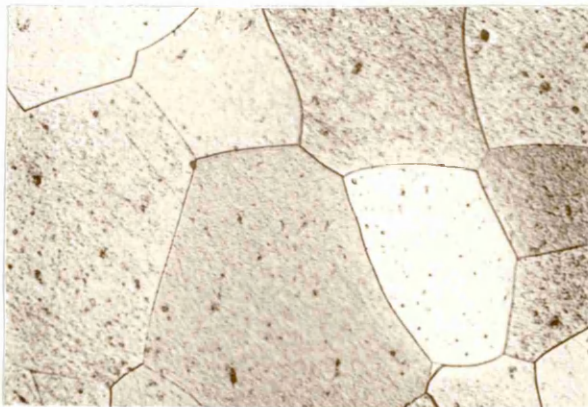
FIG.18

THE MICROSTRUCTURE OF PURE
IRON ANNEALED AT 900°C
LIGHT MICROSCOPE X500
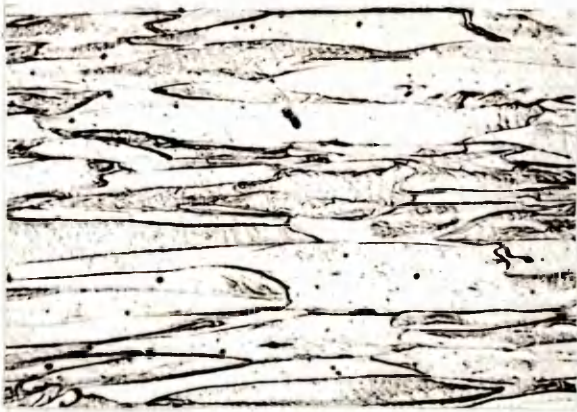
FIG. 19

THE MICROSTRUCTURE OF PURE IRON
ANNEALED AT 800°C, DRAWN 1.24
STRAIN. SPECIMEN CUT PARALLEL TO
WIRE AXIS.
LIGHT MICROSCOPE   x 500

FIG. 20

THE MICROSTRUCTURE OF PURE IRON
ANNEALED AT 800°C, DRAWN 1.24
STRAIN. SPECIMEN CUT PERPENDICULAR
TO WIRE AXIS.
LIGHT MICROSCOPE   x 500

FIG. 21

THE MICROSTRUCTURE OF PURE IRON
ANNEALED AT 800°C, DRAWN 2.27
STRAIN. SPECIMEN CUT PARALLEL TO
WIRE AXIS.
LIGHT MICROSCOPE   x 500

FIG. 22

THE MICROSTRUCTURE OF PURE IRON
ANNEALED AT 800°C, DRAWN 2.27
STRAIN. SPECIMEN CUT PERPENDICULAR
TO WIRE AXIS.
LIGHT MICROSCOPE   x 500
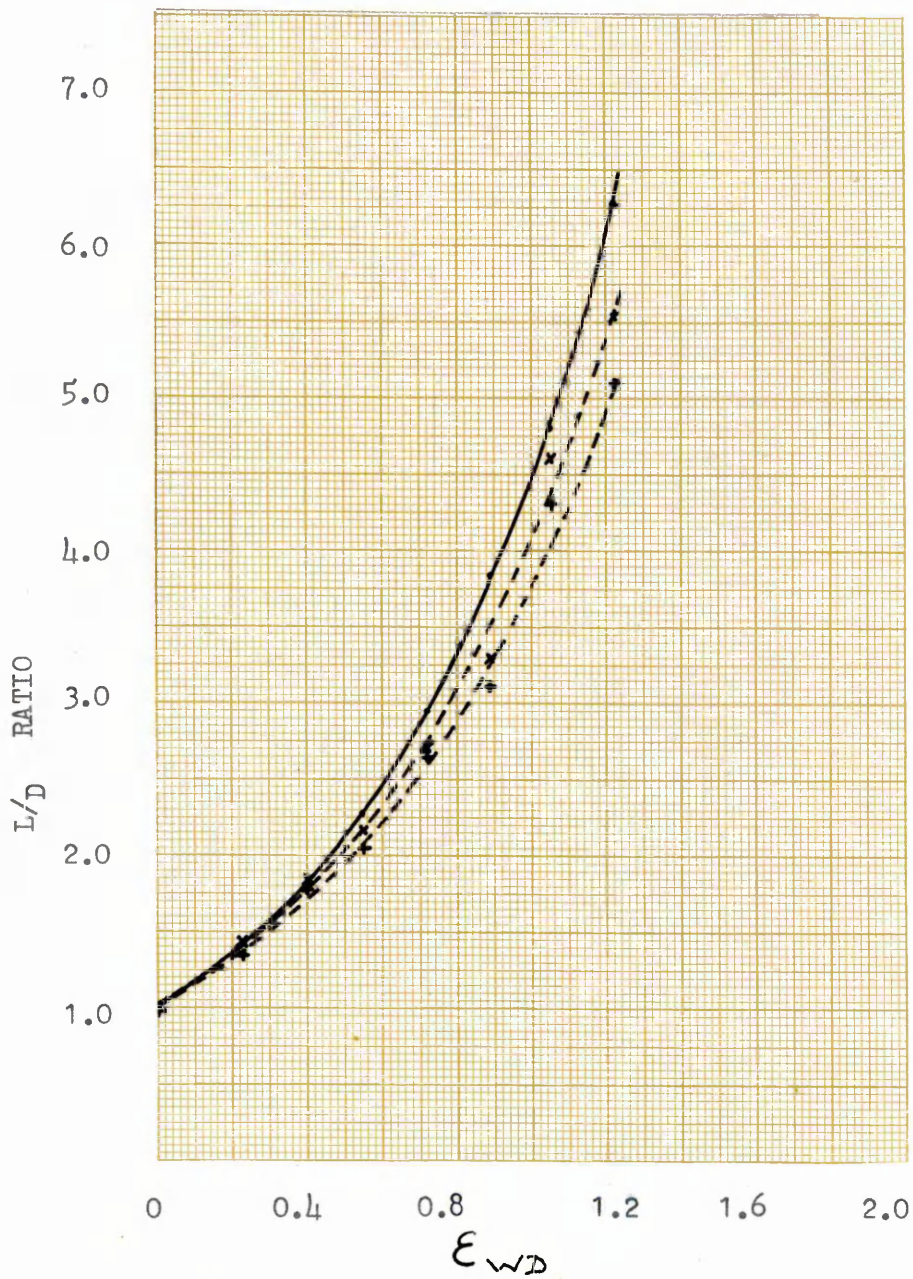
KEY TO SYMBOLS

• THEORETICAL PREDICTED RELATIONSHIP
× GRAINS AT WIRE SURFACE
+ GRAINS AT WIRE AXIS

FIG.23

THE RATIO OF THE GRAIN DIMENSION PARALLEL TO THE WIRE AXIS TO THE
GRAIN DIMENSION PERPENDICULAR TO THE WIRE AXIS FOR GRAINS AT THE
SURFACE AND AXIS OF A DRAWN IRON WIRE AS A FUNCTION OF WIREDRAWING
STRAIN.
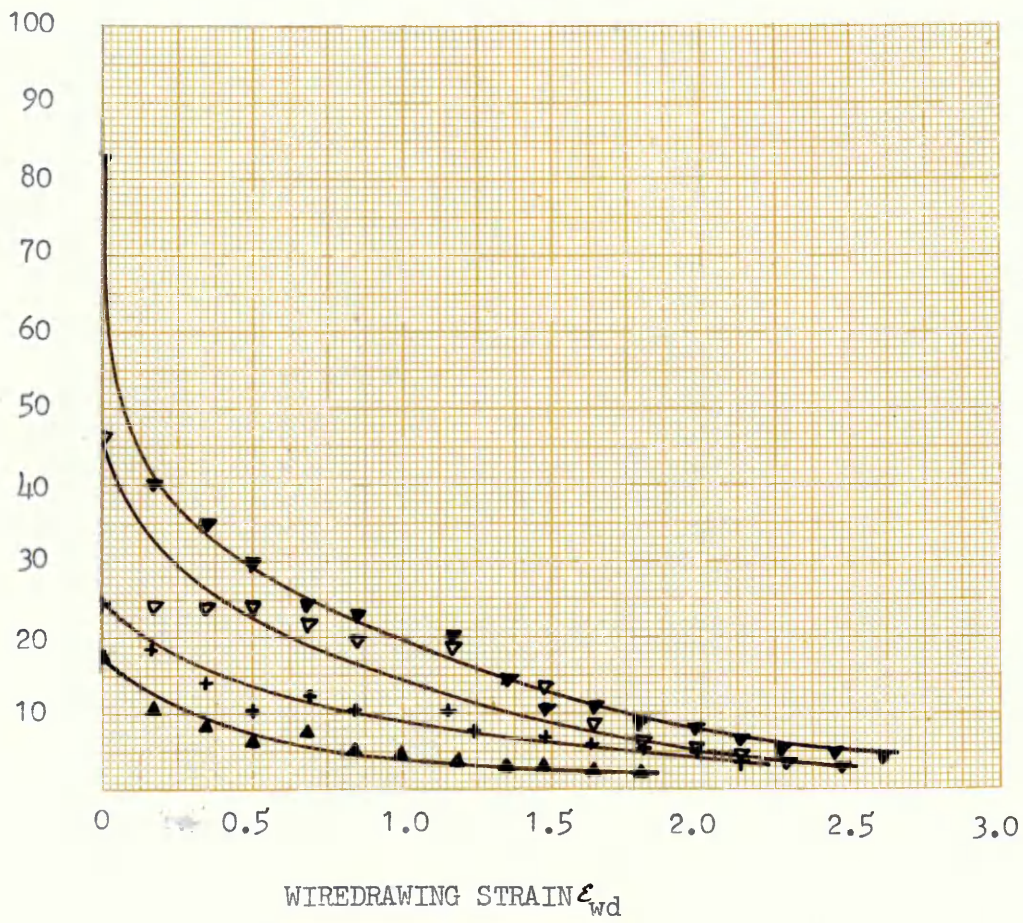
KEY TO SYMBOLS

▲ 0.18% CARBON STEEL ANNEALED AT 650°C
+ PURE IRON ANNEALED AT 800°C
▽ PURE IRON ANNEALED AT 850°C
▼ PURE IRON ANNEALED AT 900°C

FIG.24

THE MEAN GRAIN BOUNDARY INTERCEPT DISTANCE FOR DRAWN IRON AND
0.18% CARBON STEEL WIRES AS A FUNCTION OF WIREDRAWING STRAIN.

FIG.25

THE MICROSTRUCTURE OF 0.18% CARBON STEEL ANNEALED
AT 650°C. LIGHT MICROSCOPE X500
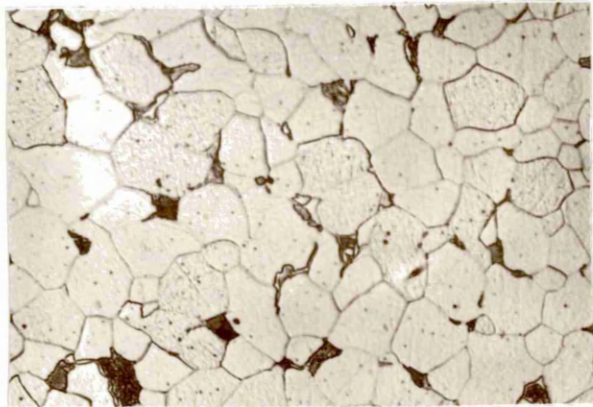
FIG.26

THE MICROSTRUCTURE OF 0.18% CARBON STEEL AS HOT ROLLED
LIGHT MICROSCOPE X500

FIG.27

THE MICROSTRUCTURE OF 0.18% CARBON
STEEL AS HOT ROLLED AFTER 2.3
WIREDRAWING STRAIN. SPECIMEN CUT
PARALLEL TO WIRE AXIS.
LIGHT MICROSCOPE X500.

FIG.28

THE MICROSTRUCTURE OF 0.18% CARBON
STEEL AS HOT ROLLED AFTER 3.2
WIREDRAWING STRAIN. SPECIMEN CUT
PARALLEL TO WIRE AXIS.
LIGHT MICROSCOPE X500.

FIG.29

THE MICROSTRUCTURE OF 0.18% CARBON
STEEL AS HOT ROLLED AFTER 3.9
WIREDRAWING STRAIN. SPECIMEN CUT
PARALLEL TO WIRE AXIS
LIGHT MICROSCOPE X500.

FIG.30

THE MICROSTRUCTURE OF 0.18% CARBON STEEL
QUENCHED IN 5% SODIUM HYROXIDE SOLUTION AT 0°C
FROM 950°C TEMPERED 10 MINS AT 400°C.
ELECTRON MICROSCOPE CARBON REPLICA X20.000

FIG.31

THE MICROSTRUCTURE OF 0.18%
CARBON STEEL QUENCHED AND
TEMPERED AFTER 1.14 WIREDRAWING
STRAIN
ELECTRON MICROSCOPE, CARBON,
REPLICA X20,000
SPECIMEN CUT PARALLEL TO THE
WIRE AXIS
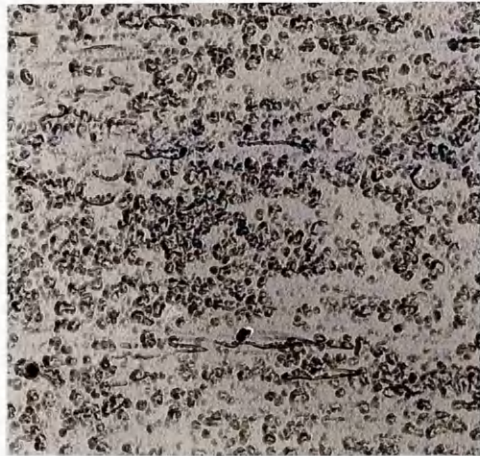
FIG.32

THE MICROSTRUCTURE OF 0.18%
CARBON STEEL QUENCHED AND
TEMPERED AFTER 2.10 WIREDRAWING
STRAIN
ELECTRON MICROSCOPE, CARBON
REPLICA X20,000
SPECIMEN CUT PARALLEL TO THE
WIRE AXIS
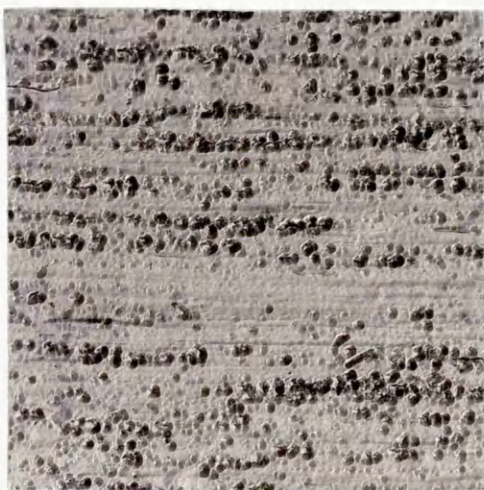
FIG.33.

THE MICROSTRUCTURE OF 0.18%
CARBON STEEL, QUENCHED AND
TEMPERED, AFTER 4.03 WIREDRAWING
STRAIN
ELECTRON MICROSCOPE, CARBON
REPLICA X20,000
SPECIMEN CUT PARALLEL TO THE
WIRE AXIS

FIG.34

THE MICROSTRUCTURE OF 0.18%
CARBON STEEL QUENCHED AND
TEMPERED, AFTER 4.82 WIREDRAWING
STRAIN
ELECTRON MICROSCOPE, CARBON
REPLICA X20,000
SPECIMEN CUT A PARALLEL TO THE
WIRE AXIS
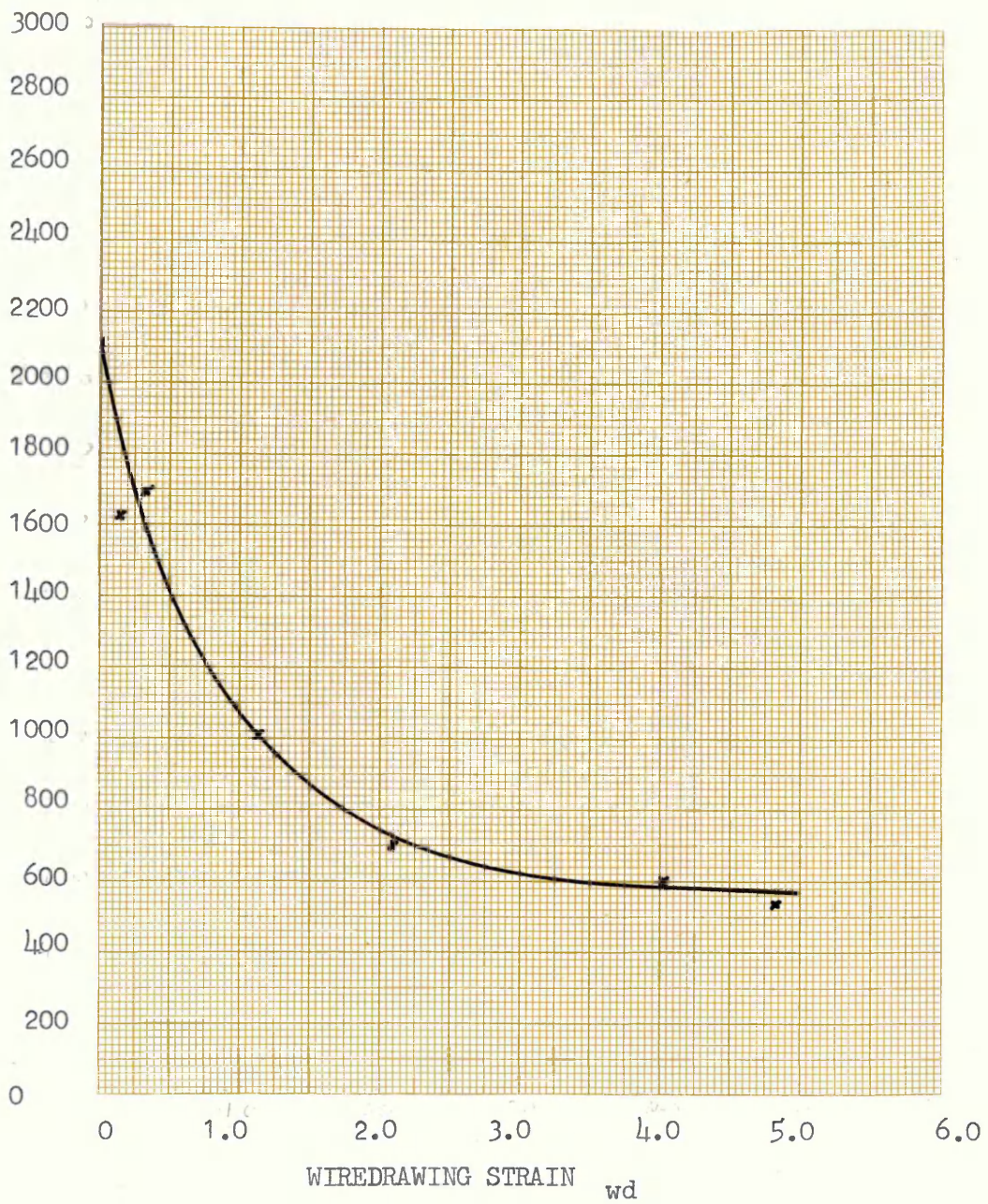
FIG. 35 THE MEAN FREE FERRITE PATH LENGTH FOR 0.18% CARBON
STEEL QUENCHED AND TEMPERED BEFORE DRAWING, AS A
FUNCTION OF WIREDRAWING STRAIN.
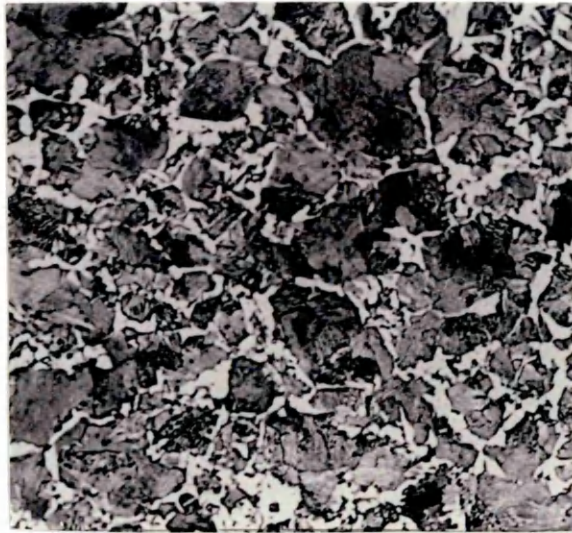
FIG.36

THE MICROSTRUCTURE OF 0.44% CARBON STEEL. LEAD PATENTED
LIGHT MICROSCOPE X500

FIG.37(a)   FIG.37(b)

SLIP LINES IN PEARITE. 0.44% CARBON STEEL. LEAD PATENTED
0.23 WIREDRAWING STRAIN.

LIGHT MICROSCOPE X1750
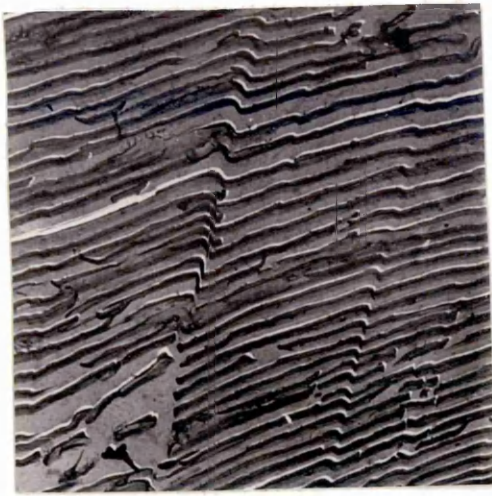
FIG. 38

SLIP IN PEARLITE. O. 44% CARBON
STEEL. LEAD PATENTED. O. 23
WIREDRAWING STRAIN.
ELECTRON MICROSCOPE
CARBON REPLICA
X 7500
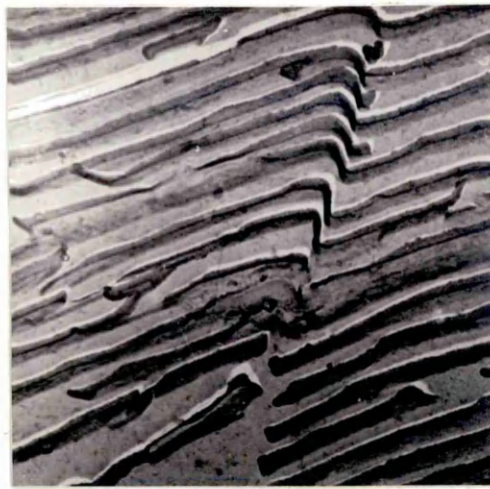
FIG. 39

SLIP IN PEARLITE. O. 44% CARBON
STEEL. LEAD PATENTED. O. 23
WIREDRAWING STRAIN.
ELECTRON MICROSCOPE
CARBON REPLICA
X 15000

FIG. 40

FIG. 41

SLIP IN PEARLITE. O. 44% CARBON STEEL
LEAD PATENTED. O. 23 WIREDRAWING STRAIN
ELECTRON MICROSCOPE. CARBON REPLICA
X 15000
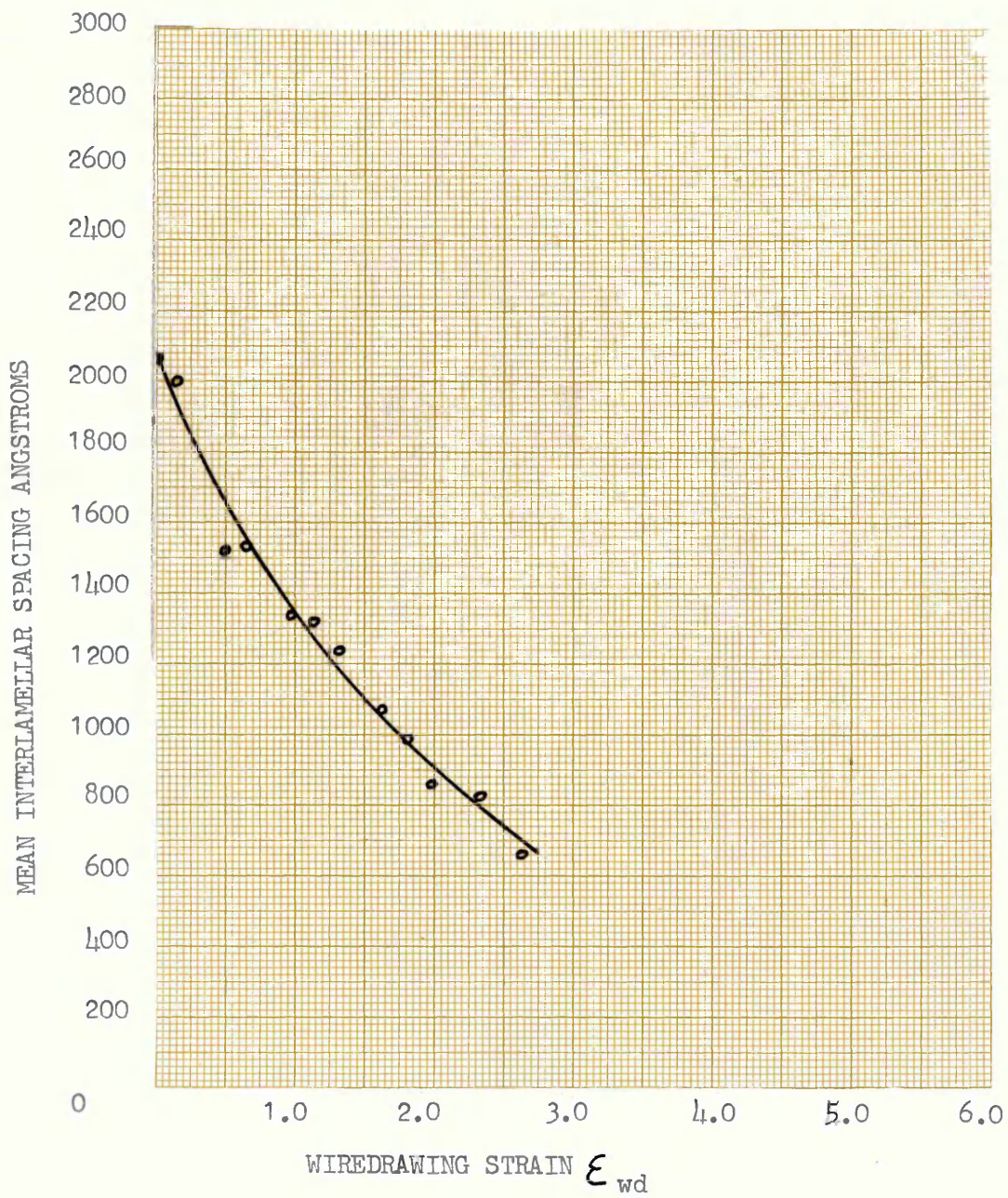
FIG.42   THE MEAN INTERLAMELLAR SPACING OF 0.44% CARBON STEEL
LEAD PATENTED BEFORE DRAWING, AS A FUNCTION OF WIRE-
DRAWING STRAIN.

FIG.43

THE MICROSTRUCTURE OF 0.44% CARBON STEEL QUENCHED
FROM 950°C IN 5% SODIUM HYDROXIDE SOLUTION AT 0°C,
AND TEMPERED FOR 10 MINUTES AT 400°C.
ELECTRON MICROSCOPE, CARBON REPLICA X200,000
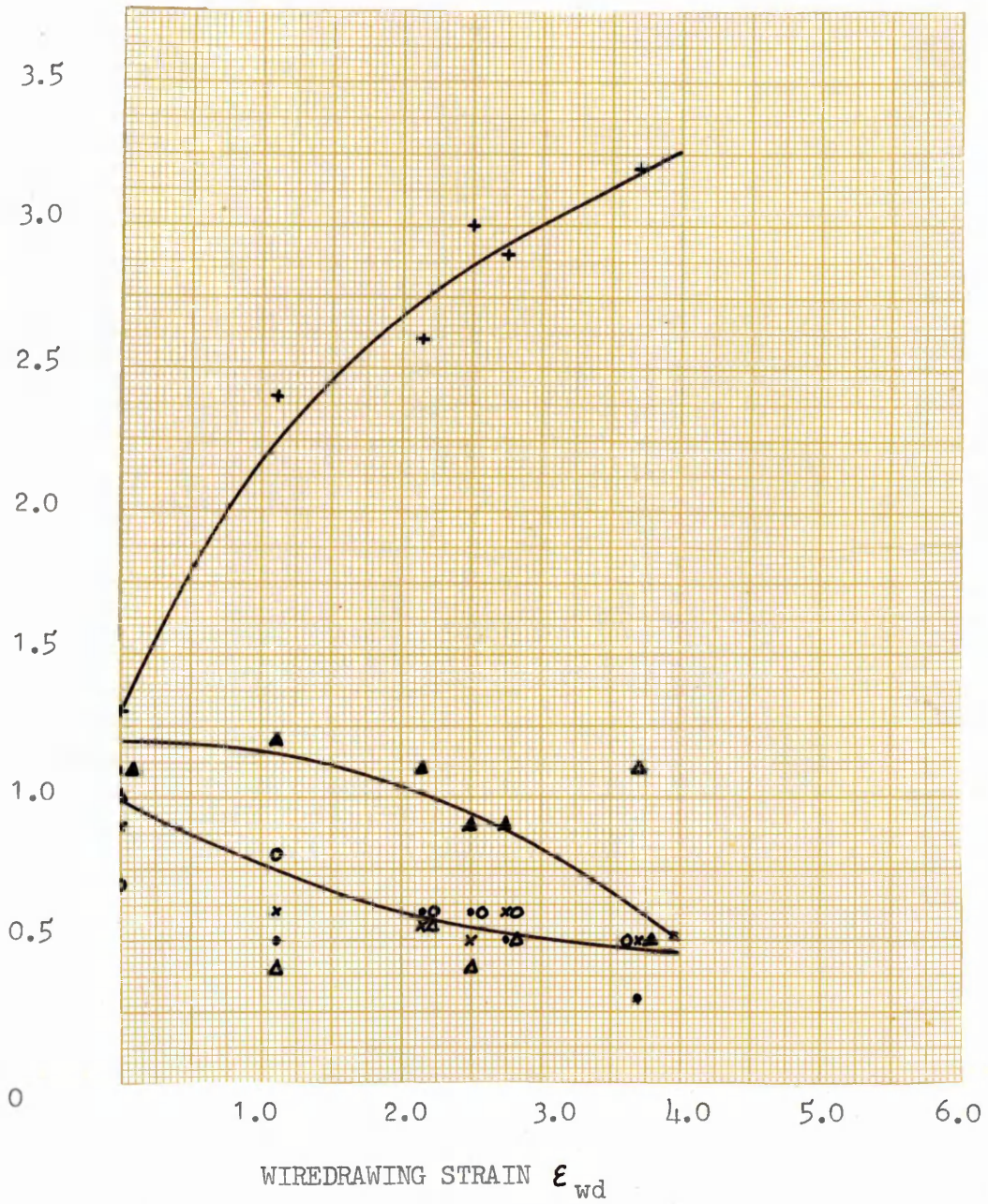
KEY TO SYMBOLS

- • (200) PLANE REFLECTION
- x (211) PLANE REFLECTION
- + (220) PLANE REFLECTION
- ▲ (310) PLANE REFLECTION
- △ (222) PLANE REFLECTION
- o (321) PLANE REFLECTION

FIG.44 THE TEXTURE COEFFICIENTS FOR REFLECTIONS FOR PURE IRON
WIRES AS A FUNCTION OF WIREDRAWING STRAIN.
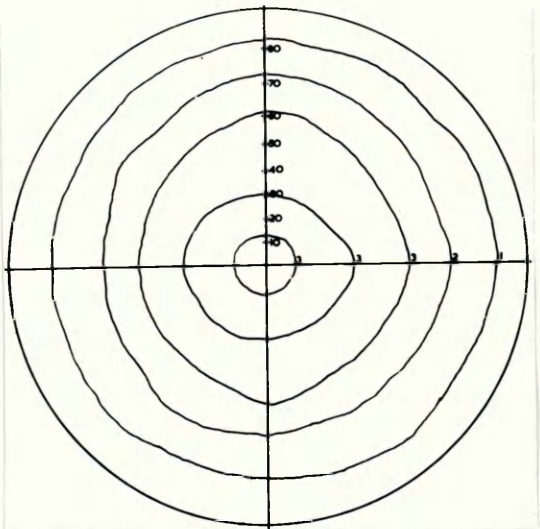
WIREDRAWING STRAIN = 0
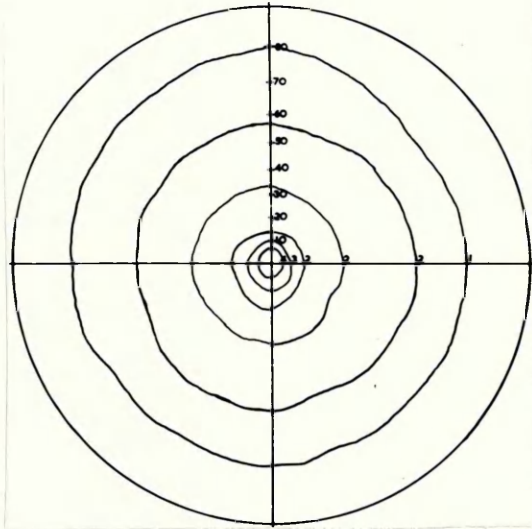
WIREDRAWING STRAIN = 1.13
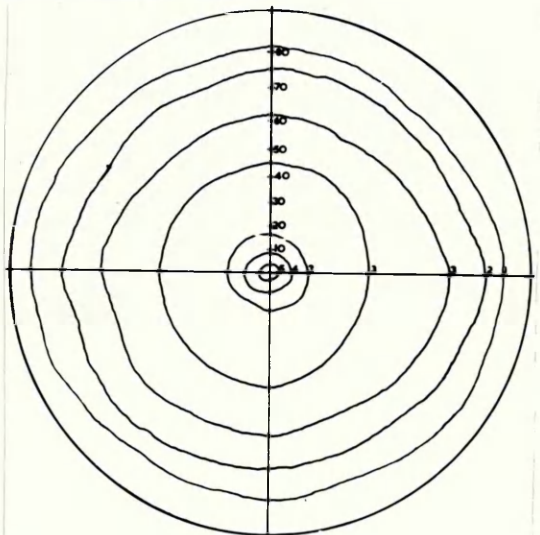
WIREDRAWING STRAIN = 1.97
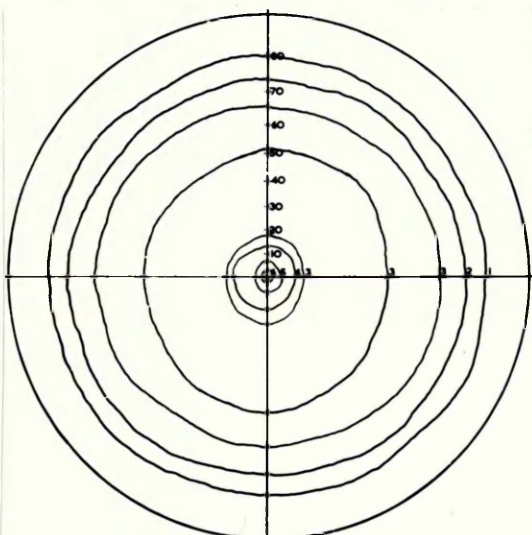
WIREDRAWING STRAIN = 2.60
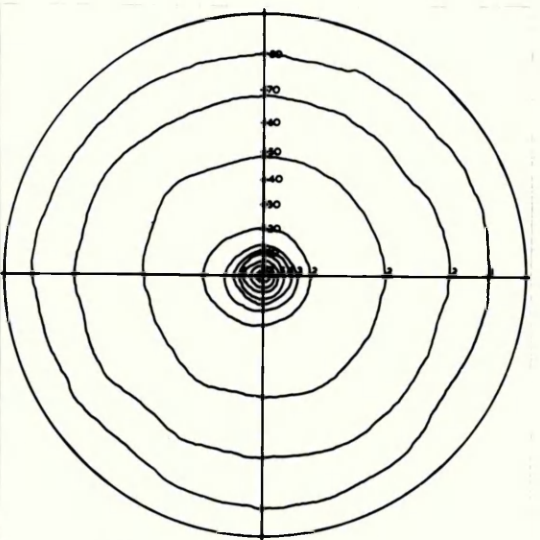
WIREDRAWING STRAIN = 5.27

FIG.45

(110) POLE FIGURES FOR PURE
IRON SAMPLES ANNEALED AT 850°C
AND DRAWN
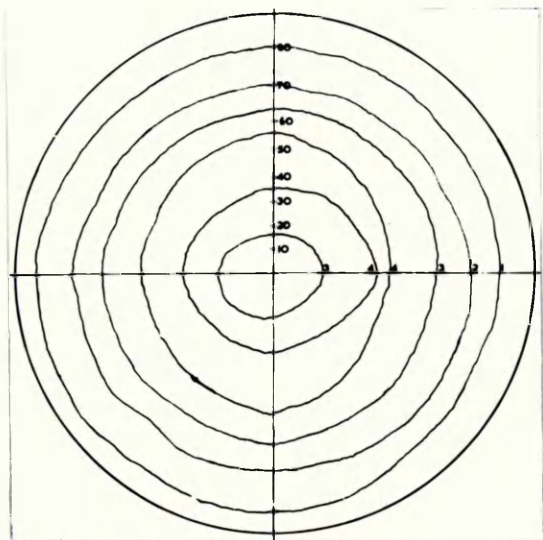
WIREDRAWING STRAIN = 0
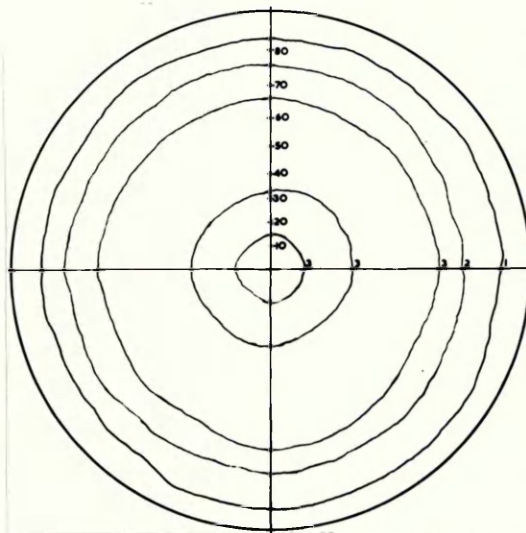
WIREDRAWING STRAIN = 1.13
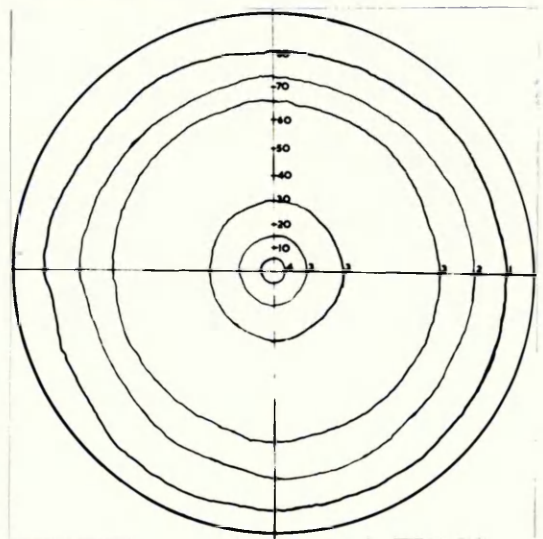
WIREDRAWING STRAIN = 1.97
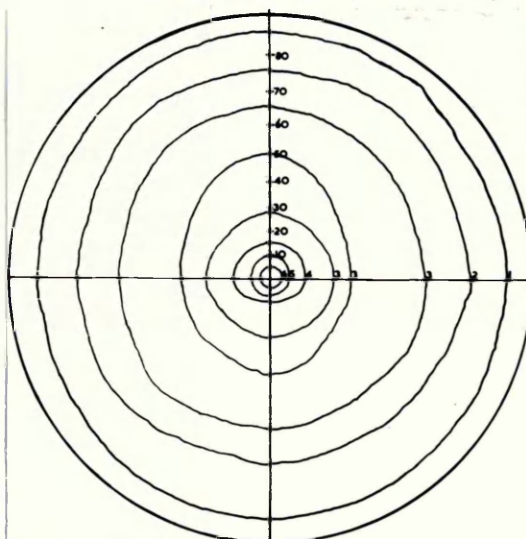
WIREDRAWING STRAIN = 2.60
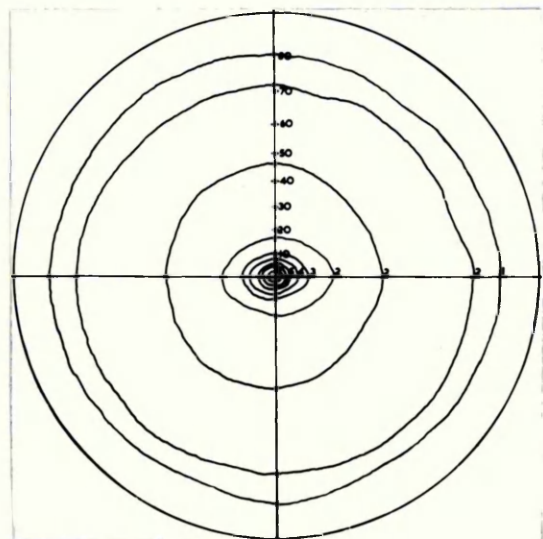
WIREDRAWING STRAIN = 5.27

FIG.46

(110) POLE FIGURES FOR 0.18%
CARBON STEEL SAMPLES ANNEALED
AT 650°C AND DRAWN
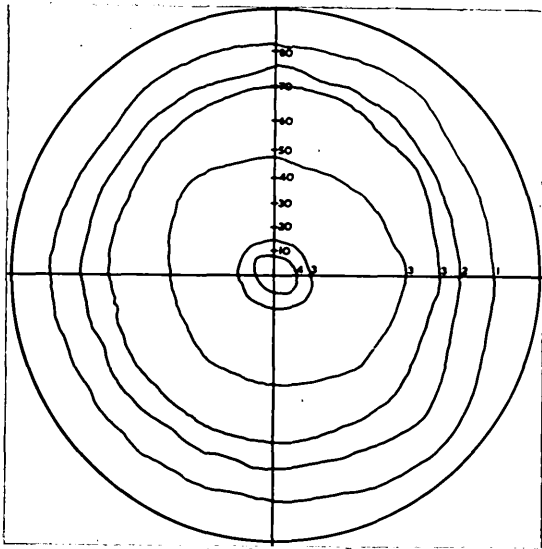
WIREDRAWING STRAIN = 0
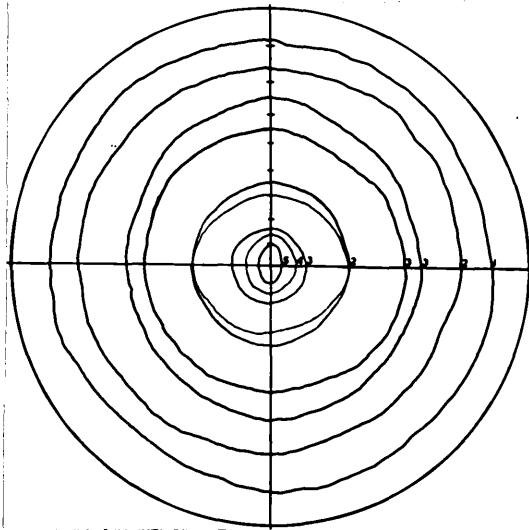
WIREDRAWING STRAIN = 0.98
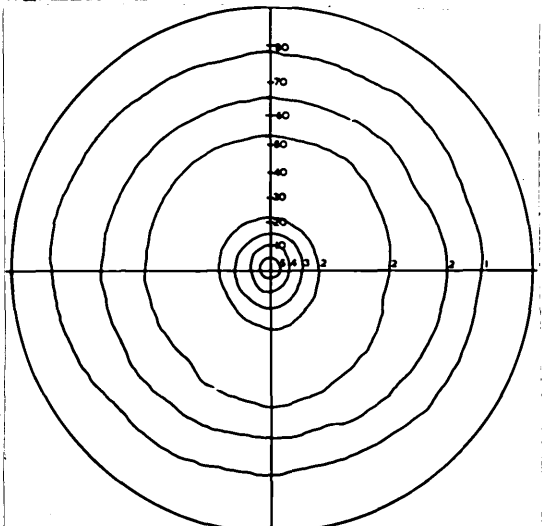
WIREDRAWING STRAIN = 1.95
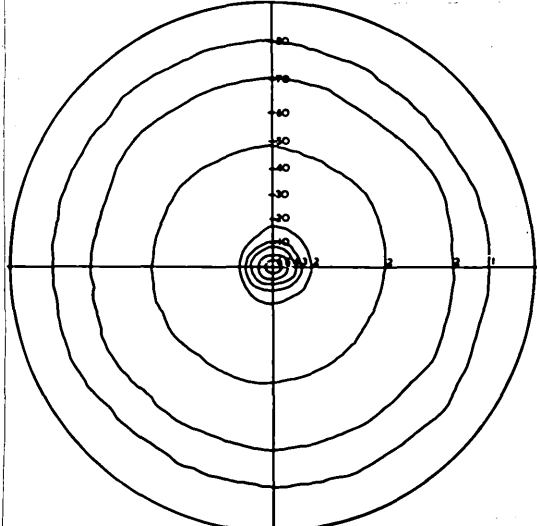
WIREDRAWING STRAIN= 2.60
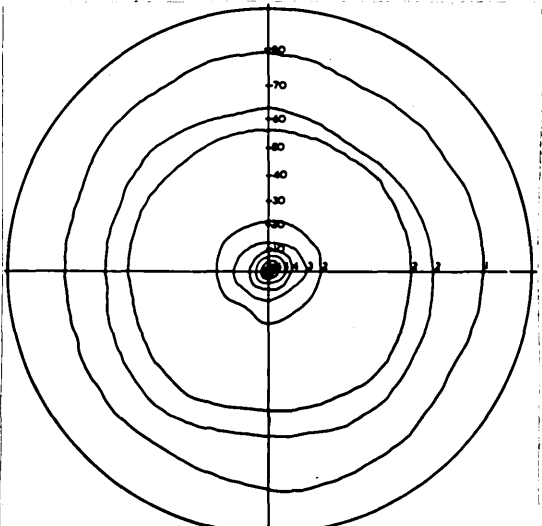
WIREDRAWING STRAIN = 5.00

FIG. 47

(110) POLE FIGURES FOR 0.18%
CARBON STEEL SAMPLES QUENCHED
AND TEMPERED AND DRAWN
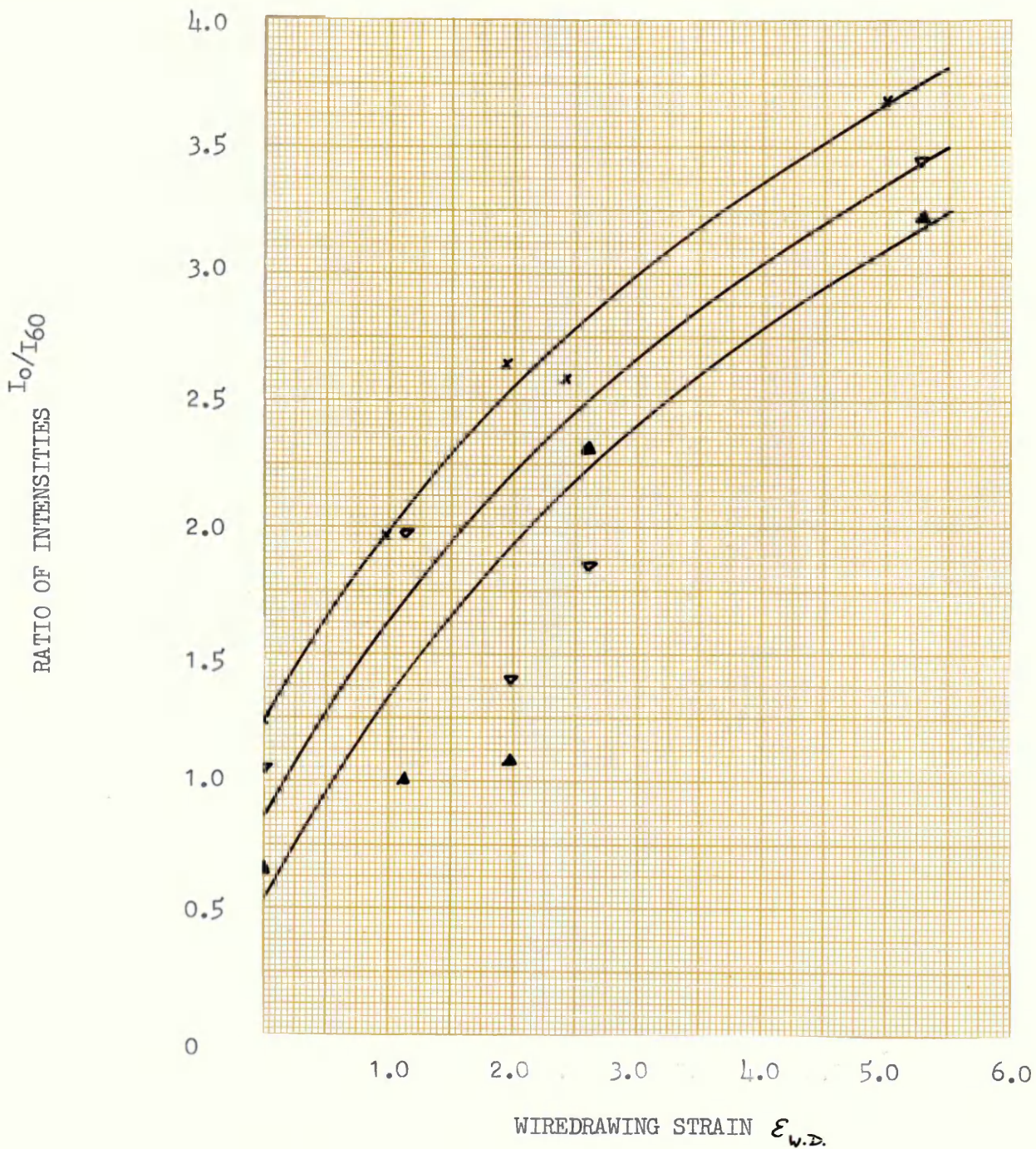
KEY TO SYMBOLS

x 0.18% CARBON STEEL QUENCHED AND TEMPERED
▲ 0.18% CARBON STEEL ANNEALED AT $650^{\circ}C$
▽ PURE IRON ANNEALED AT $850^{\circ}C$

FIG.48

THE RATIO OF PEAK INTENSITY AT 0° TO PEAK INTENSITY AT 60° TO THE WIRE
AXIS FOR (110) PLANE REFLECTIONS OF PURE IRON AND STEEL WIRES AS A
FUNCTION OF WIREDRAWING STRAIN.

MEAN STRAIN RATE

TAN α
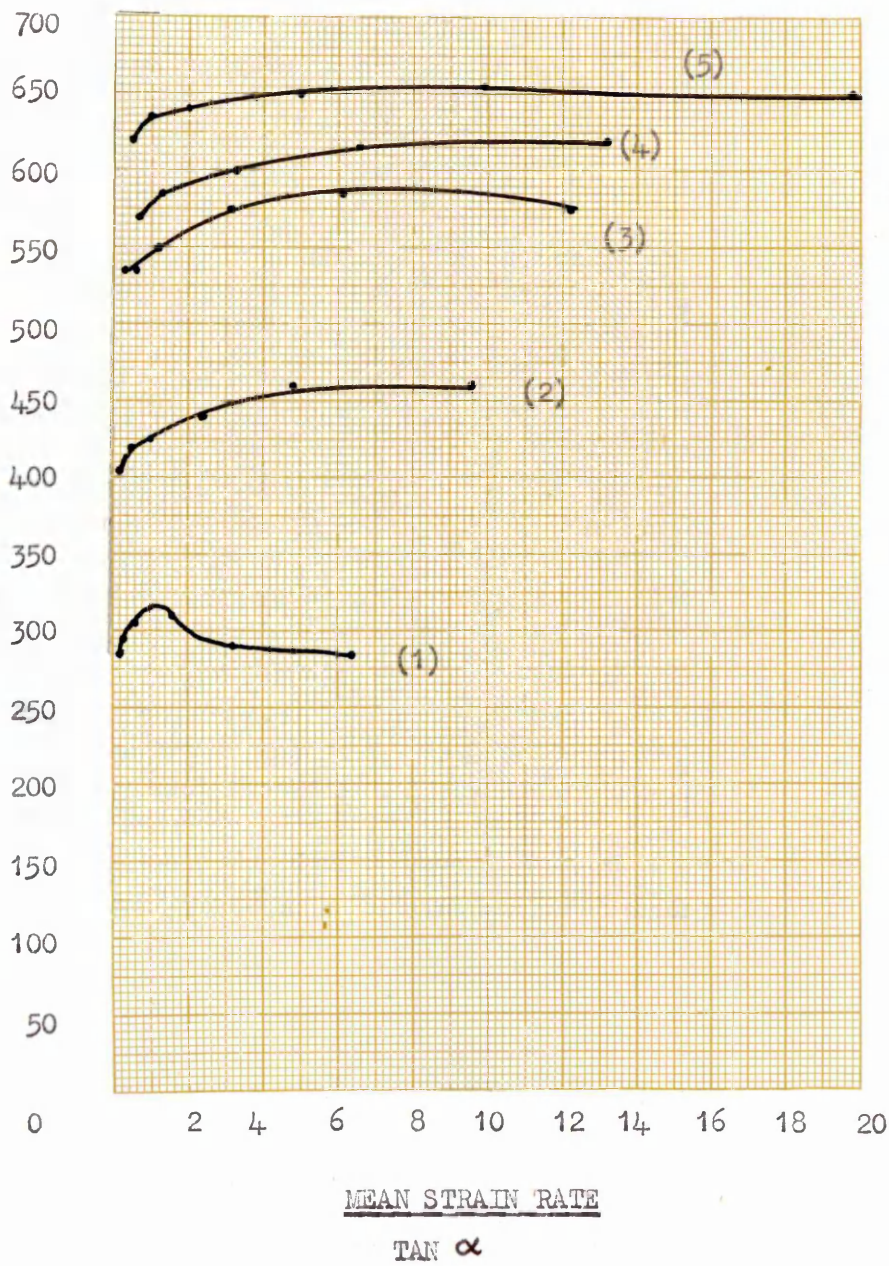
KEY TO LINE NUMBERS

(1) Prior wiredrawing strain = 0.17
(2) Prior wiredrawing strain = 1.02
(3) Prior wiredrawing strain = 1.47
(4) Prior wiredrawing strain = 1.63
(5) Prior wiredrawing strain = 2.45

FIG. 49

THE WIREDRAWING LOAD KGF PER MM^2 OF PROJECTED AREA FOR 0.44% CARBON
STEEL QUENCHED AND TEMPERED AS A FUNCTION OF MEAN STRAIN RATE/TAN
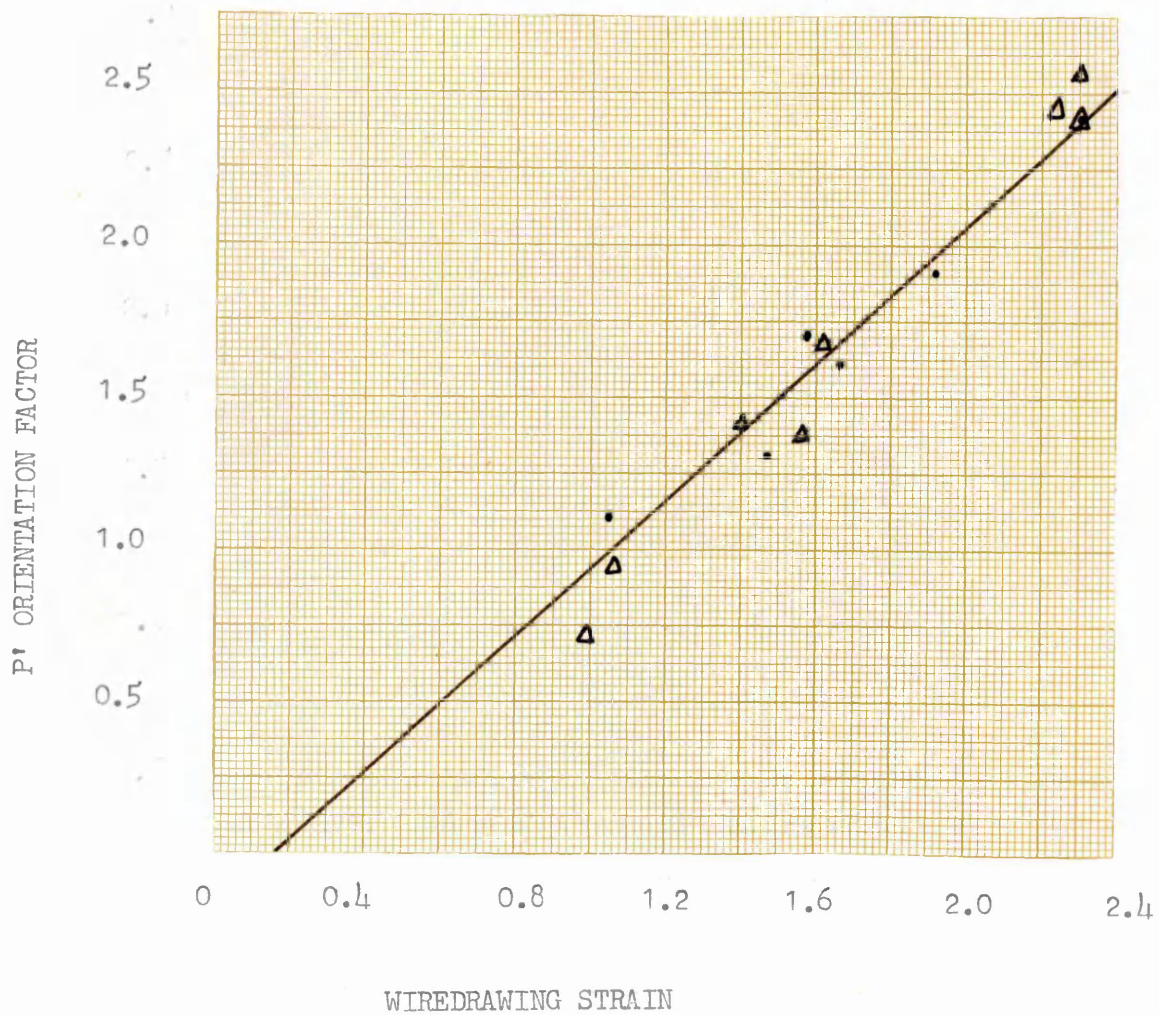
KEY TO SYMBOLS

• TEXTURE COEFFICIENT FROM INVERSE POLE FIGURES

Δ INTENSITY RATIO I_0/I_{60} FROM FULL SPIRAL POLE FIGURES

FIG. 50: THE RELATIONSHIP BETWEEN ORIENTATION FACTOR P'
AND THE SQUARE ROOT OF WIREDRAWING STRAIN.
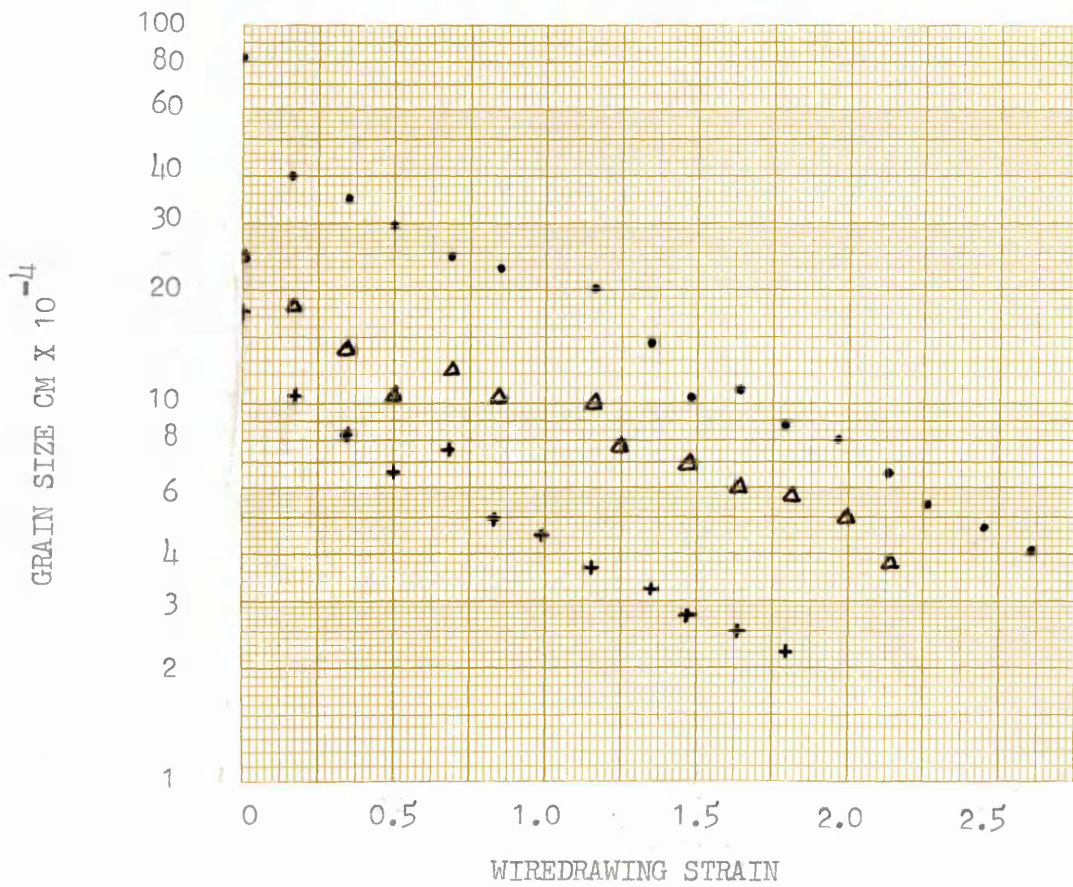
FIG.51:   LOGARITHM OF GRAIN SIZE OF FERRITIC STRUCTURES
           AS A FUNCTION OF WIREDRAWING STRAIN.

           KEY TO SYMBOLS

•   PURE IRON ANNEALED AT 900°C
△   PURE IRON ANNEALED AT 800°C
+   0.18% CARBON STEEL ANNEALED AT 650°C
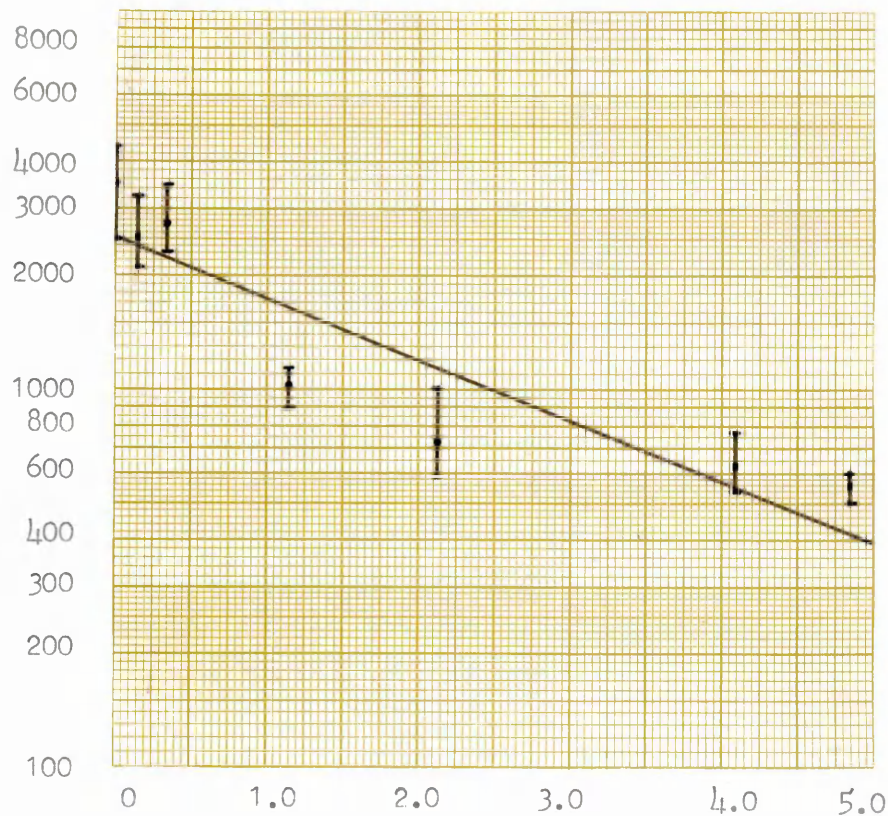
FIG.52: LOGARITHM OF MEAN FREE FERRITE PATH LENGTH OF WIRES
DRAWN FROM 0.18% CARBON STEEL QUENCHED AND TEMPERED
ROD AS A FUNCTION OF WIREDRAWING STRAIN.
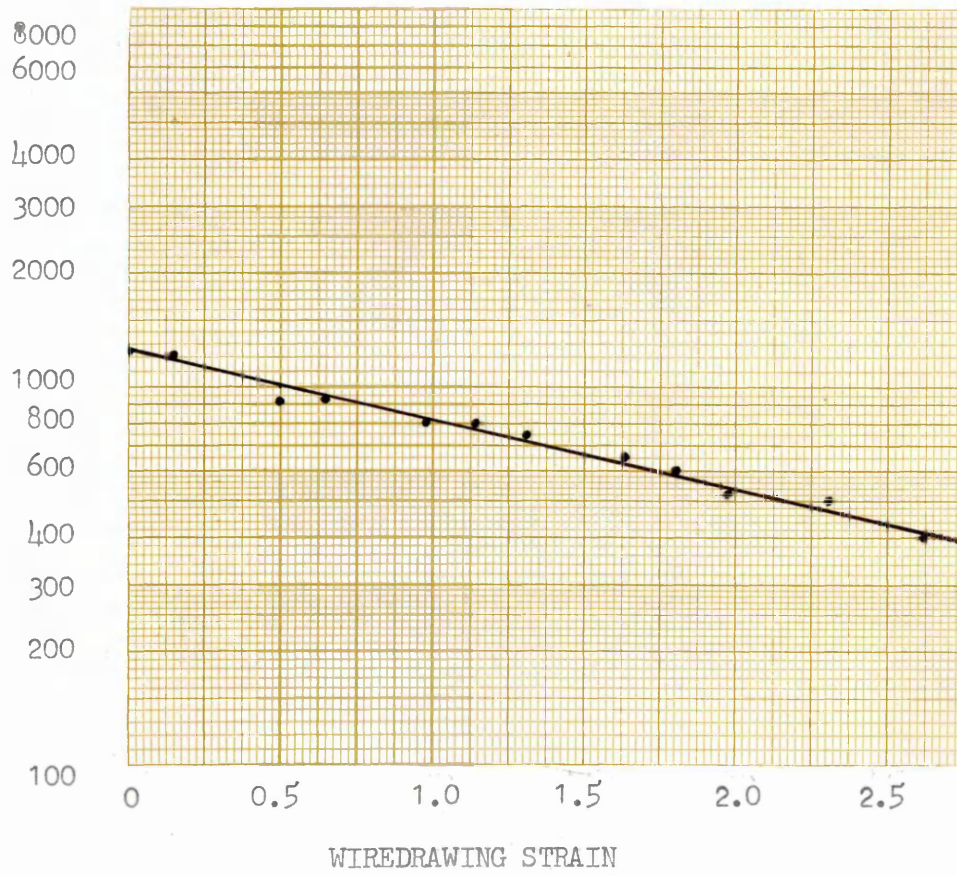
FIG.53: LOGARITHM MINIMUM PEARLITE SPACING AS A FUNCTION
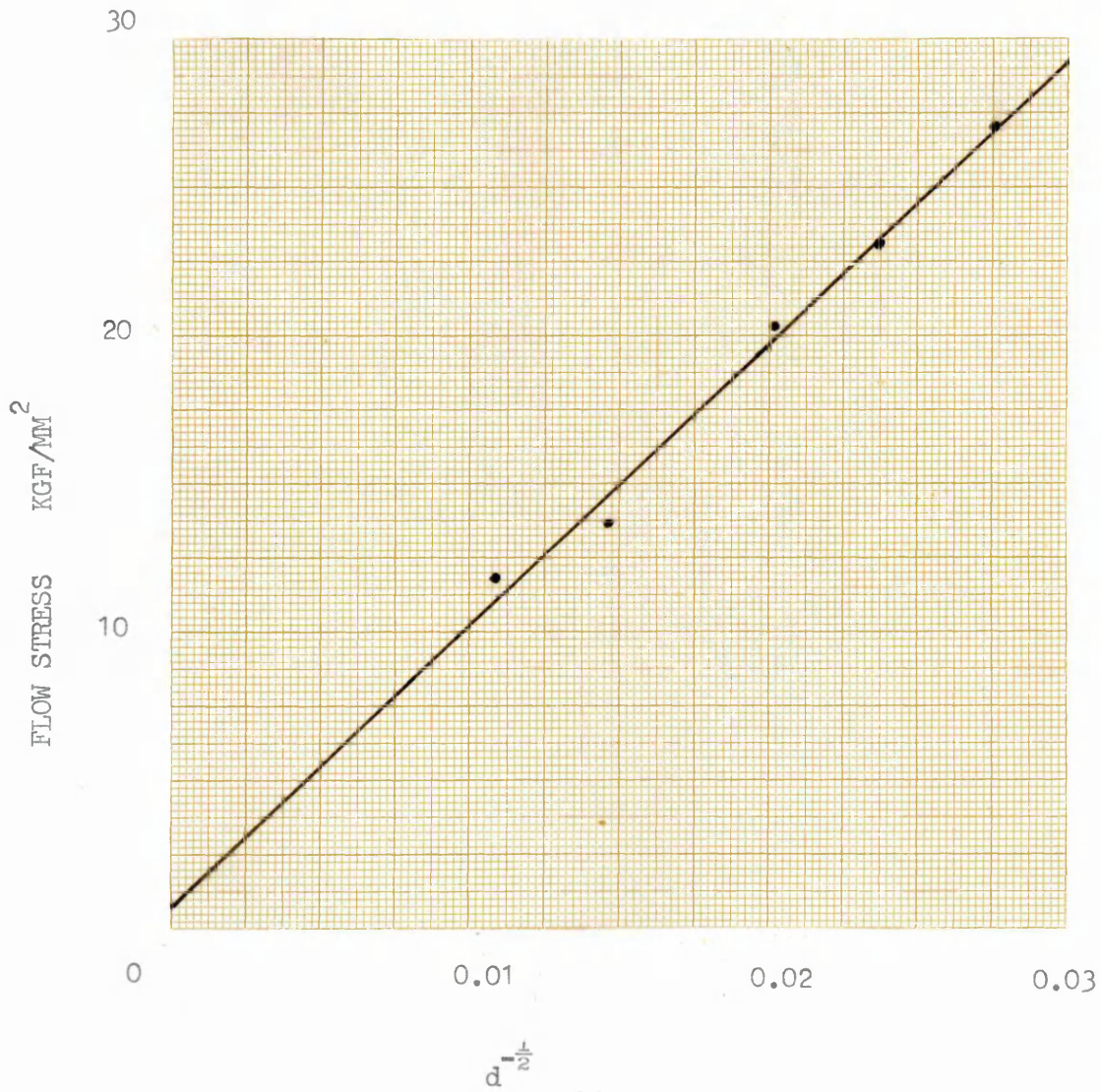OF WIREDRAWING STRAIN FOR 0.44% CARBON STEEL
WIRE DRAWN FROM LEAD PATENTED ROD

FIG.54: THE FLOW STRESS OF AS HEAT TREATED PURE IRON AND 0.18% CARBON STEEL AS A FUNCTION OF THE RECIPROCIL SQUARE ROOT OF GRAIN SIZE.

FIG.55

THE FLOW STRESS OF FERRITIC
STRUCTURES AS A FUNCTION OF
LOG ε_{wD}

KEY TO SYMBOLS

+ 0.18% CARBON STEEL ANNEALE
  AT 650°C

△ PURE IRON ANNEALED AT 800°

• PURE IRON ANNEALED AT 900°

WIREDRAWING STRAIN ε_{wD}
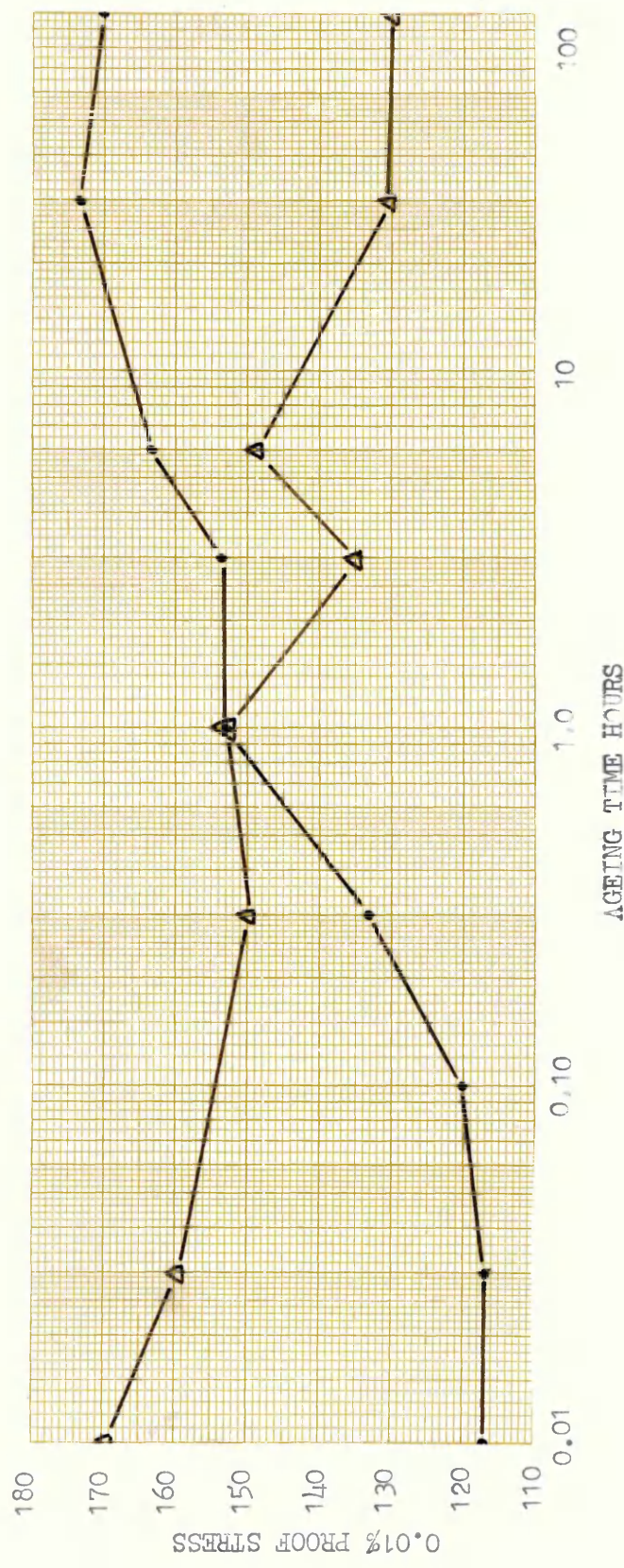
FLOW STRESS σ_f KGF/MM²

AGEING TIME HOURS
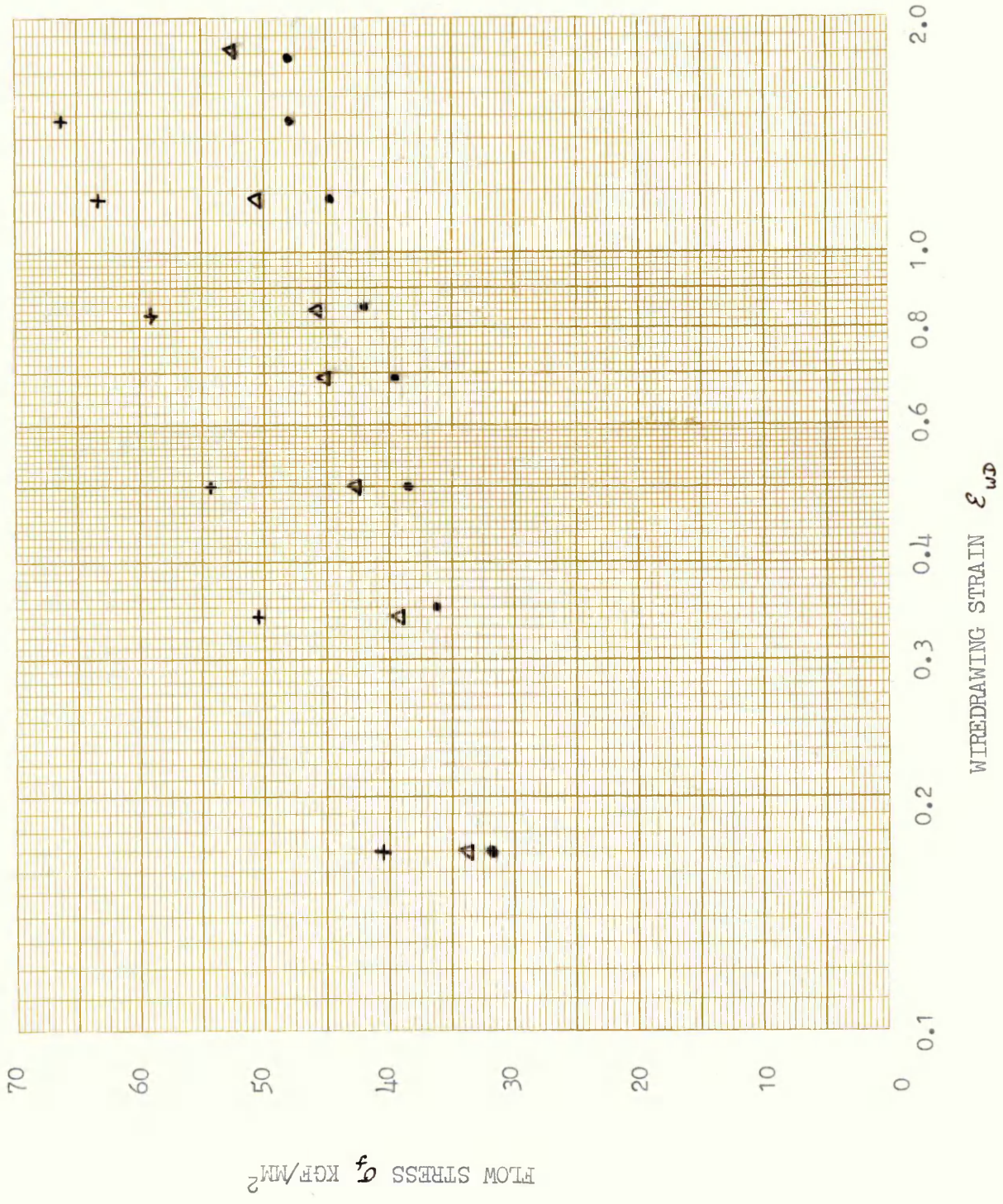
FIG. 56

THE EFFECT OF AGEING ON A 0.18% CARBON STEEL WIRE DRAWN 98% FROM QUENCHED AND TEMPERED ROD
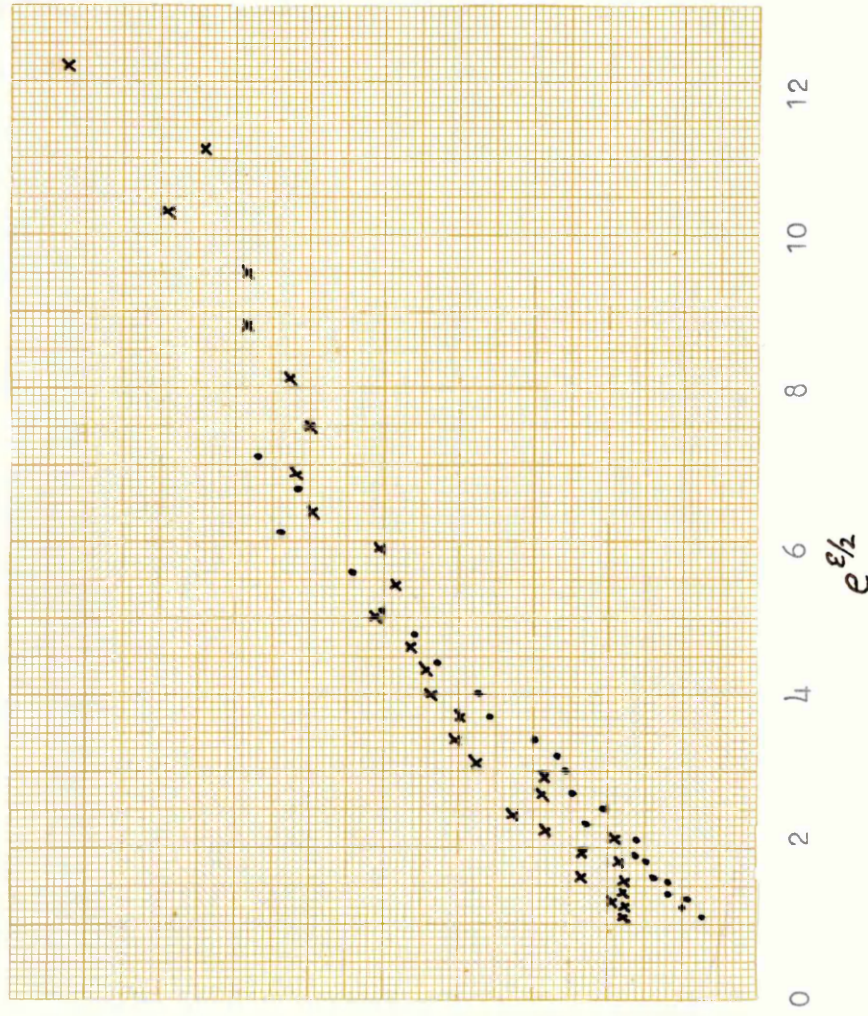
KEY TO SYMBOLS

△ AGED AT 400°C

● AGED AT 200°C

FIG.57

THE FLOW STRESS OF 0.18% CARBON
STEEL WIRES QUENCHED AND TEMPERED
BEFORE DRAWING AND 0.44% CARBON
STEEL WIRES LEAD PATENTED BEFORE
DRAWING AS A FUNCTION OF

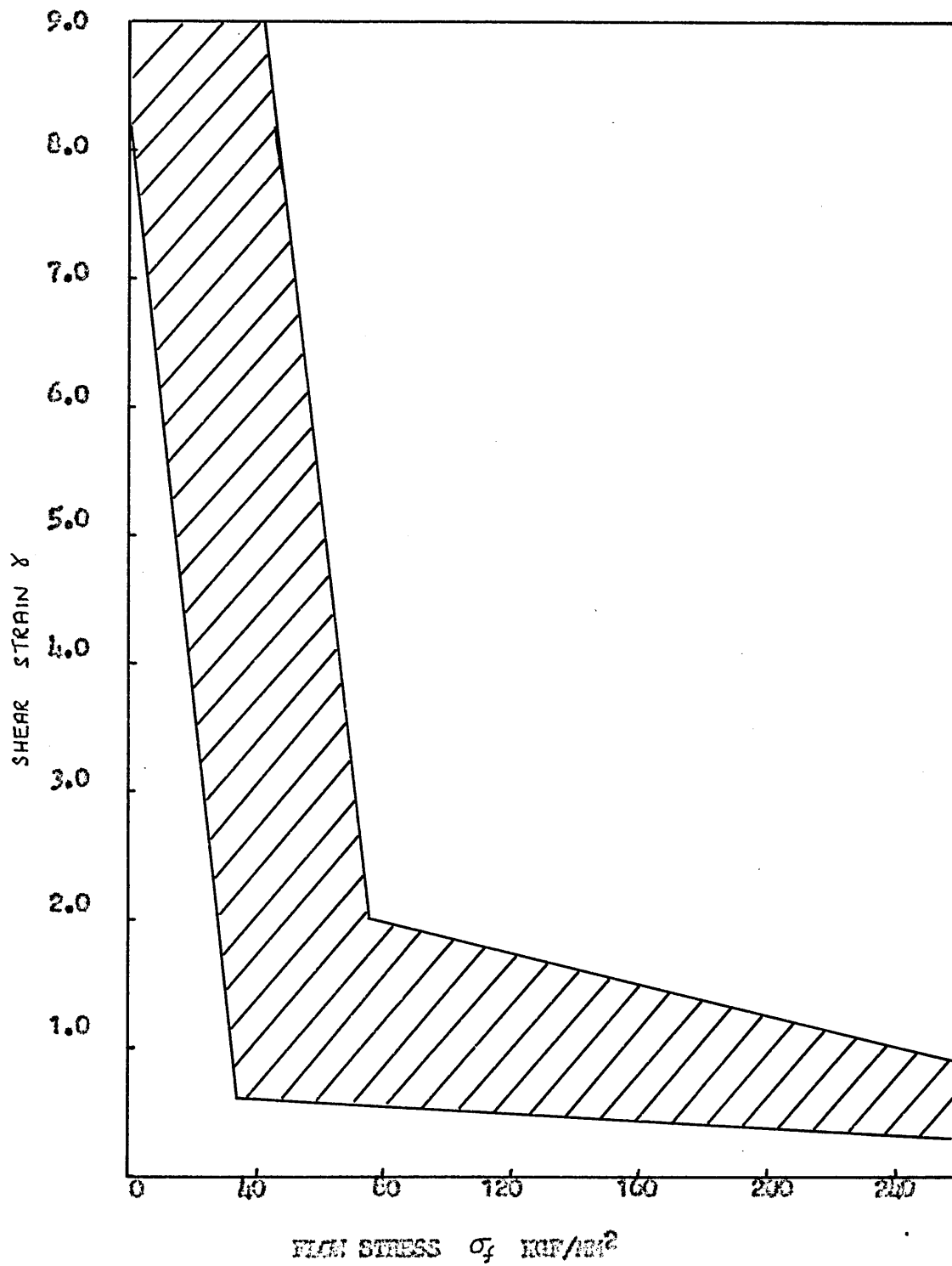KEY TO SYMBOLS

X   0.18% CARBON STEEL
·   0.44% CARBON STEEL

FIG.58: THE RELATIONSHIP BETWEEN TORSIONAL DUCTILITY AND
FLOW STRESS FOR ALL MATERIALS INVESTIGATED.

THE CALCULATION OF SHEAR STRESS AND STRAIN FROM TORQUE/TWIST TEST DATA

1. SHEAR STRESS LESS THAN TORSIONAL YIELD STRESS

Fig. A1 represents a solid bar, of length L, diameter D, subjected to a twisting for M_T.   Then:-

M_T is opposed by yhe **resistance** of the material and the stress γ acting on a segment, distance r from the centre of the rod may be given by

$$M_T = \int_{r=0}^{r=a} \gamma r \; dA = \frac{\gamma}{r} \int_0^a r^2 dA \qquad (1)$$

but $\int r^2 dA$ is the polar moment of inertia of the area with respect to the bar axis, hence

$$M_T = \frac{\gamma}{r} J$$

$$\therefore \qquad \gamma = \frac{M_T}{J} \qquad (2)$$

Since the shear stress is zero at the axis of the bar, and a maximum at the surface, and the polar moment of inertia at the surface $J = \pi D^4 / 32$

$$\gamma_{max} = M_T \frac{D/2}{(D^4/32)\pi} = \frac{16 M_T}{D^3 \pi} \qquad (3)$$

$$\text{Shear strain} = \gamma = \tan \phi = \frac{r\theta}{L} \qquad (4)$$

where θ = angle of twist in radians

The shear stress over a cross section of the bar is no longer a linear function of the distance from the axis. The derivation of the method of calculating shear stress is due to Nadai.

Re-arranging equation (4)

$$\gamma = r\theta' \quad \text{where} \quad \theta^1 = \theta/L \tag{5}$$

Equation (1) may be re-written as

$$M_T = 2\bar{\Pi} \int_0^a \tau\, r^2 dr \tag{6}$$

Shear stress is related to Shear strain by the stress/strain curve in shear i.e.

$$\tau = f(\gamma)$$

Re-writing Equation (6), and changing the variable from r to γ by use of equation (5)

$$M_T = 2\bar{\Pi} \int_0^{\gamma_a} f(\gamma)\, \frac{\gamma^2}{(\theta^1)^2}\, \frac{d\gamma}{\theta^1}$$

or

$$M_T (\theta^1)^3 = 2\bar{\Pi} \int_0^{\gamma_a} f(\gamma)\, \gamma^2 d\gamma \quad \text{where } \gamma_a = a\theta^1$$

Differentiating with respect to θ^1

$$\frac{d}{d\theta^1} (M_T \theta^{13}) = 2\bar{\Pi}\, a\, f(a\theta^1) a^2\, (\theta^1)^3$$

$$= 2\bar{\Pi}\, a^3\, (\theta^1)^2 f(a\theta^1)$$

The maximum shear stress at the surface of the bar is $\tau_a = f(a\theta^1)$

$$\therefore \quad \frac{d(M_T \theta^{13})}{d\theta^1} = 2\bar{\Pi}a^3(\theta^1)^2 \tau_a$$

i.e. $3 M_T (\theta^2)^2 + (\theta^1)^3 \dfrac{dM_T}{d\theta^1} = 2\bar{\Pi} a^3(\theta^1)^2 \tau_a$

$$\therefore \quad \tau_a = \frac{3 M_T (\theta)^2 + (\theta^1)^3 \dfrac{dM_T}{d\theta^1}}{2\overline{\pi} a^3 (\theta^1)^2}$$

$$= \frac{1}{2\overline{\pi} a^3} \left[3M_T + \theta' \frac{dM_T}{d\theta^1} \right] \tag{7}$$

Fig.A2 illustrates the method of plotting Torque/Twist data, and from the geometry

$$\tau = \frac{1}{2\overline{\pi} a^3} \left[BC + 3\ CD \right] \tag{8}$$

It should be noted that, at the maximum torque the term $\left(dM_T/d\theta^1 \right)$ is zero, therefore the maximum shear stress is given by:-

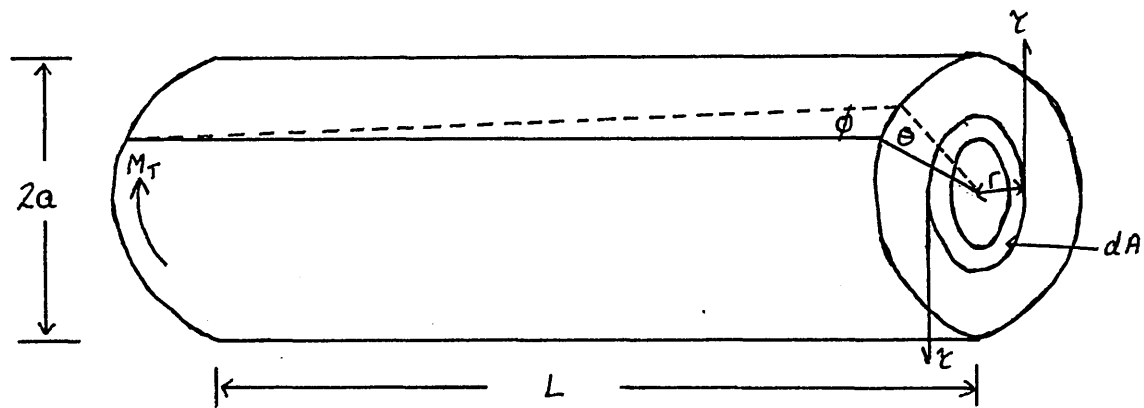$$\tau_\mu = \frac{3M_T}{2\overline{\pi} a^3} \tag{9}$$

FIG.A1.1.   THE PRINCIPLES OF TORSION FOR A SOLID
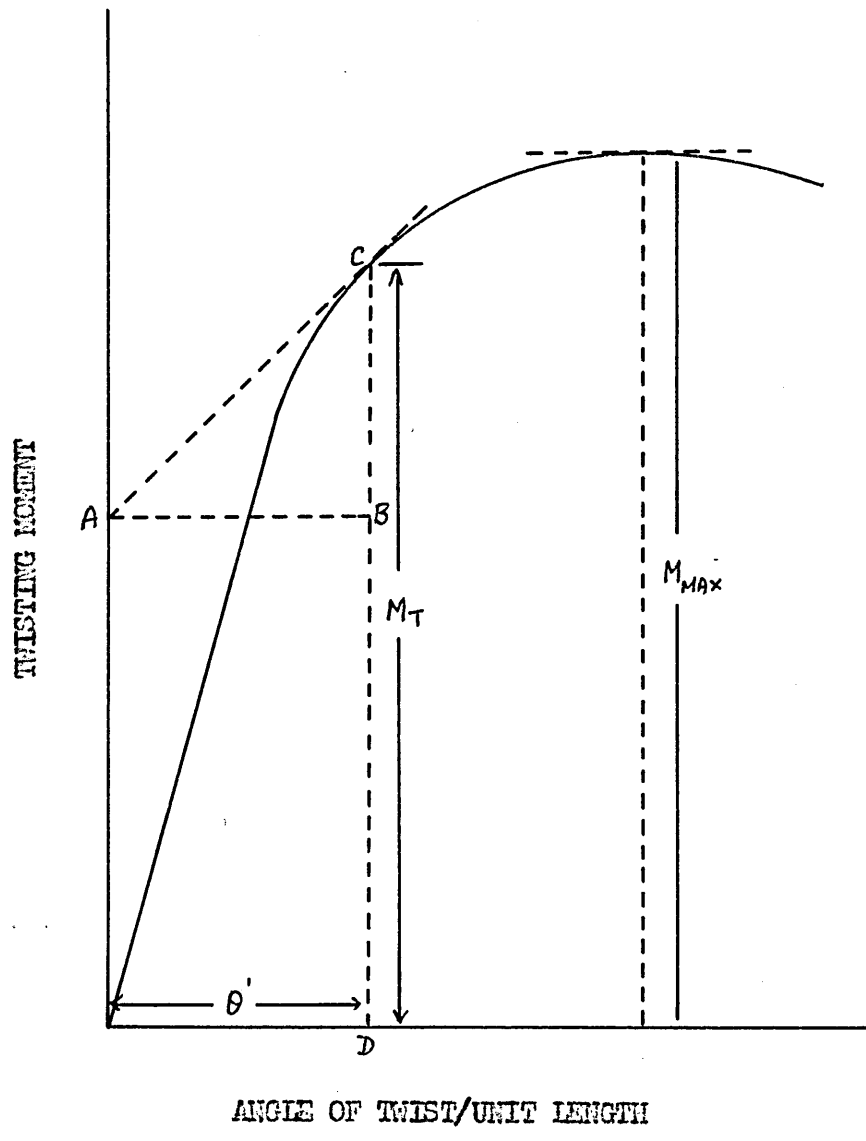CYLINDRICAL TEST PIECE.

FIG AI.2.   CONSTRUCTION USED TO DETERMINE TRUE SHEAR
STRESS/SHEAR STRAIN DATA.

THE CALCULATION OF VOLUME FRACTION OF CEMENTITE IN CARBON STEEL

All the materials used in the experimental work for this thesis were plain carbon steels, and either cooled or transformed at temperatures such that the expected carbide form would be cementite Fe_3C, or were tempered for a period of time such that again all carbides should be cementite. The following assumptions have been made:—

1. That all carbon present in the steel took the form of cementite Fe_3C.

2. That the composition of the carbides was stoichiometric.

3. That the steel was a binary solid solution of cementite in pure iron.

The Volume Fraction of the components of a binary solid solution is given by[1]:—

$$\phi_1 = \frac{N_1 V_1}{N_1 V_1 + N_2 V_2} \qquad \text{and} \qquad \phi_2 = \frac{N_2 V_2}{N_1 V_1 + N_2 V_2}$$

where N_1, N_2 are the number of molecules of components 1 and 2 respectively and V_1, V_2 are the molecular volumes of the components.

The percentage composition by weight can be converted to the atom fraction as follows[1]:—

$$n_1 = \frac{\% W/W_{(1)}}{M_1}$$

$$n_2 = \frac{\% W/W_{(2)}}{M_2}$$

where m_1, m_2 are the atomic weights of the respective elements and
n_1, n_2 are the number of atoms of each element present per 100 gm.

Assuming that the basic structure cell of the constituents may be regarded as the molecule, for volume determination we have :-

(a) Cementite Fe_3C [2]. Orthorhombic unit cell, containing 12 iron atoms, 4 carbon atoms. Cell dimensions :-

$$a = 4.5235 \; A^{\circ}$$
$$b = 5.0888 \; A^{\circ}$$
$$c = 6.7431 \; A^{\circ}$$

(b) Pure Iron [2]. Body centred cubic unit cell, containing 2 atoms of iron. Cell dimension :-

$$a = 2.8664 \; A^{\circ}$$

The molecular volume of cementite and iron are then given by :-

$$V_1 = 4.5235 \times 5.0888 \times 6.7431 = 155.22067 \; A^{\circ 3} \text{(cementite)}$$
$$V_2 = 2.8664^3 = 23.551055 \; A^{\circ 3} \text{ (iron)}$$

The number of cementite cells N_1 per unit volume may be calculated as follows :-

$$N_1 = \frac{n_1}{100} \times 4$$
$$N_2 = \frac{1 - N_1}{2}$$

then
$$f = \frac{N_1 V_1}{N_1 V_1 + N_2 V_2}$$

where
N_1 = number of cementite unit cells / unit volume

V_1 = volume of cementite unit cell = $155.22067 \; A^{\circ 3}$

N_2 = number of iron unit cells / unit volume

V_2 = volume of iron unit cell = $23.551055 \; A^{\circ 3}$

f = Volume fraction of cementite

The Volume Fraction of cementite in plain carbon, hypo eutectoid steels was calculated from these formulae, and is shown as a function of weight percentage carbon in Fig.II.1

References

(1) Darken and Gurry-Physical Chemistry of Metals.McGraw-Hill

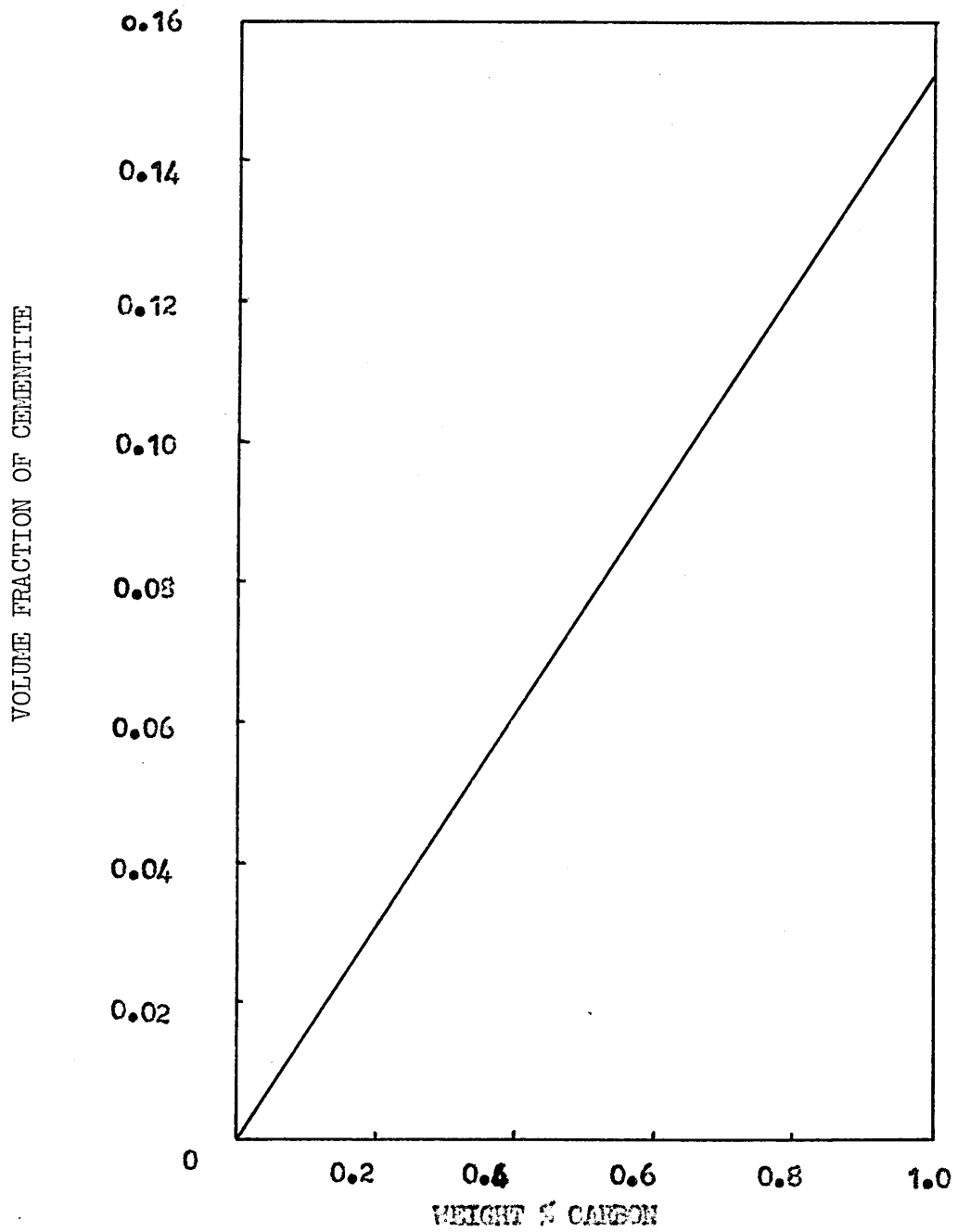(2) Barrett and Massalski - Structure of Metals. McGraw-Hill

FIG. A11.1 CALCULATED VOLUME FRACTION OF CEMENTITE
AS A FUNCTION OF WEIGHT % CARBON

METHODS OF STATISTICAL ANALYSIS

Several methods of statistical analysis were employed in this work. The formulae used are shown in this Appendix, with no attempt to provide derivations. The following definitions will apply throughout.

Let $\quad x_1 \;=\;$ Variable 1

$\qquad x_2 \;=\;$ Variable 2

$\qquad y \;=\;$ resultant variable

$\qquad N \;=\;$ number of sets of data

$$\text{Variation in } y = \Sigma(y-\bar{y})^2 = \Sigma y^2 - \frac{(\Sigma y)^2}{N}$$

$$\text{Variation in } x = \Sigma(x-\bar{x})^2 = \Sigma x^2 - \frac{(\Sigma x)^2}{N}$$

$$\text{Co-variation in } x \text{ and } y = \Sigma(x-\bar{x})(y-\bar{y}) = \Sigma xy - \frac{(\Sigma x)(\Sigma y)}{N}$$

$$\text{Regression Coefficient} = \frac{\Sigma(x-\bar{x})(y-\bar{y})}{\Sigma(x-\bar{x})^2}$$

$$\text{Variance Accountable for by the regression} = \frac{\left[\Sigma(x-\bar{x})(y-\bar{y})\right]^2}{\Sigma(x-\bar{x})^2}$$

$$\text{Correlation Coefficient} = \frac{\Sigma(x-\bar{x})(y-\bar{y})}{\sqrt{\Sigma(x-\bar{x})^2 \; \Sigma(y-\bar{y})^2}}$$

The regression constant was calculated from the equation

$$(y-\bar{y}) = a(x-\bar{x})$$

where a is the Regression Coefficient

A multiple regression technique was used which required calculation of the following for each set of data:-

1. Variation in x_1 $\qquad\qquad \Sigma x_1^2$

2. Variation in x_2 $\Sigma^1 x_2^2$

3. Co-variation in x_1 and x_2 $\Sigma^1 x_1 x_2$

4. Variation in y $\Sigma^1 y^2$

5. Covariation in x_1 and y $\Sigma^1 x_1 y$

6. Covariation in x_2 and y $\Sigma^1 x_2 y$

These can then be fitted to the two pairs of simultaneous equations

$$Ca_1 \, \Sigma^1 x_1^2 + Ca_2 \Sigma^1 x_1 x_2 = 1$$
$$Ca_1 \, \Sigma^1 x_1 x_2 + Ca_2 \, \Sigma^1 x_2^2 = 0$$

     }   Pair 1

$$C_{b1} \, \Sigma^1 x_1^2 + C_{b2} \Sigma^1 x_1 x_2 = 0$$
$$C_{b1} \, \Sigma^1 x_1 x_2 + C_{b2} \, \Sigma^1 x_2^2 = 1$$

     }   Pair 2

However a systematic approach, which is more usually employed
for multiple reqression of three or more variables, was adopted
as less susceptible to errors. This reproduced the basic
techniques of equation solving in a tabular form, as follows

C_a	C_b	1st Set	2nd Set
$\Sigma^1 x_1^2$	$\Sigma^1 x_1 x_2$	1	0
$\Sigma^1 x_1 x_2$	$\Sigma^1 x_2^2$	0	1

This can be seen to be identical to the pairs of equations above.
The solutions of the equations can then be used to calculate the
regression coefficients, and their standard error.

$$b_{1.2} = C_{a1} \, \Sigma^1 y x_1 + C_{a2} \Sigma^1 y x_2$$

$$b_{2.1} = C_{b1} \, \Sigma^1 y x_1 + C_{b2} \, \Sigma^1 y x_2$$

Residual Variance $\sigma_r^2 = \dfrac{1}{n-3} \left[\mathcal{E}^1 y^2 - b_{1.2} \mathcal{E}^1 yx_1 - b_{2.1} \mathcal{E}^1 yx_2 \right]$

Standard error of $b_{1.2} = \sqrt{C_{a1}\, \sigma_r^2}$

Standard error of $b_{2.1} = \sqrt{C_{b2}\, \sigma_r^2}$

The significance of the regression coefficients was then estimated by calculating

$$t = \dfrac{b_{1.2}}{\sqrt{C_{a1}\, \sigma_r^2}}$$

and comparing this with the values in the Table of t at n-3 degrees of freedom.

References

M.J.Moroney "Facts from Figures"

K.A.Brownlee "Industrial Experimentation"

D.V.Lindley and J.C.P.Miller "Cambridge Elementary Statistical Tables"